Mathematical Modelling of Bread Dough Sheeting

A thesis presented in partial fulfilment of the requirements for the degree of

Doctor of Philosophy in Food Engineering

at Massey University, Palmerston North, New Zealand.

Richard John Love

2003

Massey University
COLLEGE OF SCIENCES

Institute of Food, Nutrition and Human Health
Te Kura Hangarau o Kai-oranga-ā-tāngata
Private Bag 11 222,
Palmerston North,
New Zealand
Telephone: 64 6 350 4336
Facsimile: 64 6 350 5657

CANDIDATE'S DECLARATION

This is to certify that the research carried out for my Doctoral thesis entitled "Mathematical Modelling of Bread Dough Sheeting", in the Institute of Food, Nutrition and Human Health, College of Sciences, Massey University, Palmerston North, New Zealand is my own work and that the thesis material has not been used in part or in whole for any other qualification.

Candidate's Name Richard Love

Signature R. S. Love

Date 23/12/03

Massey University
COLLEGE OF SCIENCES

Institute of Food, Nutrition and Human Health
Te Kura Hangarau o Kai-oranga-ā-tāngata
Private Bag 11 222,
Palmerston North,
New Zealand
Telephone: 64 6 350 4336
Facsimile: 64 6 350 5657

SUPERVISOR'S DECLARATION

This is to certify that the research carried out for the Doctoral thesis entitled "Mathematical Modelling of Bread Dough Sheeting", was done by Richard Love in the Institute of Food, Nutrition and Human Health, College of Sciences, Massey University, Palmerston North, New Zealand. The thesis material has not been used in part or in whole for any other qualification, and I confirm that the candidate has pursed the course of study in accordance with the requirements of the Massey University regulations.

Supervisor's Name Yacine HEMAR

Signature

Date 23/12/03

Massey University
COLLEGE OF SCIENCES

Institute of Food, Nutrition and Human Health
Te Kura Hangarau o Kai-oranga-ā-tāngata
Private Bag 11 222,
Palmerston North,
New Zealand
Telephone: 64 6 350 4336
Facsimile: 64 6 350 5657

CERTIFICATE OF REGULATORY COMPLIANCE

This is to certify that the research carried out in the Doctoral thesis entitled "Mathematical Modelling of Bread Dough Sheeting", in the Institute of Food Nutrition and Human Health, College of Sciences, Massey University, New Zealand:

a) is the original work of the candidate, except as indicated by appropriate attribution in the text and/or in the acknowledgements;
b) that the text, excluding appendices, does not exceed 100,000 words;
c) all the ethical requirements applicable to this study have been complied with as required by Massey University, other organisations which had a particular association with this study and relevant legislation.

Candidate's Name Richard Love **Supervisor's Name** Yacine HEMAR

Signature R.J.Love **Signature**

Date 23/12/03 **Date** 23/12/03

Abstract

Bread dough sheeting is an important operation in the bread making industry. The process involves the passing of a mass of dough between two, or more, rotating rollers. The function of sheeting can be: i) to shape the dough, ii) to laminate layers of product together or iii) to develop the gluten network, which gives dough many of its properties.

The model developed, in this thesis, describes the dough sheeting process using a continuum mechanics approach, solved using a perturbation technique. The bread dough rheology is described using the Criminale-Ericksen-Filbey (CEF) viscoelastic constitutive equation. It was thought that this approach may model the process better than the viscous models used elsewhere. The perturbation technique, used in solution, meant that the model remained computationally swift. The CEF equation was used as it is reasonably simple mathematically and measuring the required dough properties was quite straightforward, although, as was discovered, reproducibly measuring the properties of bread dough is never easy, not least because of the history dependent nature of bread dough. Some important assumptions made, in this model, on the basis of literature and preliminary experiments, were that: the process is two-dimensional; the process is at steady state; the process is unaffected by inertia, temperature or gravity; some parts of the process (conveyor belt speeds, for example) are unimportant; and that the dough is incompressible.

It was found that such a model can be used to predict the exit height of the dough, the forces and torques experienced by the rollers, and velocity and pressure profiles in the dough. The predictions were qualitatively consistent with validation data gathered on a pilot plant sheeter, but there were some large quantitative inaccuracies, particularly with the exit height prediction (as there is with viscous models). The inaccuracies suggest that such an approach to modelling bread dough sheeting misses some important facet of the process, possibly the compressibility of the dough. That is, a viscoelastic description of the process material will not, alone, lead to a complete model of the dough sheeting process.

Acknowledgements

I would like to acknowledge the assistance of:

Supervisors: Osvaldo Campanella, Li Chong, Yacine Hemar, Robert McKibbin and Marco Morgenstern.

Leanne Hiroti, for assistance in gathering experimental data.

John Love, for proof reading.

Staff of Massey University and Crop and Food Research Ltd., for their advice.

The Foundation for Research Science and Technology, for funding.

Contents

List of Symbols Used

The following symbols and their units are used in this thesis. Definitions are also given in the main text.

a, b, c, d	constants	–
C_p	specific heat capacity	kJ kg^{-1} K^{-1}
De	Deborah number	–
DS	digital signal	–
		kJ kg^{-1} or
E	energy input during sheeting	W h kg^{-1}
F	force	N
g	acceleration due to gravity	m s^{-2}
G	modulus of elasticity	Pa
G^*	complex modulus of elasticity ($= G' + iG''$)	Pa
h	height of dough sheet	m
H	gap between viscometer plates	m
I	2nd moment of inertia	m^4
i,j	index variables	–
K	power-law consistency index	Pa s^n
I_{ij} (j_{ij})	elongation tensor (rate of elongation tensor) (section 4.2)	(s^{-1})
m	mass	kg
m	power law flow behaviour index (1st normal stress coefficient)	–
n	power law flow behaviour index	–
p, P	pressure	Pa
R	radius (roller)	m
R	Pearson correlation coefficient	–
Re	Reynolds number	–
s	Laplace co-ordinate variable	–
t	time co-ordinate	s
T, M	torque	N m
U, v, w	x, y, z velocity components	m s^{-1}
u_r	tangential velocity at roller surface	m s^{-1}
W	width of dough sheet	m

x, y, z	co-ordinate directions	m
$\overline{X}$	Laplace transform of variable X	–
Θ	reduction ratio $\left(=\frac{h_i}{\delta}\right)$	–
Ω	angular velocity of parallel plate viscometer	rad s^{-1}
Ψ_1, Ψ_2	1st and 2nd Normal Stress coefficient	Pa s^{-2}
α, θ	angle	o
β, x	response coefficient for coded variable x	–
δ	nip gap between the rollers	m
δ_{ij}	Kronecker delta	–
ε	geometry ratio $\left(=\sqrt{\frac{\delta}{R}}\right)$	–
$\gamma_{ij}\ (\dot{\gamma}_{ij})$	strain tensor (rate of strain tensor)	(s^{-1})
η	viscosity	Pa s
η^*	complex viscosity ($= \eta' + i\eta''$)	
λ	time constant	s
μ	friction coefficient	–
ρ	density	kg m^{-3}
σ_{ij}	total stress tensor	Pa
$\tau_{ij}\ (\dot{\tau}_{ij})$	deviatoric or shear stress tensor (rate of …)	Pa
ω	oscillatory strain frequency	Hz

1. Introduction and Literature Review

1.1. The Sheeting Process

Dough sheeting is a processing step used in the production of baked products, including breads, tortillas and pastries. The critical action in sheeting is the passing of a mass of dough between a rotating roller and a hard surface (usually another roller). This produces a continuous sheet of dough. A photograph and a simplified schematic of a dough sheeter are given in Figure 1.1.

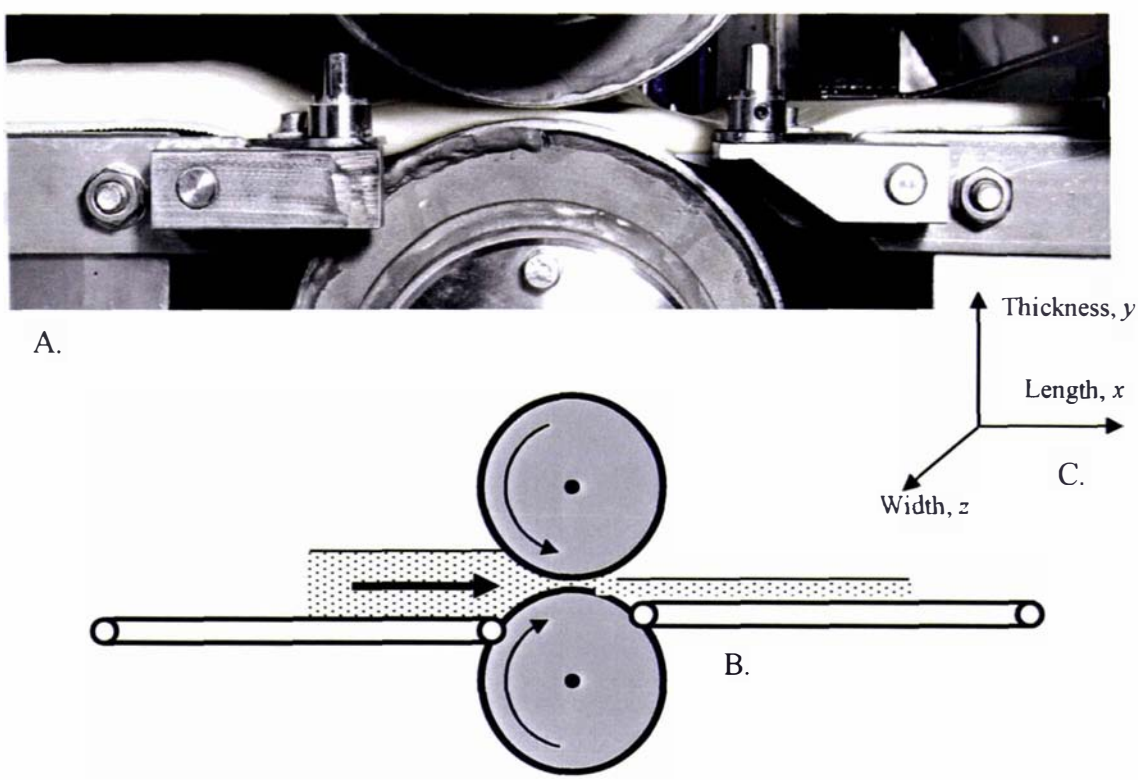

Figure 1.1 Simple Sheeter Photograph and Schematic. A. Dough passing under a roller. The rollers are 150 mm in diameter. B. Schematic (not to scale), demonstrating: roller position and direction of rotation, dough, conveyor belts. C. Coordinate directions.

Figure 1.2 demonstrates another more complicated L-Shaped sheeter geometry. Gorton (1997) described a sheeter where the upper surface consists of many smaller rollers; it was claimed that this reduces the "stresses" in sheeting.

In some circumstances the dough may be sheeted several times either by returning the sheet to the sheeter or by passing the sheet through a chain of sheeters. Levine & Drew (1989) gave an overview of some of the physical equipment associated with sheeting.

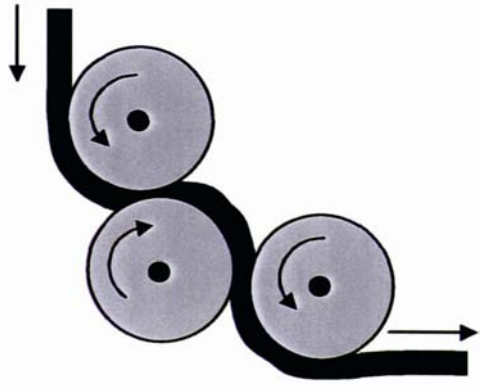

Figure 1.2 A Complicated L-Shaped Sheeter Geometry, that might be found in a moulder. Demonstrates roller positions and direction of rotation.

1.2. Similar Processes

Apart from its use in the baking industry, the sheeting of materials is an important industrial unit operation in, for example, polymer processing such as the formation of PVC sheets, pulp and paper processing and sheet metal processing. These fields have their own literature, with a more established history than dough sheeting. Literature from related industrial processes has been included in this review.

The sheeting of polymeric materials, referred to as calendering within the field, is particularly relevant to dough sheeting, as dough is fundamentally a complex tangle of protein biopolymers. An analysis of dough sheeting (Levine & Drew, 1989) is based substantially upon a polymer processing textbook by Middleman (1977). Polymer calendering does differ, however, from dough sheeting in that it is conducted at elevated temperatures, with heated rolls. This means that heat transfer affects the calendering operation (Finston, 1951). The elevated temperatures also mean that the pre-rolled condition of the polymer is a free-flowing liquid, as opposed to a semisolid sheet as in dough sheeting. In polymer calendering the process material is usually homogeneous and well defined. This is also different from the situation with dough sheeting.

1.3. Sheeting Purpose

In the baking industry bread dough is sheeted usually for three purposes: Shaping, Lamination and Structural Development.

1.3.1. Shaping

The primary function of sheeting is to shape the bread dough. That is, the thickness of the dough as it exits the sheeter is the important outcome. As well as a deformation in terms of height, sheeting also results in a length and width change. Figure 1.3 shows an example of this type of deformation.

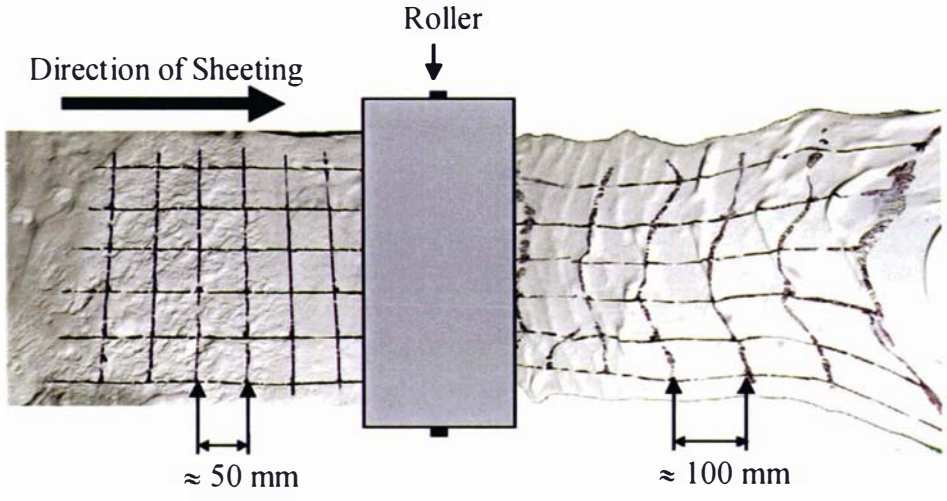

Figure 1.3 Width and Length Deformation due to Sheeting (Looking down upon the sheeter). This photograph indicates how the sheet surface can be damaged and the shape of the sheet deformed by the sheeting process. It is important to understand the conditions under which undesirable deformation occurs.

1.3.2. Laminating

Sheeting is also a part of the process by which layers of either different doughs or dough and fat are laminated together, for example in the manufacture of puff pastries. In this case an important outcome is the conditions under which re-circulation occurs. Re-circulation can occur in the region prior to the dough entering sheeter (See Figure 1.4)

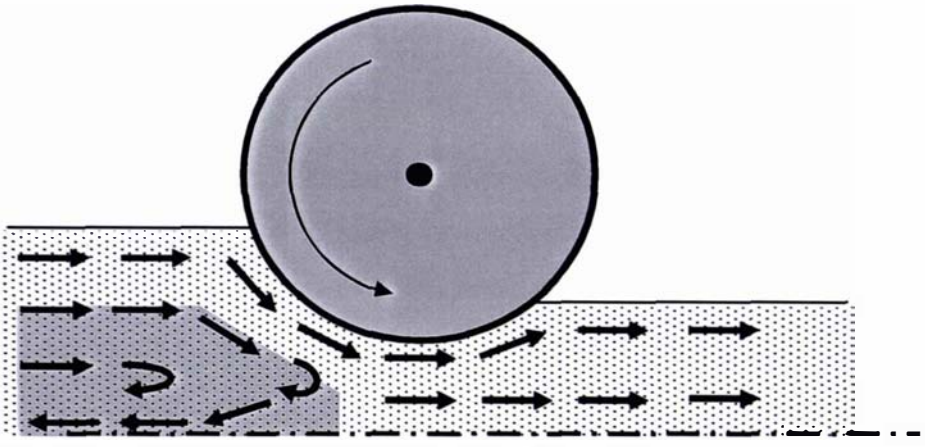

Figure 1.4 Stylised re-circulation region indicated by the shaded area.

Morgenstern & Ross (1998) found, experimentally, that a reduction ratio (ratio of inlet thickness to the gap between the rollers) of less than 4 resulted in no re-circulation when dough is sheeted, while for reduction ratios of more than 8 re-circulation was always observed. When laminating a dough re-circulation must be avoided, as it destroys the layers which the process is designed to form.

1.3.3. Structural Development

Sheeting can be used as an alternative, energetically efficient, method of dough development (Kilborn & Tipples, 1974). Dough development, which is discussed in more detail in section 1.5.3, is the process by which the dough gluten proteins are hydrated and form a dough gluten network, which gives bread dough many of its properties. In short-time bread production processes such as the Chorleywood Bread Process and Mechanical Dough Development Process (MDD) (French and Fish, 1981), dough is developed during the mixing process, which is costly in terms of energy use. Dough can also be developed during a fermentation processing step. In order to compare the sheeting process to the mixing process an understanding of the energy expended in sheeting is required.

Bread dough contains air bubbles, which can be significant in processing steps downstream of the sheeting operation, for example baking. Sheeting can be used to affect the structure and distribution of the bubbles in a bread dough.

1.4. Model Purpose and Requirements

The purpose of this study was to develop a model which can be used to gain an understanding of the sheeting process. In particular, how changes in the sheeter's geometry and the process material's properties affect the sheeting system's responses were to be examined. Such a model is important for two reasons: first, it allows a plant operator to predict and compensate for changes that might occur during processing; second, it allows a designer to specify both the sheeter geometry and the dough properties that are required to give a particular response.

There are two approaches, empirical and fundamental, to the development of a model of a system. An empirical model is one where historical data, which describes a system's responses to particular sets of conditions, is used to make a prediction about the system's behaviour at an arbitrary set of conditions. Curve-fitting and regression analysis are common tools for developing these types of models. An empirical model can be thought of as a method of summarising experimental data, the accuracy of the summary being dependent on the relative numbers of model parameters and historical data points. An empirical model makes no claim to describe what is actually occurring in the system under study; it is merely a calculating device for predicting the behaviour of the system. A disadvantage is that empirical models are not generally applicable. For example, if the conditions of interest differ from the conditions with which the model was formulated, then the model results may not be valid.

In this study an attempt was made to model the dough sheeting process using a fundamental model. Some authors (Raghavan et al., 1996) have modelled the process using empirical models. These models are of limited usefulness in understanding the system.

A fundamental model is one where the system is described through the use of fundamental relationships, which have been independently validated to be true for various cases. In this case, historical data, of the performance of the particular system under study, is only used to validate or confirm the model predictions. The advantage of a fundamental model is that it aids in understanding the behaviour of a system—rather than merely predicting the behaviour of the system. A fundamental model claims

to describe what actually happens in the system, but may be computationally or mathematically difficult to apply to complex problems. Partly this is because in order to apply a fundamental model it is necessary to be able to identify and describe all relevant parts of the system according to a fundamental theory. This is sometimes difficult, particularly for poorly defined systems, like food systems.

A useful model of the dough sheeting process should model the responses that are important to the applications of dough sheeting. The exit height at which the sheet leaves the sheeter should be modelled. A model should also identify conditions under which re-circulation might occur, that is describe the velocity profile of the process material. A model should also be able to estimate the energy expended during sheeting. This is valuable in comparing various methods of dough development. It is also useful for a model to describe the forces acting on the rollers and other process equipment, as this information can be used to specify materials of construction of a sheeting system.

To successfully model the sheeting system both the process material (dough) and the sheeting geometry and conditions need to be investigated. Section 1.5, Dough Properties, summarises progress that has been made in describing bread dough. Section 1.6, Sheeter Geometry and Conditions, describes common assumptions made about the sheeting system and their validity. Finally Section 1.7 Modelling History, describes attempts that have been made to model bread dough sheeting.

1.5. Dough Properties

A model of dough sheeting obviously needs to take into account the properties of the bread dough. In particular the rheological properties - descriptions of how the dough deforms - are required. An important difficulty is that dough properties are affected by the deformation history of the dough; thus the previous processing steps are significant.

1.5.1. Composition

One of the most important factors influencing dough rheology and hence sheeting is dough composition. When describing dough compositions it is conventional to give compositions as weight percentages relative to the flour component. Thus a dough might consist of X kg of flour (10 kg, for example) and 50 % water (5 kg). Usually the

dough used for a sheeted bakery product has a water content of 50 % to 70 %. A typical wheat flour might consist of 76 % starch, 10 % protein, 12 % moisture, 1 % lipids and trace minerals (mostly phosphorus, potassium, selenium, magnesium and calcium), vitamins and acids (US Department of Agriculture, 2002). The exact properties are dependent upon the variety of wheat used, field conditions and to a certain extent the milling conditions. Small quantities of salt, yeast, sugar, fats, emulsifiers, and redox agents are also added. Wheat selection and additives are highly dependent upon the intended use of the dough.

1.5.2. Structure

When dough is mixed, in a high-speed mixer, a significant amount of air is entrained with it. Campbell et al. (1998) demonstrated that a porosity, the percentage of bulk dough volume that is air, of almost 10 % occurs during mixing, which has an effect on the bread produced. The amount of entrained air directly affects the compressibility of the dough. This is important during the sheeting operation. In general dough-sheeting models assume that the dough is incompressible. This is a legacy from models of the traditional polymer calendering process where it is reasonable to assume that air is not entrained, as the polymer is present as a melt, rather than a mixed bulk, prior to sheeting. Levine (1998) suggested that errors of up to 20 % occur when modelling the dough sheeting process without taking compressibility into account, and attempted to account for this by introducing empirical factors into a model which used a power law model to describe the bread dough (see Section 1.5.5.5).

Dough also consists of two phases. Larsson & Eliasson (1996) showed that dough can be separated (using ultra-centrifugation) into a protein phase, the "gluten network", and a liquid phase, consisting of dispersed starch and solubles. At low moisture content only the gluten network exists. This suggests that water is first "consumed" through hydration of the gluten network. If excess water is present, another phase containing soluble starches forms. The gluten network provides the viscoelastic properties of the dough (Larsson & Eliasson, 1996). The model by Phan Thein et al. (1997) is one of the few dough rheological models that explicitly account for the presence of two aqueous phases.

1.5.3. Dough Development

Dough consists of a gluten network that entraps a starch suspension. To obtain the hydrated gluten network, water is obviously required, but if development is to occur in a reasonable time mechanical work is also required (Eliasson & Larsson, 1993). This can be achieved by high-speed / short-time mixing (Bloksma, 1990). It is unclear exactly why mechanical work is required. Perhaps a shearing action is needed to properly entangle the gluten molecules. Kilborn & Tipples (1974) demonstrated that repeated sheeting could achieve dough development with less energy input required, thereby decreasing manufacturing cost. Morgenstern et al. (1999) confirmed that less than 25% of the energy required for traditional mixing was required for development by multi-pass sheeting. As development increases, the properties and hence the quality of the bread finally produced changes.

Dough development also means that the degree of changes in the properties of the dough during a processing step depends upon the previous processing steps to which it has been exposed. For example, Kilborn & Preston (1982) showed that there is a significant difference, in terms of power requirement, between the first pass through a sheeter and subsequent passes. This phenomenon indicates that the properties of the dough have been changed by the sheeting operation. Completely specifying the properties of a partially processed dough is therefore very difficult. This will affect the accuracy of any model that depends upon property measurements.

Dough that is prepared at – 8 °C using ice instead of water and then allowed to thaw at room temperature, becomes hydrated without mechanical work. This "undeveloped" dough shows less resistance to deformation than dough prepared normally (Campos et al., 1997)

1.5.4. Measurement of Dough Properties

As discussed above, dough, like most food products, is a very complex substance. The properties of the dough are influenced by the variety of wheat used, the conditions under which the wheat is grown, the mixture composition (moisture content, salt, fat, etc) and the deformation history of the dough (Castell-Perez & Steffe, 1992). As the precise effect these parameters have upon the dough are poorly understood, it is very

difficult to compare data from different sources, particularly as many of these parameters are not reported in the literature. This effectively means that data from the literature is only useful for orders-of-magnitude studies, and any relationship developed using a single set of data may not be applicable to other data sets.

Some experimenters have simplified measurements of dough properties by using a "model dough" that consists of only flour and water (Phan-Thien et al., 1997). Others (Wang & Kokini 1995a) use "chemical dough" formed from gluten powder and water. Barney et al. (1965) made a flour and water dough and then removed the starch through a series of washes and freeze drying operations.

Obviously, these doughs are different to (and have different properties to) "real" dough used in a baking application. However, a model dough does allow the study of the responses that a particular application (sheeting, for example) has to the idealised properties exhibited by the model dough. The idealised responses can then be used as a guide to determining the responses of the application to the more complicated properties of a real dough.

Another problem with experimental techniques that are available is the distinction between fundamental and empirical instruments. Many instrumental techniques for dough date back to the 1920s. These early techniques include instruments like the Farinograph, the Chopin Alveograph and the Extensigraph (Walker & Hazelton, 1996). These instruments perform arbitrary, proprietary measurements that can be used to develop empirical models. Originally these instruments were designed to simulate the behaviour of specific processing equipment. The problem is that the complex geometry of the instruments and the combination of actions occurring within them make it difficult or impossible to calculate fundamental properties from the instrumental readings (Anderssen et al., 1997). This means that comparison of the measurements from different instruments is unwise and it is difficult to gain a general understanding of the dough rheology. Furthermore these instruments sometimes test dough under conditions different from those found in baking operations (Menjivar, 1989). As dough properties are very dependent upon the measurement conditions, extrapolation from testing to practical conditions is questionable.

The alternative is to use fundamental rheological instruments (Hibberd & Parker, 1975; Zheng, 1998). Some of these that have been used for dough are: slit rheometer (Bhattacharya,1993; Dus & Kokini, 1990); extensometer (Morgenstern et al., 1996); capillary rheometer (Sharma et al., 1993; Dus & Kokini, 1990); rotational rheometer (Launay & Bure, 1973; Wang & Kokini, 1995a). The results gained from some of these instruments are discussed in Section 1.5.5.

1.5.5. Constitutive Equations

In rheology, a constitutive equation is used to describe how a material behaves when it is deformed. Many authors have attempted to describe dough using a constitutive equation.

1.5.5.1. General Constitutive Equation

The general form of the constitutive equation is:

$$\sigma_{ij} = p\delta_{ij} + \tau_{ij} \tag{1.1}$$

where p is the pressure [Pa], σ_{ij} is the total stress tensor [Pa] and τ_{ij} is the deviatoric or shear stress tensor [Pa]. Some authors use a different sign convention with $-p$ instead of p. δ_{ij} is defined as:

$$\delta_{ij} = \begin{bmatrix} 1 & 0 & 0 \\ 0 & 1 & 0 \\ 0 & 0 & 1 \end{bmatrix} \tag{1.2}$$

Therefore equation (1.1) states that when we are referring to a normal stress, $i = j$ (= 1 for example), the total stress is given by: $\sigma_{11} = p + \tau_{11}$. For non-diagonal shear stresses ($i \neq j$) the stress tensor equals the shear stress tensor, $\sigma_{ij} = \tau_{ij}$.

The shear stress tensor is often written as a function of the rate-of-strain tensor, $\dot{\gamma}_{ij}$ (s^{-1}) which is given by (Ferry, 1980):

$$\dot{\gamma}_{ij} = \begin{bmatrix} 2\frac{\partial u}{\partial x} & \frac{\partial v}{\partial x} + \frac{\partial u}{\partial y} & \frac{\partial w}{\partial x} + \frac{\partial u}{\partial z} \\ \frac{\partial v}{\partial x} + \frac{\partial u}{\partial y} & 2\frac{\partial v}{\partial y} & \frac{\partial v}{\partial z} + \frac{\partial w}{\partial y} \\ \frac{\partial w}{\partial x} + \frac{\partial u}{\partial z} & \frac{\partial v}{\partial z} + \frac{\partial w}{\partial y} & 2\frac{\partial w}{\partial z} \end{bmatrix} \tag{1.3}$$

where: x, y and z are the coordinate directions and u, v and w are the velocity components in each direction, respectively.

1.5.5.2. Determining an Appropriate Constitutive Equation

Constitutive equations are proposed from either theoretical consideration of how the material deforms or by mathematical convenience. Typically the constitutive equation is then written in a form such that the "response" to a particular type of deformation (that which occurs in the rheometer) is easily studied. For example many rheological tests study the response to an oscillatory strain.

Such "response" based models are good for the analysis of rheological tests, where the type of deformation experienced by the sample is strictly controlled (that is, in cases where what the material is responding to is well defined); but constitutive equations based on a "response" may be unrealistic when applied to a "real" application where many ill-defined deformations may be experienced by the material.

Some authors (Keentok et al., 2002) have provided "responses" for the deformation of dough, which could be used to validate constitutive equations.

1.5.5.3. Newtonian Constitutive Equation

The Newtonian constitutive equation (for an incompressible fluid) is the simplest fluid model. It is:

$$\tau_{ij} = -\eta\dot{\gamma}_{ij} \qquad (1.4)$$

where η is the viscosity [Pa s].

It should be noted that the negative sign in equation 1.4 is part of the sign convention used in this thesis. This follows the sign conventions used in Bird et al. (1987), some authors use a different sign convention.

Bread dough has been described as a Newtonian material, but, due to the non-linearity of the rheological behaviour of dough, various values have been reported in the literature for η. Literature values of the apparent η usually range from 10^4 to 10^6 Pa s, although values as low as 3×10^2 Pa s have been reported (Bloksma, 1972).

η can be obtained using standard rheological instruments. An apparent viscosity can be also be obtained using traditional dough measuring instruments, for example a Brabender Farinograph (Bloksma, 1972).

1.5.5.4. Hookean Constitutive Equation

The Hookean constitutive equation is a simple model of a purely elastic solid:

$$\tau_{ij} = -G\gamma_{ij} \tag{1.5}$$

where G is the modulus of elasticity [Pa]. (Again the negative sign is due to the sign convention).

The Hookean constitutive equation has not been used to describe dough.

1.5.5.5. Power-Law Constitutive Equation

A common, simple modification to the Newtonian constitutive equation is to introduce a function for η, in equation 1.4:

$$\eta = K\dot{\gamma}_{ij}^{\,n-1} \tag{1.6}$$

where K, [Pa s^n], and n are the consistency index and the flow behaviour index, respectively.

This is the most widely used relationship in engineering rheology (Tanner, 1985) largely because it is simple and works adequately for many materials, including many polymers.

As dough properties vary with composition it is difficult to compare the power-law parameters of different authors. Several styles of instrument have been used to determine power-law constants, for example the capillary rheometer (Sharma et al., 1993) and the rotational rheometer (Launay & Bure, 1973). Some values that have been reported are listed in Table 1.1:

K [Pa s^n]	n	Author
3650	0.42	Levine (1998).
24000-46000	0.23-0.26	Morgenstern et al. (1996).
2395	0.35	Sharma, et al. (1993).
4450	0.35	Levine and Drew (1989).
2800-5300	0.32-0.37	Launay and Bure (1973).

Table 1.1 Power-law Constants, reported by different authors.

Water content is by far the component with the most influence upon rheological properties (Faubion & Hoseney, 1989). Raghavan et al. (1995) have developed power-law constitutive equations that include a dependence upon moisture, salt and fat content.

1.5.5.6. Carreau-Yasuda Constitutive Equation

Related to the power-law constitutive equation is the Carreau-Yasuda constitutive equation. It can be written as:

$$\frac{\eta - \eta_\infty}{\eta_0 - \eta_\infty} = \left[1 + (\lambda\dot{\gamma})^a\right]^{(n-1)/a} \tag{1.7}$$

where: η_0 is the zero shear rate viscosity [Pa s], η_∞ is the infinite shear rate [Pa s], n and a are constants and λ is a characteristic time, [s].

This constitutive equation divides the viscosity into three regions. At low shear rates, $\eta = \eta_0$. At high shear rates, $\eta = \eta_\infty$. Between the two extremes is a power-law region, whose location is controlled by a. The Carreau-Yasuda constitutive equation performs well for a wide variety of polymer solutions (Bird et al., 1987) but does not appear to have been used for dough.

1.5.5.7. Voigt-Kelvin Constitutive Equation

The Hookean and Newtonian equations can be simply combined (in parallel) to give the Voigt-Kelvin model of viscoelasticity:

$$\tau_{ij} = -G\gamma_{ij} - \eta\dot{\gamma}_{ij} \tag{1.8}$$

This equation has been used in dough rheology (Launay & Bure, 1973; Launay, 1990). To introduce non-linearity, a power-law relationship for η is used, as in Equation 1.6. A cone and plate viscometer can be used to determine these parameters. Typical values are: K = 5000 Pa s^n, n = 0.3 and G = 500 Pa (Launay, 1990). Launay, 1990 gives the power-law parameters a dependency upon moisture content, temperature etc, but the value of G is given as constant for a flour type.

1.5.5.8. Maxwell Constitutive Equation

Another simple viscoelastic equation is the Maxwell constitutive equation, which can be written as:

$$\tau_{ij} + \lambda_1\dot{\tau}_{ij} = -\eta\dot{\gamma}_{ij} \tag{1.9}$$

where λ_1 is the first Maxwell time constant [s]. The Maxwell constitutive equation can be thought of as a series combination of the Hookean and Newtonian constitutive equations (c.f. Voigt-Kelvin constitutive equation).

The Maxwell equation has been applied to dough (Bagley et al., 1988; Bagley et al., 1990). Typical parameters observed were η = 38000 Pa s, λ_1 = 15 s. The equation did not perform well when applied over a large range of strains (Bagley et al., 1988). The Maxwell constitutive equation was also found to be inadequate for modelling the viscoelasticity of other materials (for example, polymers), which led to the introduction of more complex constitutive equations (Bird et al, 1987).

1.5.5.9. Jeffrey's Constitutive Equation

The Maxwell equation can be refined by adding additional linear relationships between τ_{ij} and $\dot{\gamma}_{ij}$ (Bird et al, 1987). Once such refinement is the Jeffrey's model, which can be written as:

$$\tau_{ij} + \lambda_1 \dot{\tau}_{ij} = -\eta\left(\dot{\gamma}_{ij} + \lambda_2 \ddot{\gamma}_{ij}\right) \tag{1.10}$$

where (in this case) λ_1 is the "relaxation time" [s] and λ_2 is the "retardation time" [s].

The Jeffrey's equation does not appear to have been used to describe bread dough.

1.5.5.10. Generalised Maxwell Constitutive Equation

Another method of extending the Maxwell model is The Generalised Maxwell Model. It is a linear superposition of Maxwell models:

$$\tau_{ij} = \sum_{k=1}^{\infty} \tau_{k,ij} \tag{1.11}$$

$$\tau_{k,ij} + \lambda_k \dot{\tau}_{k,ij} = -\eta_k \dot{\gamma}_{ij} \tag{1.12}$$

where λ_k is the k^{th} Maxwell time constant [s] and η_k is the k^{th} Maxwell viscosity [Pa s].

Using measurements of steady shear and oscillatory shear (measured with capillary and parallel plate viscometers, respectively), Wang & Kokini (1995a) were able to apply a variant on the generalised Maxwell equation to dough. They modified the generalised Maxwell equation to include a dampening function. The values of the generalised Maxwell parameters are given in Table 1.2.

k	1	2	3	4	5	6	7	8	9	10	11	12	>12
λ (s)	10^{7}	10^{6}	10^{5}	10^{4}	10^{3}	10^{2}	10^{1}	10^{0}	10^{-1}	10^{-2}	10^{-3}	10^{-4}	0
η_n (Pa s)	5.5×10^{5}	5.55×10^{5}	1.75×10^{6}	1.5×10^{6}	3.33×10^{5}	4.49×10^{4}	4.98×10^{3}	9.39×10^{2}	2.82×10^{2}	3×10^{2}	1×10^{1}	1×10^{1}	0

Table 1.2 Generalised Maxwell Parameters.

The dampening function that was added to equation 1.11 was:

$$\tau_{ij} = \left[a\exp\left(b\gamma_{ij}\right) + c\exp\left(d\gamma_{ij}\right)\right]\sum_{k=1}^{\infty}\tau_{k,ij} \qquad (1.13)$$

where a, b, c and d are constants with values of: 0.39, -0.80362, 0.61 and -0.009 respectively.

1.5.5.11. Criminale-Ericksen-Filbey (CEF) Constitutive Equation

An important equation in the study of polymers is the Criminale-Ericksen-Filbey (CEF) constitutive equation. It has been successfully used to model the behaviour of viscoelastic polymers in conditions close to steady state (Bird et al., 1987). The CEF equation has not been used to model bread dough, but it has been used to model the calendering of polymers (Mitsoulis, et al., 1985). The CEF constitutive equation is discussed in more detail in Section 6.2.

1.5.5.12. Complex Constitutive Equation

Other constitutive equations have been proposed for dough, some of which are given below. Despite their realism, these constitutive equations are mathematically too complex to be easily used for modelling applications.

1.5.5.12.1. Bird-Carreau Constitutive Equation

Dus & Kokini (1990) and Wang & Kokini (1995b) attempted to use the Bird-Carreau constitutive equation to model dough rheological properties. The Bird-Carreau equation is semi-empirical, with 5 empirically determined constants. Dus & Kokini (1990) used a combination of data from slit and capillary rheometers to determine the parameters.

1.5.5.12.2. Phan-Thien et al. Constitutive Equation

Phan-Thien et al. (1997) proposed a complicated constitutive equation for dough, based on the assumption that dough consisted of a permanent, elastic, network of polymers (the gluten network) and a suspension of particles and loose chains (representing starch

and other components). Each component (elastic network and fluid suspension) makes an independent contribution to the constitutive equation. The fluid suspension component is similar to the generalised Maxwell constitutive equation. Phan-Thien et al. found parameter values using a rotational viscometer.

1.5.5.12.3. Morgan et al. Constitutive Equation

Morgan et al. (1989) developed a complex model, of protein (soy) doughs, intended to be used for extrusion modelling. Their model began with a "power law" style relationship relating viscosity to shear rate, to which corrections for temperature, moisture, temperature history and shear history, were added. Mackey & Ofoli (1990) modified this constitutive equation for use with maize dough. The model provides a value for η. This particular model is not necessarily correct for bread dough, but it does demonstrate an empirical approach that may be taken in the development of a constitutive equation.

1.6. Sheeter Geometry and Conditions

Defining the system under study is an important element of modelling. Figure 1.5 demonstrates the important features of the sheeter geometry:

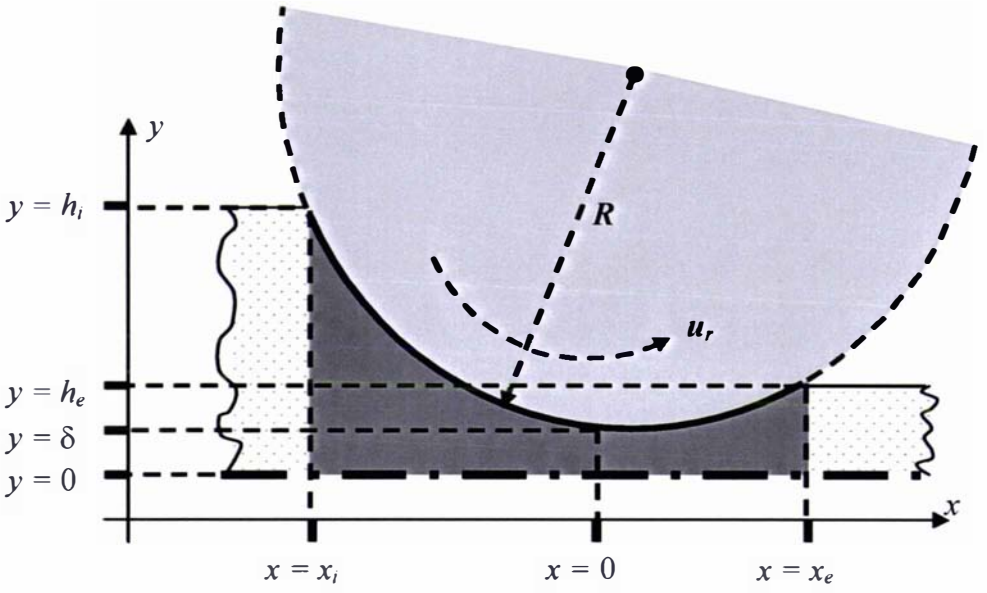

Figure 1.5 Sheeter Geometry (Not to Scale). Where:

x	horizontal coordinate [m].	y	vertical coordinate [m].
R	roller diameter [m].	δ	height* between the rollers [m].
h_i	inlet height* of dough [m].	x_i	inlet distance of dough [m].
h_e	exit height* of dough [m].	x_e	exit distance of dough [m].

u_r tangential, surface speed of the roller [m s^{-1}].

*** in this figure "height" is half the "thickness" defined in Figure 1.1 (c).**

1.6.1. Two Dimensional

The models presented in this thesis assume that the system is two dimensional, that nothing significant happens in the width direction (defined in Figure 1.1 (c)). However, when sheeting pellets, as is done in the production of some cereals, dramatic changes occur in the width direction (Levine & Levine, 1997). Some industrial dough sheeters produce sheets less than 0.5 m wide. For such a scale of operation effects at the edges may become significant, meaning a 2-D model is insufficient. Chong (1968) suggested that for PVC sheeting a 3-D model would be required to accurately model the nerve-like patterns that have been seen on the surface of PVC sheets. Levine et al. (2002) describe a model which successfully describes the width (z) of a sheet (for a power law fluid). When the initial width of the sheet (W_0) is much greater than δ ($W_0 > 80\delta$), then width effects were not significant. For example, if $\delta = 5$ mm then width effects are not significant for sheets greater than 400 mm wide.

1.6.2. Limited Region

Only the region shaded ■ in Figure 1.5 is considered in the models presented here. This is the region defined by:

$$x_i \le x \le x_e \tag{1.14}$$

$$0 \le y \le h = R + \delta - \sqrt{R^2 - x^2} \tag{1.15}$$

1.6.3. Plane of Symmetry

Implicit in the limited region of applicability is the assumption that a plane of symmetry exists in the sheeter, as shown in Figure 1.5. This implies that gravitational effects are insignificant in comparison with others and there are no other significant, external forces acting upon the system, for example the system is not in motion on an accelerating railroad carriage. This assumption can be simply validated.

During experimentation (See Chapter 2) a force per width of approximately 5000 N m^{-1} was observed on the dough. Dough travelled through the sheeter at a rate of about 0.1 m s^{-1} and the bread dough was in the sheeter for approximately 1 s. Therefore the pressure due to sheeting ($\Delta P_{sheeting}$, Pa) can be estimated:

$$\Delta P_{sheeting} = \frac{F}{Wtu_r} \approx 50\,kPa \tag{1.16}$$

where, F = downwards force [N], t = time under sheeter [s], W = width of sheet [m] and u_r = speed of dough [m s^{-1}].

By comparison the pressure due to gravity ($\Delta P_{gravity}$, Pa) on the bread dough (given that dough density, ρ, is approximately 1200 kg m^{-3}, and δ is of order 0.005 m) is:

$$\Delta P_{gravity} = \rho \delta g \approx 0.06\, kPa \qquad (1.17)$$

Therefore, as $\Delta P_{gravity} << \Delta P_{sheeting}$, the gravitational forces are insignificant in the problem.

1.6.4. Isothermal

It is assumed that no heat generation or transfer is involved in the sheeting process. Any changes in temperature in the dough occur so slowly that their time scales are insignificant compared with the motion of the material. The problem is therefore isothermal.

This assumption can be validated by an examination of the energy input (E) into the dough during sheeting. Morgenstern et al. (1999) reported that for a pass through a laboratory scale sheeter, a maximum (assuming no energy loss due to inefficient motors or friction) of 0.56 kJ kg^{-1} was transferred to the dough. The heat capacity of bread dough (C_p) is approximately 2.7 kJ kg^{-1} K^{-1} (Rahman, 1995). If all the transferred energy was used to heat the dough, and the rollers, the room and the dough are initially at the same temperature, then the adiabatic temperature rise in the dough can be estimated as:

$$\Delta T = \frac{E}{C_p} \approx 0.2\, K \qquad (1.18)$$

This value is an extreme maximum, but it is clear that only a small, irrelevant rise in temperature should be observed. This is significantly different from polymer calendering where temperature rises of 100 K, or higher, occur (Mitsoulis et al., 1985).

1.6.5. Steady State and Significant Times

It is assumed that the system reaches a steady state. Relative to the time scale of the entire sheeting operation the time to reach steady state is very small. In this context steady state means that entrance and exit effects due to the finite length of the sheet can be ignored, that is the model assumes that the sheet is continuous or at least very large.

It is also often assumed that the inertial terms in the momentum balance are insignificant. This can be justified using the Reynolds number (Re), which is the ratio of inertial forces to viscous forces. Typical values for sheeting:

$$\mathrm{Re} = \frac{\rho u_r \delta}{\eta} \approx 6 \times 10^{-5} << 1 \qquad (1.19)$$

where: Re = Reynolds number, $\rho \approx 1200$ kg m^{-3}, $u_r \approx 0.1$ m s^{-1}, $\delta \approx 0.005$ m, $\eta \approx 10000$ Pa s.

As the Reynolds number is much lower than 1, inertia effects are insignificant if dough is considered a Newtonian fluid. Of course dough is not a Newtonian fluid but a viscoelastic material.

Another dimensionless number, the Deborah number (De), is useful in characterising viscoelastic flows. The Deborah number is interpreted as the ratio of elastic character to viscous character of the material: as De $\rightarrow \infty$ the material will behave more like an elastic solid; as De $\rightarrow 0$ the material behaves like a viscous fluid (Bird et al., 1987).

$$De = \frac{\lambda}{t} \qquad (1.20)$$

where: λ is a characteristic time of the material [s] and is usually the largest time constant associated with the material; t is the characteristic time of the process [s], perhaps, the length of time the material is under the sheeter, in this case.

In the case of dough, λ is difficult to define. Using the data of Bagley et al. (1988) a value of 15 s is suggested for λ, which gives a De of 15 ($t \approx 1$ s is a reasonable estimate of the characteristic time of the process). As De is greater than 1, it appears that elastic forces will dominate over viscous. However, as De is only a single order of magnitude greater than 1, viscous forces will still be important.

1.6.6. Boundary Conditions

In order to properly define the system under consideration the boundaries need to be described.

1.6.6.1. No Slip at the Roller Surface

The no slip boundary condition means that at the roller surface, $y = h$, the dough velocity is equal to the roller surface linear velocity, u_r.

$$at\ y = h,\quad u = |u_r|\frac{\sqrt{R^2 - x^2}}{R} \tag{1.21}$$

$$at\ y = h,\quad v = |u_r|\frac{x}{R} \tag{1.22}$$

1.6.6.2. Line of Symmetry

As mentioned earlier there is a line of symmetry at $y = 0$. This means:

$$at\ y = 0,\quad v = 0 \tag{1.23}$$

$$at\ y = 0,\quad \frac{\partial u}{\partial y} = 0 \tag{1.24}$$

1.6.6.3. Inlet Condition

At the point of inlet (x_i,h_i), there is a free surface, at which the total upward stress is equal to zero:

$$at\ x = x_i,\ y = h_i,\quad \sigma_{yy} = -p + \tau_{yy} = 0 \tag{1.25}$$

1.6.6.4. Outlet Condition

At the point of exit (x_e,h_e), there is also a free surface, at which the total upward stress is equal to zero.

$$at\ x = x_e,\ y = h_e,\quad \sigma_{yy} = -p + \tau_{yy} = 0 \tag{1.26}$$

1.6.6.5. Conservation of Mass

At any value of x the integral of the horizontal velocity component (u) by y, from $y = 0$ to $y = h$, is equal to a constant. Assuming that the exit velocity profile is flat, and obeying the outlet boundary condition, then the constant is equal to $u_e h_e$ (this also assumes that the dough is incompressible).

$$\forall x,\quad u_e h_e = \int_0^h u\,dy \tag{1.27}$$

1.7. Modelling History

Polymer calendering was first rigorously modelled by Gaskell (1950). Gaskell used a

simple fluid dynamic model of polymer calendering, which included the lubrication approximation (assuming that only one direction, x, is significant). The polymer was described using both a Newtonian constitutive equation and a Bingham constitutive equation. Middleman (1977) and others have revised and extended this model to power law fluids.

Sheet metal rolling has been modelled using descriptions of the friction coefficient between process material and roller surface (Lange, 1985).

Levine & Drew (1989) applied the models of Middleman to dough sheeting. A major flaw of these models is that they do not accurately predict the thickness of the dough as it leaves the sheeting system. Attempts were made to explain the discrepancy by including corrections arising from the compressibility of dough, but an unrealistic compressibility is required, in the model, to produce realistic sheeting outcomes (Levine, 1998).

It has been proposed that a model that describes the bread dough using a viscoelastic constitutive equation may produce realistic sheeting outcomes (Morgenstern, et al., 2000). Finite element techniques have been used in the past to solve models of polymer calendering (Mitsoulis, et al., 1985; Kiparissides & Vlachopouplos, 1976). These models had difficulties with finding solutions for very viscoelastic materials. Finite element models are also, often, too computationally complex to solve in real time, for example as modifications are made to a plant during operation.

1.8. Summary of Literature

Dough sheeting is an operation used in the manufacture of many baked products. The main purposes of the operation are: shaping, laminating and/or dough development. A fundamental model of the process could help both the designer and operator to determine the response of the sheeting system to changes in sheeter geometry and also to changes in process material.

A description of the dough properties is required for the model. This is difficult because bread dough is viscoelastic and its properties are highly dependent upon

composition, particularly water content, and processing history. Many constitutive equations (which describe rheological properties) have been proposed for bread dough. Those that are accurate are mathematically difficult to apply to complex geometries.

When modelling the system, it can be assumed that the sheeting process is two-dimensional, symmetrical, at steady state and isothermal. Assumptions can also be made about the boundaries of the sheeting system, for example no slip at the sheeter roller surface. Those models that have been proposed are not accurate for dough sheeting. Possibly this is because they ignore viscoelasticity. Those models which do include viscoelasticity are computationally complex and their solutions may not be stable for highly viscoelastic materials.

2. Experimental

2.1. Pilot Plant Sheeter

To validate any model of dough sheeting a set of experimental data needs to be gathered. In this project experimental data were gathered using a pilot plant-scale sheeter located at Crop and Food Research Limited, Lincoln. The sheeter was manufactured, for the New Zealand Institute of Crop and Food Research Limited, by EFl Engineering, Christchurch NZ. Figure 2.1 is a photograph of the sheeter.

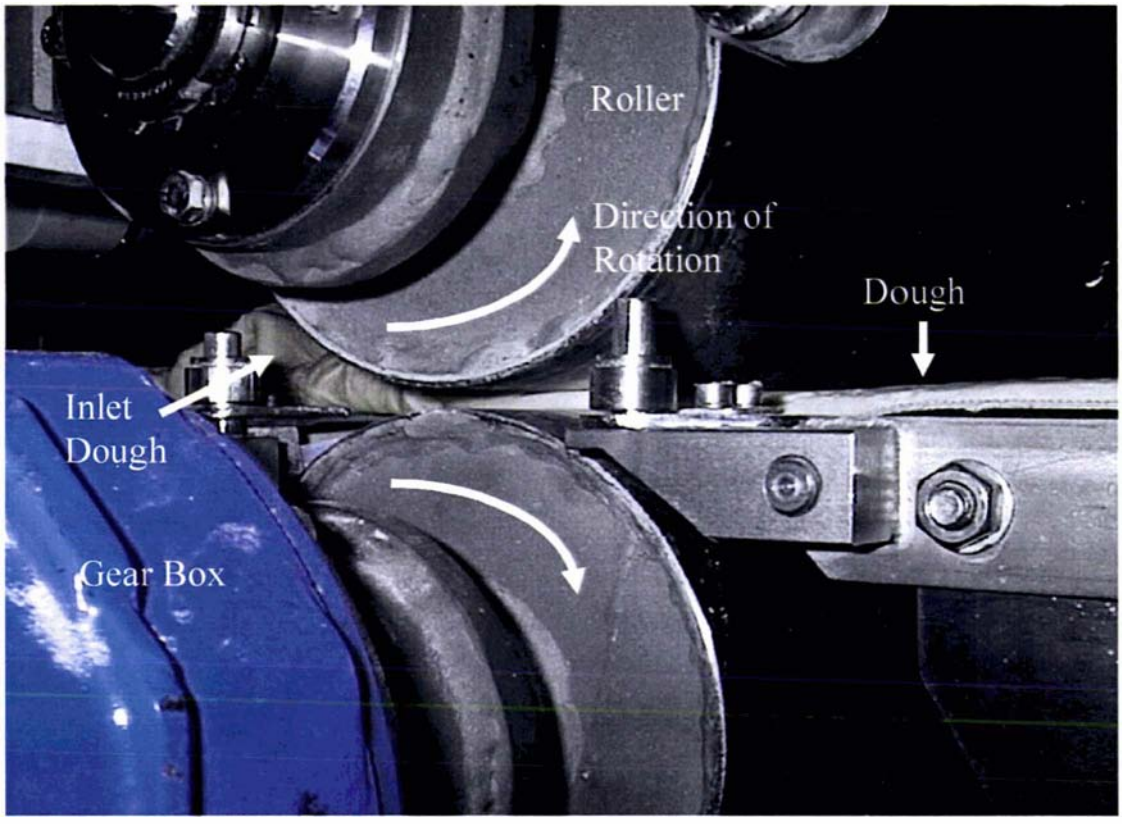

Figure 2.1 Pilot Plant Sheeter. The rollers have a radius of 135 mm. The dough is travelling from the left to the right in this picture.

2.2. Sheeter Layout

The major components of the sheeter were: i) rollers, ii) inlet and outlet conveyor belts, iii) motors, iv) torque meter, v) downwards force meter, vi) exit height meter, vii) roller

nip gap meter and viii) the data collection computer. These components were laid out as illustrated in Figure 2.2.

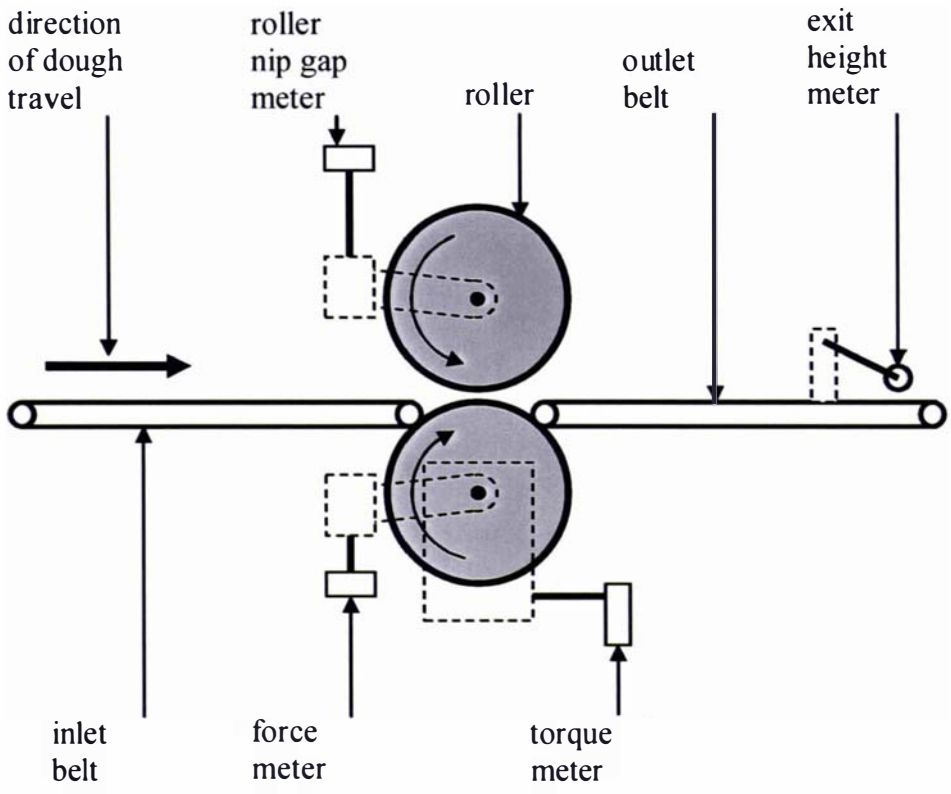

Figure 2.2 Sheeter Layout (Not to Scale), indicating relative positioning of components.

2.3. Component Details

2.3.1. Rollers

Three different rollers, with radii of 0.135 m, 0.075 m and 0.025 m, were available for the sheeter (Figure 2.3). The rollers were made of stainless steel (304 SS) and machined by the sheeter manufacturer to a surface equivalent to Brushed Finish #4. A computer controller controlled the set the roller speed and it was found that, over a range of 2 to 22 rpm, the roller speed was accurate to 0.25 %.

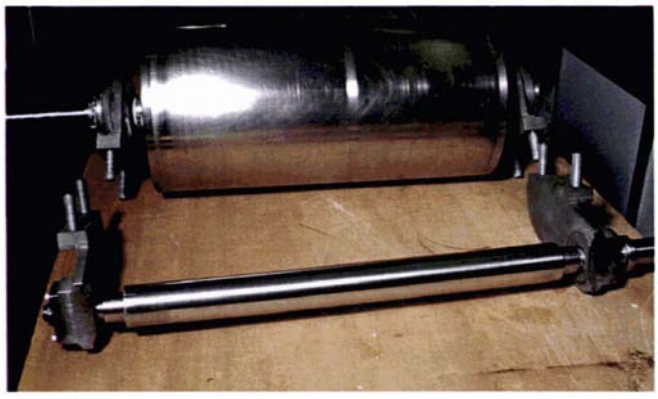

Figure 2.3 Rollers (135 mm and 25 mm radius).

2.3.2. Conveyor Belts

The inlet and outlet conveyor belt speeds were controlled by a computer and the belts were driven independently of the rollers by Crompton Greaves (Mumbai, India), 0.37 kW, 3 phase motors. The belt speeds were set as a fraction of the roller speed. It was found that the belt speeds were accurate to approximately 15%.

2.3.3. Motors

The rollers were driven by a Baldor, 7.5 kW, 3 phase, vector-drive motor (Baldor Electric Company, US).

2.3.4. Torque Load Cell

A Precision Transducers (Auckland, New Zealand), ASB 125 kg, load cell was used to measure the torque, T, on the gearbox (coloured blue on Figure 2.1) attached to the shaft that turned the lower roller. The details of the load cell calibration can be found in Appendix A. The average torque calibration error was $\pm$ 0.8 N m.

2.3.5. Downward Force Load Cell

The downward force load cell measures the total force exerted downwards (F) on the lower roller, as the dough is passed through the sheeter. A Precision Transducers, Model LPX, 1000 kg, load cell was used and was calibrated (Appendix A). Although in practice forces of 4000-5000 N are observed in sheeting, only weights equivalent to 1500 N were used in the calibrations. It was assumed that the load cell remained linear beyond this range and into the sheeting range. The average calibration error was $\pm$ 4 N.

2.3.6. Exit Height Meter

The thickness of the sheet, as it left the sheeter, was measured with a wheel attached to a rotary encoder. When the dough passed under the wheel the angle, α, was measured by the rotary encoder and a digital output (proportional to the exit height of the dough, h_e) was sent to the data collection computer. The wheel was mounted 810 mm from the nip gap. The average calibration error was $\pm$ 0.2 mm (Appendix A).

2.3.7. Roller Nip Gap Meter

The nip gap was measured with a modified set of digital callipers. This measurement was found to be accurate to 0.09%.

2.3.8. Inlet Height

The inlet height of the dough was measured and averaged over five points with a set of digital callipers.

2.3.9. Computer Controller

The computer controller logged: the time, sheeting conditions (roller speed, nip gap) and sheeting outcomes (force, torque and exit thickness). The computer logged data at a rate proportional to the speed of the roller. Approximately 50 data points are gathered per revolution of the roller.

The time logged by an earlier version of the program was found to be highly inaccurate due to time "lost" while polling digital interfaces. It was found that the program used, with improved digital interfaces, was accurate to about 1% over a period of a minute at several speeds.

2.4. Data Analysis

The data collected during sheeting was analysed using Microsoft Excel 9.0.381 (2000). A graph was produced for each run displaying the torque, force and exit thickness as a function of time. The data on this graph extended from before the dough reached the rollers, until after the dough has left the rollers. A selection was made of the data to give a data set "while dough was sheeted". As the selected data covered the time while

a large quantity of dough was sheeted, the data could be averaged to give estimates of steady state values. Figure 2.4 shows the output for an example sheeting run.

The conditions and outcomes for the example run were:

Sheeting Conditions			
Roller Radius:	135 mm	Nip Gap:	3.6 mm
Dough Type:	*Epic*: short mix*	Inlet Height:	74 mm
Sheeting Outcomes			
Maximum Torque:	157 N m	Maximum Force:	3087 N
Average Torque:	95 N m	Average Force:	2225 N
Average Exit Height:	16.34 mm		

Table 2.1 Summary of Sheeter Output Example (* see Section 2.6.3.2)

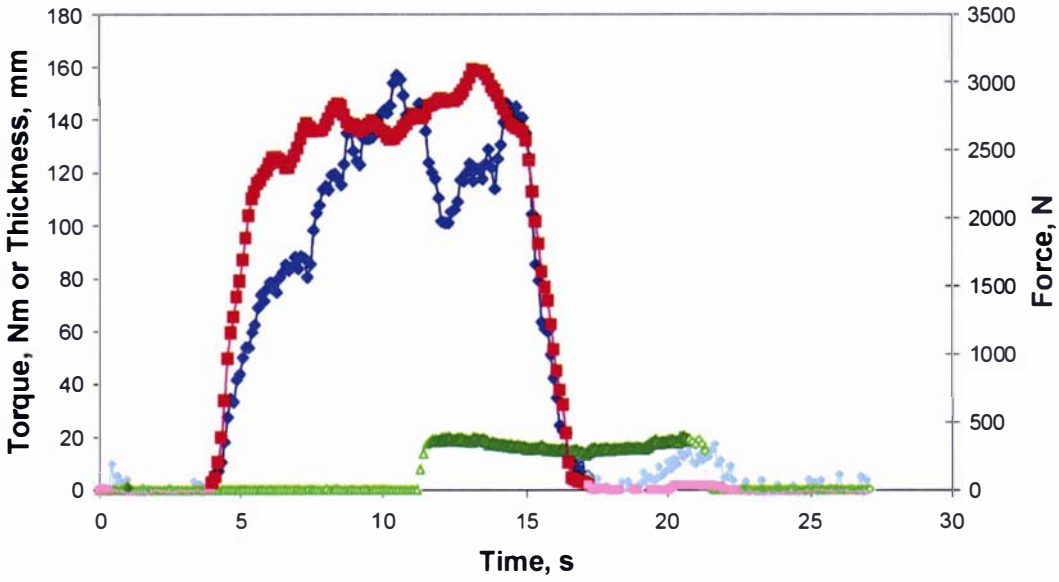

Figure 2.4 Example of Sheeter Output. The dark-hued points are the points selected for analysis. Red squares are the downward force, N; blue diamonds are the torque, N m; and green triangles are the exit thickness, mm.

2.5. Significant Geometric Factors

2.5.1. Aim

A factorial experiment was conducted to determine which of the sheeting system's geometric properties had a significant effect on the measured sheeting outcomes (force, torque and exit height). The conclusions from this were used to guide a more complete investigation of the significant factors.

2.5.2. Method

The seven factors examined were: nip gap, roller diameter, reduction ratio, dough type, roller speed, and inlet and outlet conveyor belt speeds. The reduction ratio is the ratio of the inlet thickness of the dough to the nip gap. The levels used for each are given in Table 2.2. The experiment used a fractional factorial 2^{7-3} design (Montgomery, 1997). There were sixteen experimental runs, each duplicated, in a semi-random order (the roller diameter factor was not randomised due to the time required to switch between rollers). Table 2.3, indicates the levels of the factors for each experimental run.

Factor		-	+
Nip Gap	[mm]	3	6
Roller Diameter	[mm]	150	270
Reduction Ratio	-	5	10
Dough Type	-	I	II
Roller Speed	[rpm]	6	12
Inlet Conveyor Speed	*	50%	70%
Outlet Conveyor Speed	*	80%	100%

* as a % of the surface roller speed.

Table 2.2 Levels for Significance Experiment

Experiment	Order Performed	Nip Gap	Red. Ratio	Dough Type	Roll Diameter	Roll Speed	Inlet Speed	Outlet Speed
1	5	- 1	- 1	- 1	+ 1	- 1	- 1	- 1
2	1	+ 1	- 1	- 1	+ 1	+ 1	- 1	+ 1
3	6	- 1	+ 1	- 1	+ 1	+ 1	+ 1	- 1
4	2	+ 1	+ 1	- 1	+ 1	- 1	+ 1	+ 1
5	4	- 1	- 1	+ 1	+ 1	+ 1	+ 1	+ 1
6	7	+ 1	- 1	+ 1	+ 1	- 1	+ 1	- 1
7	3	- 1	+ 1	+ 1	+ 1	- 1	- 1	+ 1
8	8	+ 1	+ 1	+ 1	+ 1	+ 1	- 1	- 1
9	13	- 1	- 1	- 1	- 1	- 1	+ 1	+ 1
10	11	+ 1	- 1	- 1	- 1	+ 1	+ 1	- 1
11	14	- 1	+ 1	- 1	- 1	+ 1	- 1	+ 1
12	12	+ 1	+ 1	- 1	- 1	- 1	- 1	- 1
13	9	- 1	- 1	+ 1	- 1	+ 1	- 1	- 1
14	15	+ 1	- 1	+ 1	- 1	- 1	- 1	+ 1
15	10	- 1	+ 1	+ 1	- 1	- 1	+ 1	- 1
16	16	+ 1	+ 1	+ 1	- 1	+ 1	+ 1	+ 1

Table 2.3 Order of experimental runs for Significance Experiment

2.5.3. Dough Recipe

The two types of dough used, type I and type II, had very different properties. Type I was viscoelastic and was similar to a production dough, although for ease of use it contained neither yeast nor fat. Type II dough was less elastic and behaved more like the idealised doughs used in developing some models (Levine and Drew, 1989). The recipes for the doughs are shown in Table 2.4 .

Type I dough was mixed at a speed of 300 rpm in an ECS 35 mixer (manufactured by ECS Engineering, Christchurch, New Zealand) for 150 s. Type II dough was mixed for 90 s at speed 3 in a Hobart mixer (manufactured by the Hobart Manufacturing Co. Ltd). Both doughs were formed to a uniform thickness of 15 mm, by gently sheeting at a low reduction ratio, in a consistent manner before the sheeting experiments were begun. See Section 2.6.4 for details of the sheeting procedure (noting that in these preliminary experiments the complete mixed dough was sheeted, it was not divided into two batches).

Type I Dough		Type II Dough	
Epic Flour*	6.000 kg	*Epic* Flour	1.840 kg
Iced Water at ≈ 2 ^{0}C	3.120 kg	Hot Water at ≈ 92 ^{0}C	2.600 kg
Salt	0.108 kg	Salt	1.520 kg
		Oil	0.052 kg
		Cream of Tartar	0.040 kg

Table 2.4 Dough Recipes for Significance Experiment. * Manufactured by Champion Flour Mills, Christchurch, New Zealand.

2.5.4. Results

The averages of the duplicate responses in each experiment are presented in Table 2.5. Table 2.6 to Table 2.8 are summaries of the analyses of the response variables, in the form of regression equations, made up of the most significant factors. The regression equations take the form of:

$$\text{Response} = \beta_o + \sum_i [\beta_i][x_i] \qquad (2.1)$$

where β_0 is the average response, β_i is the coefficient for factor i, and x_i is a coded variable that is equal to −1 when the factor is at its low value and + 1 when at its high value.

A factor was considered "significant" if it accounted for 5% or more of the observed variation in the response.

Experiment	Torque [N m]	Force [N]	Exit Thickness [mm]
1	39.19	2805	7.40
2	34.51	2382	11.84
3	57.49	4018	9.67
4	61.80	3509	14.44
5	23.52	1802	5.31
6	17.74	775	7.98
7	20.15	1279	4.49
8	22.73	911	8.97
9	30.51	2649	6.16
10	25.50	2184	9.59
11	38.24	3466	7.26
12	16.56	1372	9.05
13	10.97	1089	4.78
14	7.33	483	6.10
15	6.74	652	3.22
16	4.62	241	6.31

Table 2.5 Responses for Significance Experiment

Exit Thickness

$$\text{Exit Thickness [mm]} = 7.66 + 1.62[x_{NipGap}] - 1.77[x_{DoughType}] + 1.10[x_{RollDiameter}] \quad (2.2)$$

Factor	Variation Accounted For
Nip Gap	34 %
Dough Type	40 %
Roll Diameter	16 %
	90 % ($R^2 = 0.89$)

Table 2.6 Exit Thickness Response Equation

Force on the Roller

$$\text{Force [N]} = 1851 - 369[x_{NipGap}] - 947[x_{DoughType}] + 334[x_{RollDiameter}] \quad (2.3)$$

Factor	Variation Accounted For
Nip Gap	10 %
Dough Type	68 %
Roll Diameter	8 %
	86 % ($R^2 = 0.87$)

Table 2.7 Force on the Roller Response Equation

Torque

$$\text{Torque [N m]} = 26.10 - 11.88[x_{DoughType}] + 8.54[x_{RollDiameter}] \quad (2.4)$$

Factor	Variation Accounted For
Dough Type	52 %
Roll Diameter	27 %
	79 % ($R^2 = 0.82$)

Table 2.8 Torque Response Equation

An alternative to looking at the response of the exit thickness is to look at the response of the deformation ratio. The deformation ratio is given by:

Deformation Ratio = Inlet Thickness / Exit Thickness (2.5)

If the deformation ratio is equal to 1, then the inlet and exit thicknesses of the dough are identical. This might occur for very elastic dough, which springs back into its original shape after passing between the rollers. At the other extreme, if the deformation ratio is equal to the reduction ratio, then the dough is inelastic and does not spring back after leaving the rollers. (Although in many models of the sheeting process this does not occur even for a completely inelastic Newtonian fluid. This is because of the way the exit condition is determined, see Section 1.6.6.4 or Middleman, 1977).

Deformation Ratio

$$\begin{aligned}\text{Deformation Ratio [mm]} &= 4.67 + 1.52[x_{ReductionRatio}] \\ &+ 1.20[x_{DoughType}] - 0.53[x_{RollDiameter}] \\ &- 0.63[x_{RollerSpeed}] + 0.58[x_{NipGap}][x_{RollerSpeed}]\end{aligned} \quad (2.6)$$

Factor	Variation Accounted For
Reduction Ratio	43 %
Dough Type	27 %
Roll Diameter	5 %
Roller Speed	7 %
Nip Gap . Roller Speed	6 %
	88 % ($R^2 = 0.87$)

Table 2.9 Deformation Ratio Response Equation

2.5.5. Discussion

For the response variables exit thickness, force on the roller and torque, the most influential parameter is the dough type. This means that the properties of the dough play a larger part in determining the behaviour of the material during sheeting than any

of the geometric factors. As expected the less elastic dough (type II), had a higher deformation ratio than the more elastic (type I) dough; the less elastic a dough the more it is deformed by the sheeting process. The type II dough also resulted in less force on the roller and less torque.

The roller diameter was also important for all responses, although not of equal importance for each. The results indicate that increasing roll diameter results in an increase of exit thickness, force, and torque. This suggests that large rollers are in some ways not as efficient as small rollers. However, it was noticed that with a small roller the dough was more likely to tear or have surface deformities. This type of response was not measured in these experiments, but is very important in a practical application of sheeting.

Increasing the nip gap decreased the downward force and, obviously, increased the exit thickness. The nip gap was not particularly important for the torque and deformation ratio responses.

The deformation ratio increased as the reduction ratio increased, as expected. The reduction ratio can be thought of as a measure of the target change in the sheet thickness. Similarly the deformation ratio represents the actual change in sheet thickness. The deformation ratio decreased as the roller speed increased. This is also expected as it is well known (Bird et al., 1987) that many materials exhibit a larger elastic recoil when rapidly deformed than when slowly deformed. In this case as the roller speed increased, the time during which the dough was held between the rollers decreased and therefore the more rapidly the dough was deformed.

This experiment also demonstrated that the two conveyor belt speeds, inlet and outlet, were not of significance. This means that the conveyor belts could be ignored in a sheeting model and in subsequent experiments.

2.5.6. Summary of Factorial Experiment

This factorial experiment was conducted to determine which of the studied factors were most important to the sheeting system responses exit thickness, roller force and torque.

It was found that the dough type and the two geometric parameters nip gap and roller diameter were the most important, accounting for up to 90% of the observed variability. The factors reduction ratio and roller speed were also important for the response deformation ratio, which is derived from the exit thickness.

A dough sheeting model and further experiments had, therefore, to include the factors: dough properties, roller diameter, nip gap, reduction ratio and roller speed. The belt speeds could be ignored for the responses studied.

2.6. Validation Data Experiment

2.6.1. Aim

A set of data encompassing a wide range of sheeting conditions was required to validate a model of the sheeting process.

2.6.2. Method

On the basis of the preliminary experiment described in Section 2.5 the factors considered in this experiment were:

Factor		Range of Values
Dough Recipe	-	*Epic*: short mix, *Epic*: long mix, and *Halo*.
Roller Radius	[mm]	135, 75, 25.
Nip Gap	[mm]	1.5, 2, 2.8, 3.6.
Roller Speed	[rpm]	6, 11, 19, 35.
Reduction Ratio	-	2, 3, 4, 5, 6, 7, 8, 9, 10.

Table 2.10 Factors for Validation Experiment

The experiments were conducted in as random a manner as possible over a period of several months. The major difficulty, preventing a fully random design, was the rollers; owing to the length of time required it was not practical to change the rollers between each experimental run. In order to minimise variability due to the long period of experimentation the flour used for all experiments was from the same batch, and the flour was keep in a dark refrigerated room. The flour was brought to room temperature before mixing.

2.6.3. Dough Recipe

Bread dough usually is composed of flour, water, salt, sugar, fats, yeast and other ingredients. Such a dough is difficult to characterise and is very complex rheologically, particularly as the fermentation of the yeast causes the properties to change over time. For the purposes of this study a bread dough made only from flour, water and salt was used. This much more stable material allowed the behaviour of the sheeter to be studied with a dough-like material.

2.6.3.1. Flour Composition

The flours used in these experiments were *Epic Bakers Flour* and *Halo Flour*, both milled by Champion Flour Mills. The flours were tested using a 125 g MDD dough developer (French and Fish, 1951) to determine the optimum amount of water to add (built by Crop and Food Research, Ltd). The optimum dough is one that will produce a large volume loaf with good texture and quality scores. The optimum dough is also dependent upon processing conditions; too much water and the dough will be too sticky to process well, too little water and the dough is too elastic. The optimum water addition for the *Epic* flour was 63%, and for the *Halo*: 54.5 %. Other flour properties are shown in Table 2.11:

Property	Epic Flour	Halo Flour
Moisture Content	13.9 %	14.3 %
Protein Content*	11.1 %	8.6 %
Optimum Water for development	63 %	54.5 %
Optimum Work Input	10.5 W h kg^{-1}	6.1 W h kg^{-1}

Table 2.11 Flour Properties (% given are as a mass of flour basis). * Protein Content was measured with a 14% moisture basis.

2.6.3.2. Epic Dough

Initially a dough with a composition (given in Table 2.12) based on the MDD measurements was mixed in an ECS35 dough. The percentages of the non-flour components are on a flour basis (Table 2.12).

Water at 5 °C	63 %
Salt	2 %

Table 2.12 Initial Epic Recipe

In Figure 2.5 is a picture of dough in the ECS 35 mixer. About 15 kg of dough was made in each batch.

Figure 2.5 Picture of ECS 35 mixer. Arrow indicates direction of blade motion.

The dough with a 63 % water content, determined to be optimum based upon the flour composition, was too unwieldy to sheet in the very wide range of conditions that were needed for these experiments. The dough was too sticky to sheet at high reduction ratios. Thus a drier recipe was used, the composition of which is shown in Table 2.13.

Water at 5 °C	54.5 %
Salt	2 %

Table 2.13 Second Epic Dough Recipe

The optimum sheeting time to reach dough development was then determined by examining the mixing curve of an over-developed dough, prepared in the ECS 35 mixer. On a mixing curve the "consistency" of the dough (which is proportional to the viscoisty) increases until a plateau is reached. On the plateau the dough is fully developed. If the dough is over-worked the consistency will reduce again. The point at which the mixing curve reaches the plateau is the optimum time for mixing and for this dough it was determined to be 135 s, with a work input of 16 W h kg^{-1}. This is different from the optimum work indicated by the 125 g MDD mixer, a result typical of the difficulties in scaling dough processing conditions. This dough is referred to later as *Epic*: short mix. Some experiments were also conducted with the same recipe mixed to 150 s, corresponding to a work input of 17 W h kg^{-1}, which is referred to as *Epic*: long mix. Together, the two dough types could be used to demonstrate the sensitivity of responses to a small change in processing conditions upstream of the sheeting operation. The final *Epic* recipe is shown in Table 2.14.

Flour	9 kg	
Water at 5 °C	4.905 kg	
Salt	0.180 kg	
	14.085 kg	mixed 135 s (16 W h kg^{-1}) or 150 s (17 W h kg^{-1}).

Table 2.14 Final Epic Dough Recipe

2.6.3.3. *Halo Dough*

The recipe used for the *Halo* dough is shown in Table 2.15.

Flour	9 kg	
Water at 5 °C	4.905 kg	
Salt	0.180 kg	
	14.085 kg	mixed 95 s (9.5 W h kg^{-1}).

Table 2.15 Halo Dough Recipe

It was found that the optimum mixing time was 95 s, with a work input of 9.5 W h kg^{-1}.

2.6.4. *Sheeting Procedure*

After the dough was mixed it was allowed to rest for about 10 minutes, before the dough mass was cut in half and sheeting began on the first half. Prior to each sheeting pass the weight, width and height of the dough were recorded. During a sheeting pass the torque, downward force, exit thickness and nip gap height were recorded by the computer as described above. The piece of dough was sheeted 10 times, which took about half an hour, before being discarded. The second half of the dough was then sheeted in the same manner. Between each sheeting run the dough was transferred to the inlet side of the sheeter by reversing the roller direction and conveyor belt, and increasing the nip gap to be much greater than the thickness of the sheet. Once on the inlet side of the sheeter the dough was cut and layered to (approximately) produce the desired inlet thickness for the next sheeting run.

The following graph (Figure 2.6) shows the response deformation ratio vs the time since the dough was mixed. For this example the reduction ratio was 9, the dough used was *Epic*: short mix, the nip gap was 2 mm, and the roller speed was 6 rpm. This demonstrates that the deformation ratio was constant at around 5. Therefore the time for which the dough had been standing had little effect on the measured response of the sheeting system. Thus it is valid to compare the first half of a dough mixture, sheeted from 10 min after sheeting, to the second half of the dough mixture, sheeted from approximately 40 min.

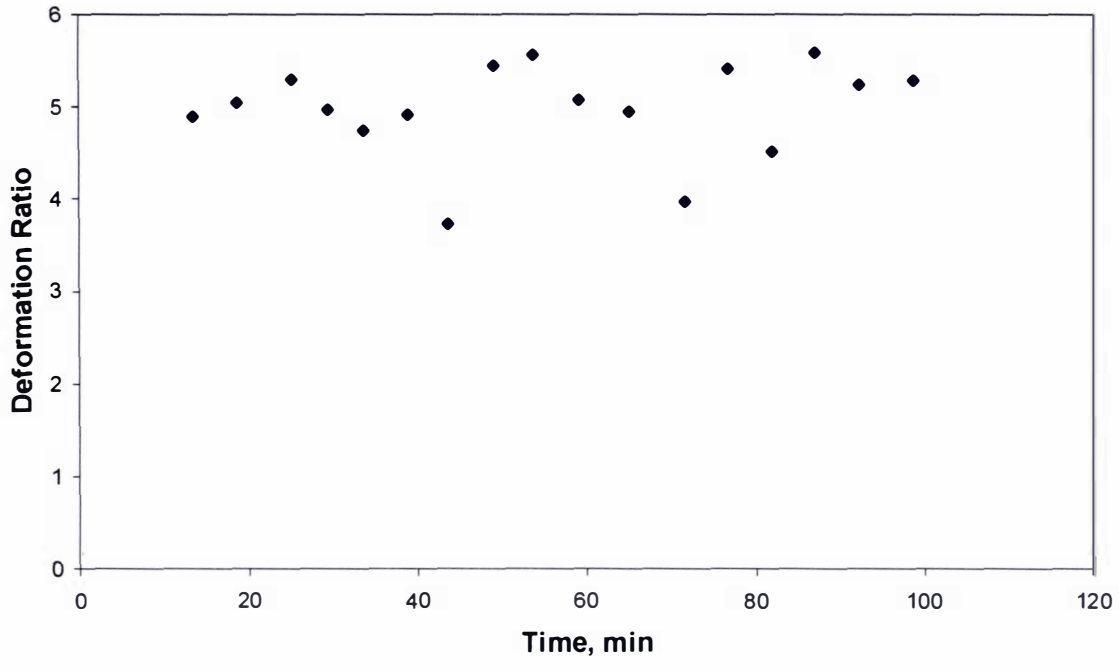

Figure 2.6 Deformation Ratio vs Time Since Mixing

The next graph (Figure 2.7) shows the deformation ratio as a function of sheeting passes (again the reduction ratio was 9, the dough *Epic*: short mix, the nip gap 2 mm, and the roller speed 6 rpm).

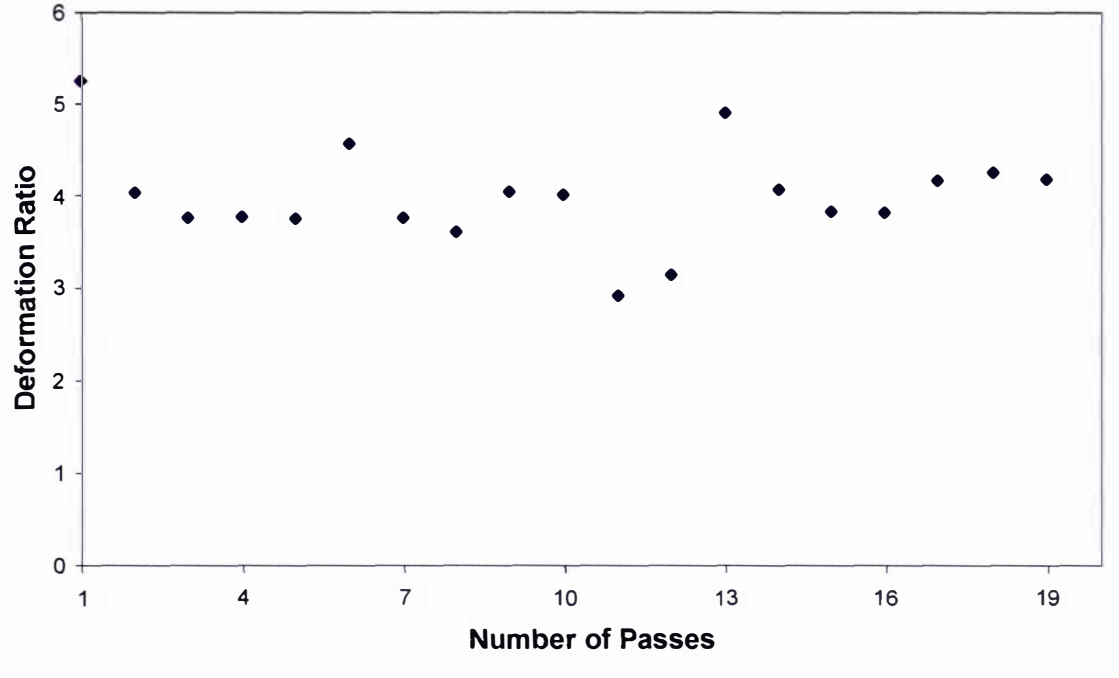

Figure 2.7 Deformation Ratio vs Pass Number

In Figure 2.7, after the first sheeting pass, where the deformation ratio is about 5, the deformation ratio is constant at around 4. This means that the sheeting procedure,

which assumes the dough is identical for 10 sheeting passes, is valid — if the first data point is ignored. In the subsequent analysis the data point collected for the first sheeting pass was ignored and only the data from passes 2 to 10 were used.

2.6.5. Results and Discussion

Representative data from the sheeting runs have been plotted in the figures below. In these figures the reduction ratio (the ratio of inlet height to nip gap) is the independent variable, plotted on the x-axis. The reason for this is that the attainment of a particular reduction in dough thickness is the main reason for using a sheeter.

2.6.5.1. Effect of Nip Gap

2.6.5.1.1. Deformation Ratio

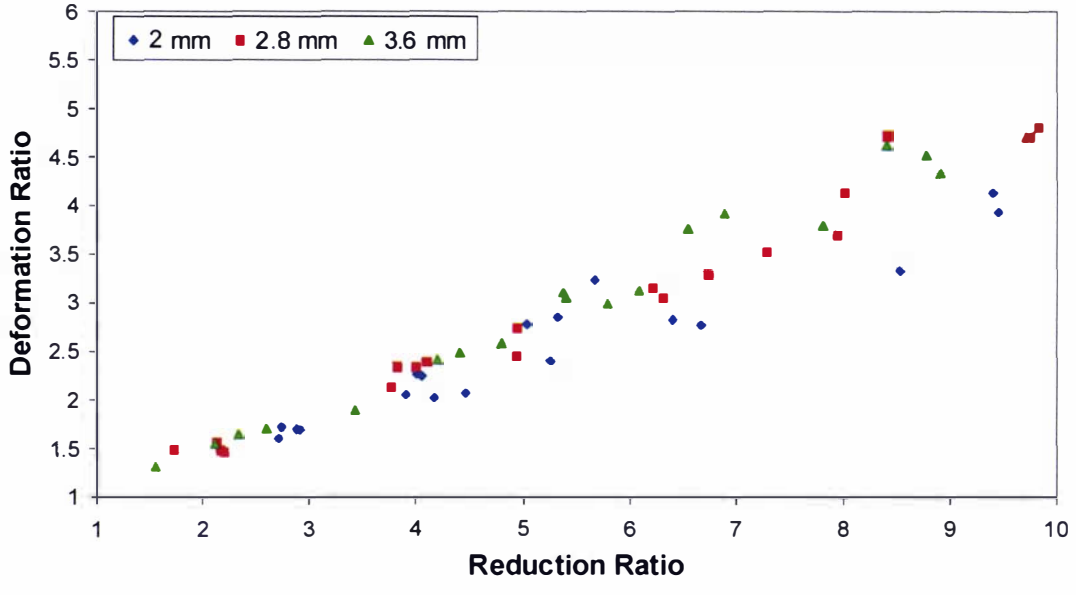

Figure 2.8 Deformation Ratio, Effect of nip gap: Blue diamonds are a 2 mm nip gap, red squares are a 2.8 mm nip gap and green triangles are for a 3.6 mm nip gap. Other conditions are: *Epic* short mix dough; 135 mm radius rollers; 19 rpm roller speed.

It was found that as the nip gap increased, the deformation ratio also increased. That is, the dough became more deformed. This does *not* mean that a piece of dough 20 mm thick, for example, will be more deformed by a 5 mm nip gap than a 2 mm gap. Instead this observation suggests that a piece of dough 10 times bigger, for example, than the nip gap will be deformed more (relative to its initial height) as the nip gap increases in size, if the initial height of the dough is also increased proportionally to the increase in

nip gap (that is, if the reduction ratio is held constant). This effect was independent of the dough mixture and the roller radius. However, as can be seen in Figure 2.8, it is difficult to separate the results for a 2.8 mm nip gap from the results for a 3.6 mm gap. It is also difficult to separate the variation due to nip gap at low reduction ratios. Finally, at lower roller speeds these effects were less pronounced. Figure 2.9 demonstrates the observed effect of variation in nip gap upon the deformation ratio at a low roller speed (6 rpm).

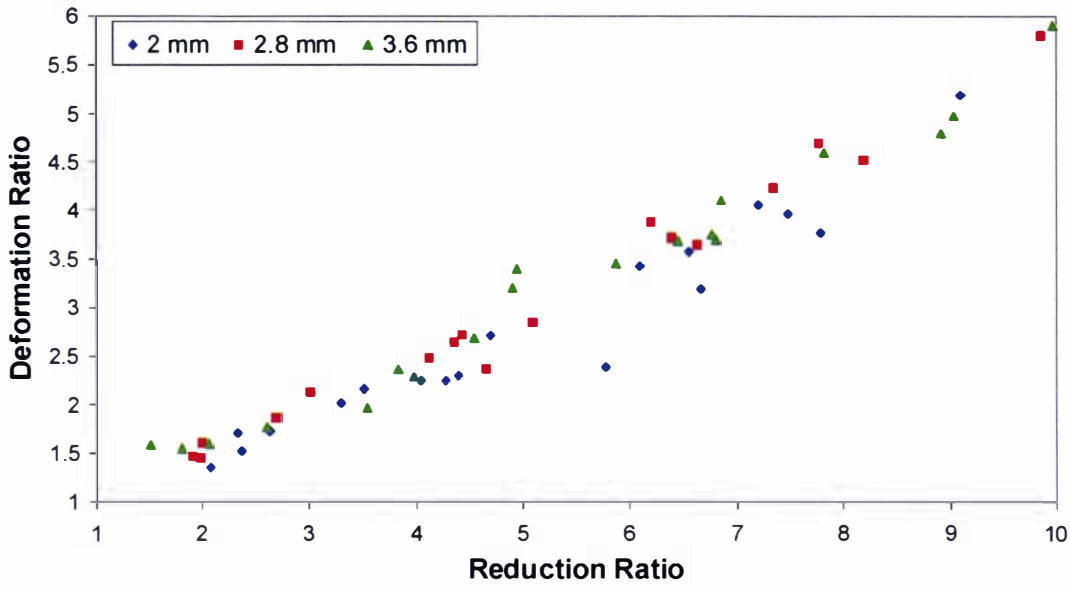

Figure 2.9 Deformation Ratio, Effect of nip gap: Blue diamonds are a 2 mm nip gap, red squares are a 2.8 mm nip gap and green triangles are for a 3.6 mm nip gap. Other conditions are: *Epic* short mix dough; 135 mm radius rollers; 6 rpm roller speed.

2.6.5.1.2. Exit Ratio

The exit ratio is the exit height divided by the nip gap, whereas the deformation ratio is the inlet height divided by the exit height. Some authors prefer to plot the exit ratio as a function of reduction ratio, instead of deformation ratio. Figure 2.10 demonstrates exit ratio for the same case as Figure 2.8. The relationship between deformation ratio and reduction ratio is close to being linear, while the relationship between exit ratio and reduction ratio is logarithmic. For this reason, the deformation ratio may be more convenient to work with than the exit ratio.

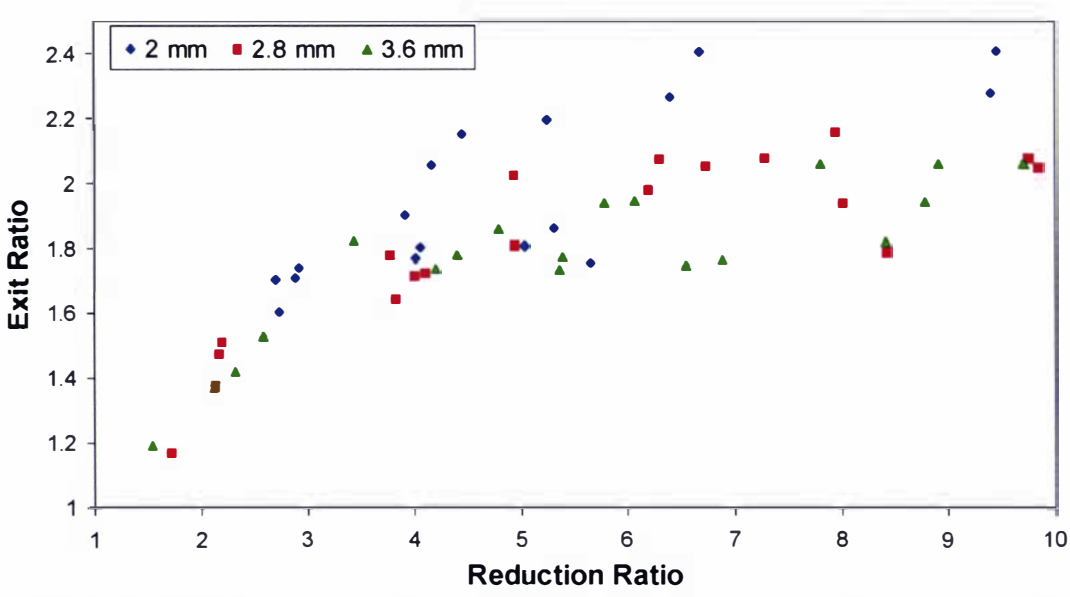

Figure 2.10 Exit Ratio, Effect of nip gap: Blue diamonds are a 2 mm nip gap, red squares are a 2.8 mm nip gap and green triangles are for a 3.6 mm nip gap. Other conditions are: *Epic* short mix dough; 135 mm radius rollers; 19 rpm roller speed.

The exit ratio is the exit height divided by the nip gap, whereas the deformation ratio is the inlet height divided by the exit height. Some authors prefer to plot the exit ratio as a function of reduction ratio, instead of deformation ratio. Figure 2.10 demonstrates exit ratio for the same case as Figure 2.8. The relationship between deformation ratio and reduction ratio is close to being linear, while the relationship between exit ratio and reduction ratio is logarithmic. For this reason, the deformation ratio may be more convenient to work with than the exit ratio.

2.6.5.1.3. Force on the Roller

The force exerted on the roller, for various nip gaps is given in Figure 2.11. It is hard to determine what the effect of nip gap is on the downward force. It appears that at low reduction ratios (3 to 5) as nip gap increases the force on the rollers decreases.

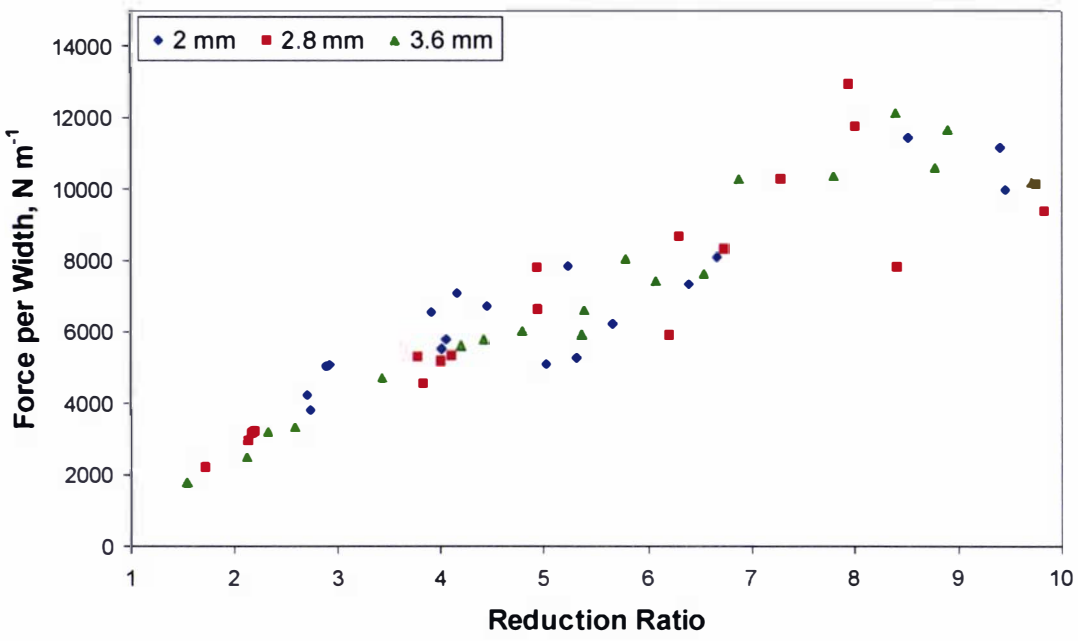

Figure 2.11 Force upon the roller, N m^{-1} (per Width of roller), Effect of nip gap: Blue diamonds are a 2 mm nip gap, red squares are a 2.8 mm nip gap and green triangles are for a 3.6 mm nip gap. Other conditions are: *Epic* short mix dough; 135 mm radius rollers; 19 rpm roller speed.

2.6.5.1.4. Torque

As for the downward force (Figure 2.11), Figure 2.12 shows that there is no clear influence of nip gap upon the torque.

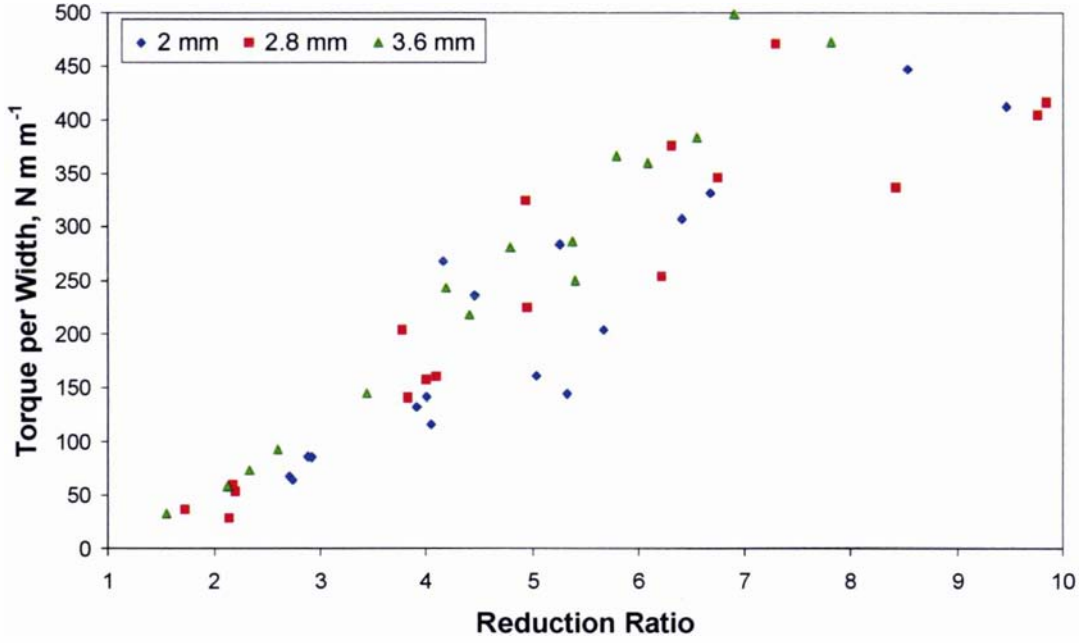

Figure 2.12 Torque, N m m^{-1} (per Width of roller), Effect of nip gap: Blue diamonds are a 2 mm nip gap, red squares are a 2.8 mm nip gap and green triangles are for a 3.6 mm nip gap. Other conditions are: *Epic* short mix dough; 135 mm radius rollers; 19 rpm roller speed.

The behaviour in Figure 2.12 is consistent with the preliminary experiments, where only dough type and roller diameter had a significant influence upon the torque measured.

2.6.5.2. *Effect of Roller Speed*

2.6.5.2.1. Deformation Ratio

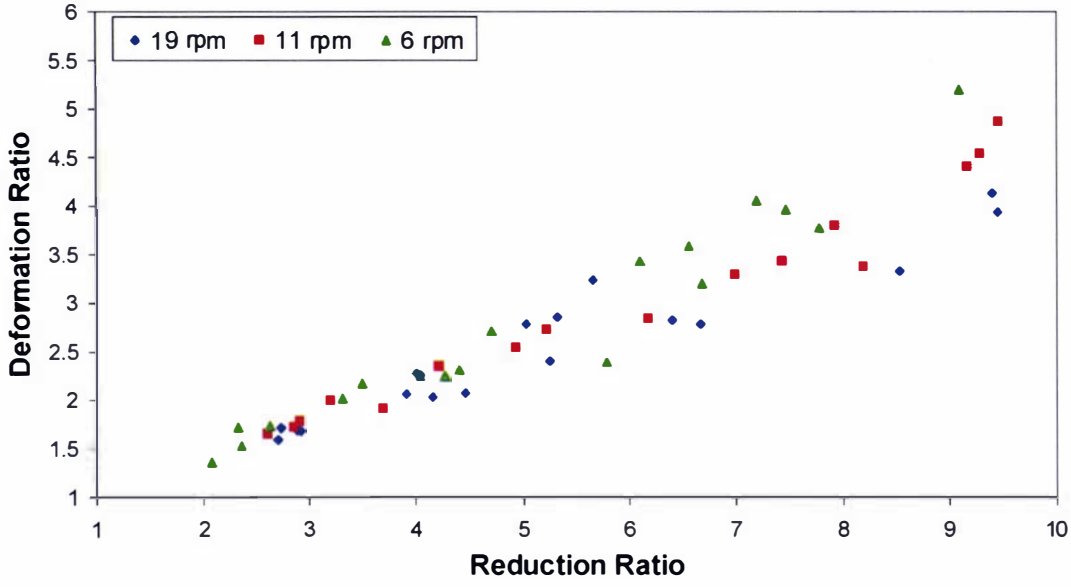

Figure 2.13 Deformation Ratio, Effect of Roller Speed: Blue diamonds are for a roller speed of 19 rpm, red squares for 11 rpm and green triangles for 6 rpm. Other conditions are: *Epic* short mix dough; 135 mm radius rollers; 2mm nip gap.

As the roller speed increases, the deformation ratio decreases (Figure 2.13). That is, the shorter the sheeting time, the less the dough is permanently deformed. This seems intuitive and is consistent with the results of the preliminary experiment.

2.6.5.2.2. Exit Ratio

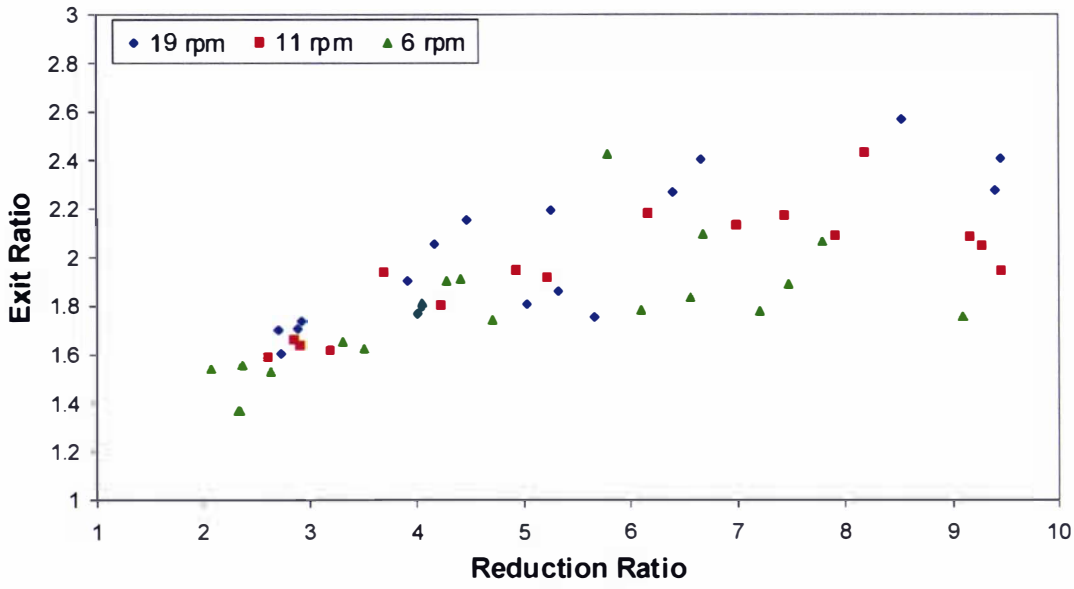

Figure 2.14 Exit Ratio, Effect of Roller Speed: Blue diamonds are for a roller speed of 19 rpm, red squares for 11 rpm and green triangles for 6 rpm. Other conditions are: *Epic* short mix dough; 135 mm radius rollers; 2mm nip gap.

The exit ratio, like the deformation ratio, demonstrates that the shorter the time the dough is under the sheeter, then the less it is deformed. That is the higher speed (19 rpm) case has a greater exit ratio than the low speed (6 rpm) case.

2.6.5.2.3. Force on the Roller

Figure 2.15 shows that the roller speed does not seem to strongly influence the force measured. This is consistent with the earlier preliminary experiments, where only nip gap, roller diameter and dough type were significant factors for determining the force upon the roller.

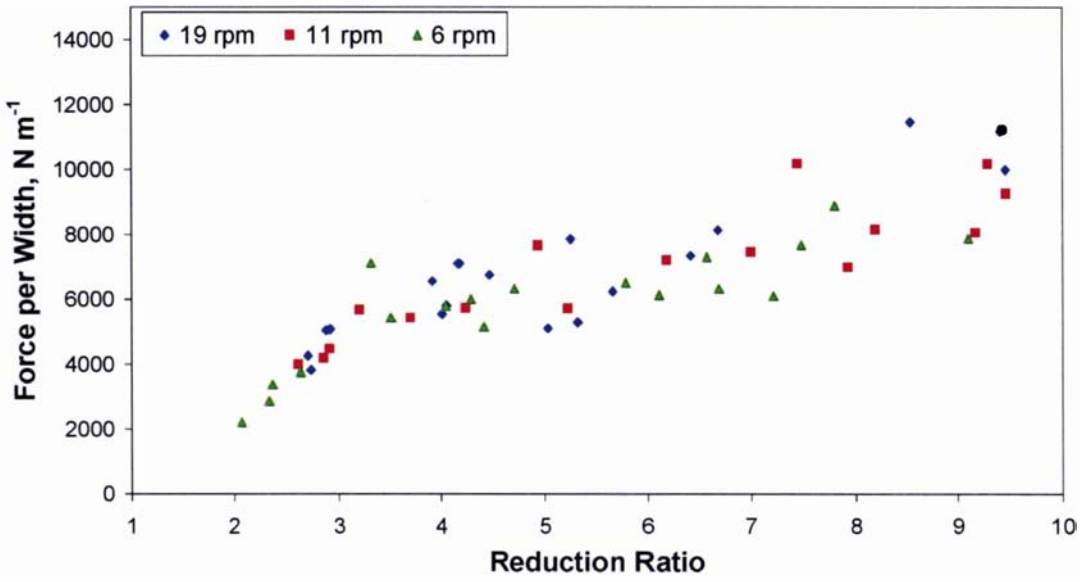

Figure 2.15 Force upon the roller, N m^{-1} (per Width of roller), Effect of Roller Speed: Blue diamonds are for a roller speed of 19 rpm, red squares for 11 rpm and green triangles for 6 rpm. Other conditions are: *Epic* short mix dough; 135 mm radius rollers; 2mm nip gap.

2.6.5.2.4. Torque

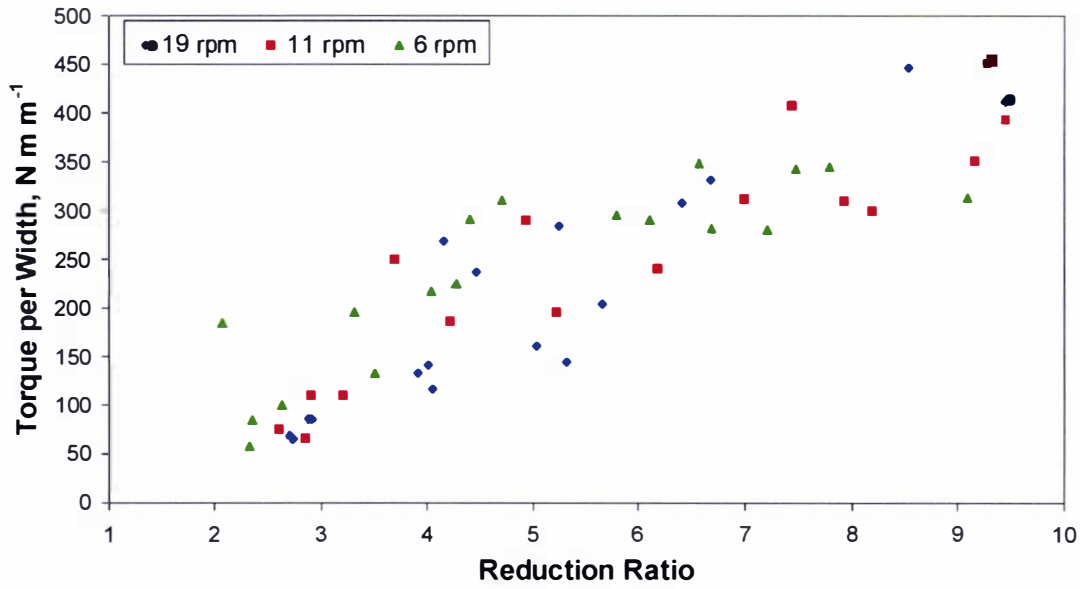

Figure 2.16 Torque, N m m^{-1} (per Width of roller), Effect of Roller Speed: Blue diamonds are for a roller speed of 19 rpm, red squares for 11 rpm and green triangles for 6 rpm. Other conditions are: *Epic* short mix dough; 135 mm radius rollers; 2mm nip gap.

At small reduction ratios it appears that a slower roller speed results in a greater torque (Figure 2.16). No trend is clear at high reduction ratios. There is a lot of scatter in the torque results.

2.6.5.3. *Effect of Roller Diameter*

2.6.5.3.1. Deformation Ratio

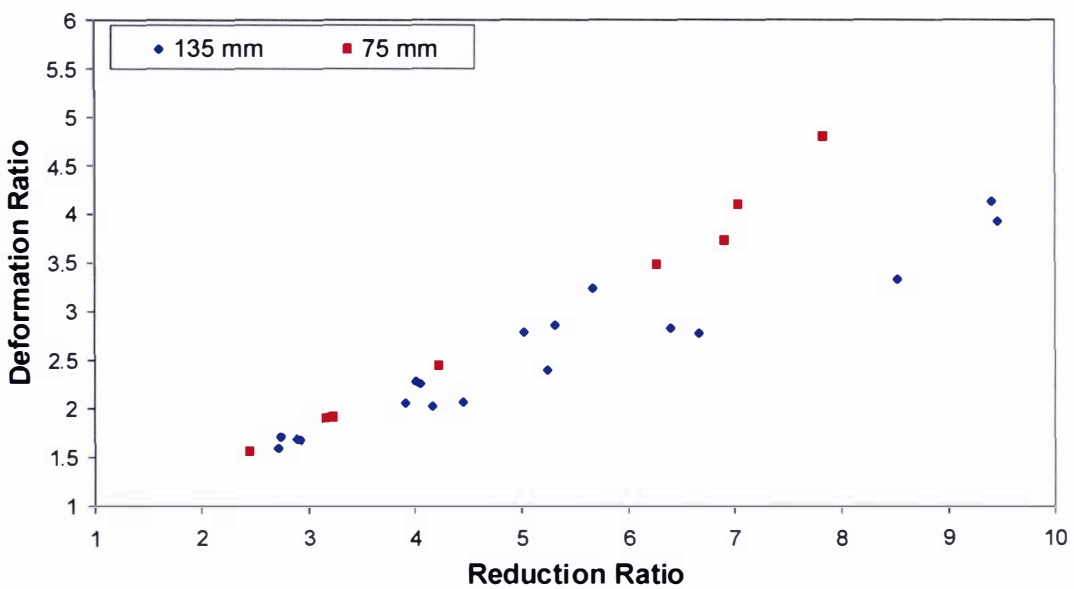

Figure 2.17 Deformation Ratio, Effect of Roller Diameter: Blue diamonds are for a roller diameter of 135 mm, red squares for 75 mm. Other conditions are: *Epic* short mix dough; 19 rpm roller speed; 2mm nip gap.

It was found that for the same nip gap, dough type and roller speed [rpm] the smaller roller results in a higher deformation ratio (Figure 2.17).

The surface speed of the roller [$m.s^{-1}$] can be calculated by:

$$u_r = \frac{2\pi RN}{60} \tag{2.7}$$

(where: R is the roller radius [m] and N is the roller speed [rpm]) and the dimensionless geometry ratio, ε, is defined (where δ is the nip gap [m]) as:

$$\varepsilon = \sqrt{\frac{\delta}{R}} \tag{2.8}$$

It was found that if the sheeting system is scaled to preserve both the roller's surface speed and the geometry ratio, ε, then the response of the deformation ratio also scales.

This is illustrated in Figure 2.18. Such a scaling relationship would be useful in scaling between production and laboratory scale systems.

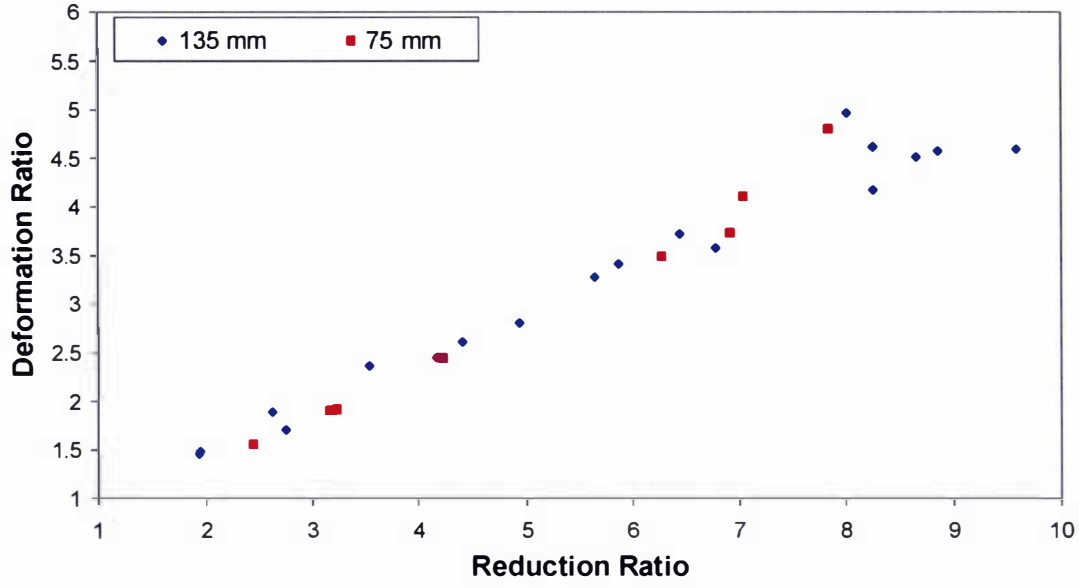

Figure 2.18 Deformation Ratio, Effect of Roller Diameter (Constant geometry ratio and surface speed): Blue diamonds are for a roller diameter of 135 mm, red squares for 75 mm. Other conditions are: *Epic* short mix dough; surface roller speed 0.15 m s^{-1}; geometry ratio 0.16.

2.6.5.3.2. Exit Ratio

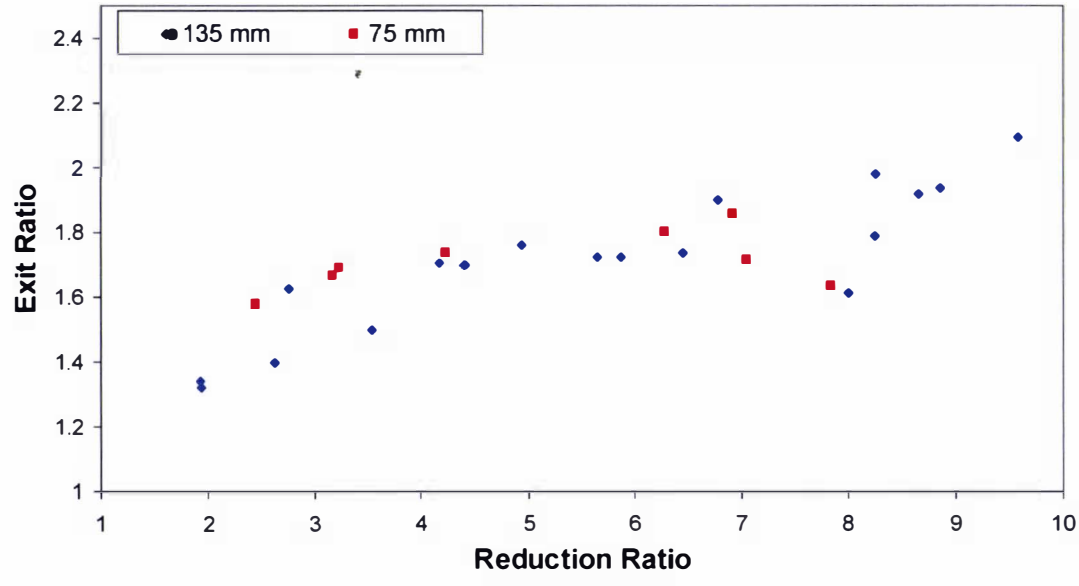

Figure 2.19 Exit Ratio, Effect of Roller Diameter (Constant geometry ratio and surface speed): Blue diamonds are for a roller diameter of 135 mm, red squares for 75 mm. Other conditions are: *Epic* short mix dough; surface roller speed 0.15 m s^{-1}; geometry ratio 0.16.

The exit ratio scales in the same manner as the deformation ratio. This is shown in Figure 2.19.

2.6.5.3.3. Force on the Roller

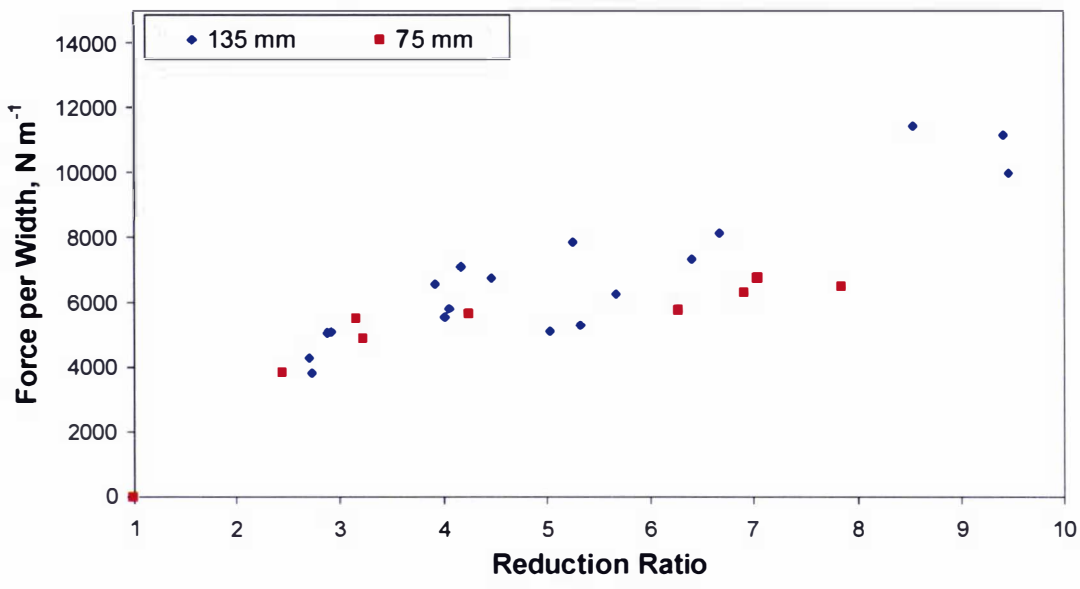

Figure 2.20 Force upon the roller, N m^{-1} (per Width of roller), Effect of Roller Diameter: Blue diamonds are for a roller diameter of 135 mm, red squares for 75 mm. Other conditions are: *Epic* short mix dough; 19 rpm roller speed; 2mm nip gap.

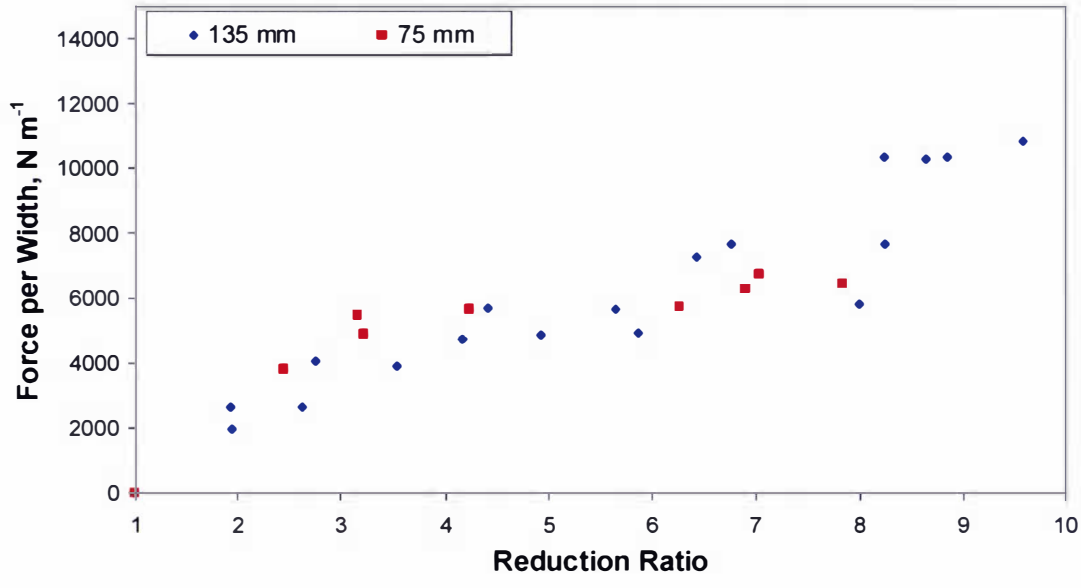

Figure 2.21 Force upon the roller, N m^{-1} (per Width of roller), Effect of Roller Diameter (Constant geometry ratio and surface speed): Blue diamonds are for a roller diameter of 135 mm, red squares for 75 mm. Other conditions are: *Epic* short mix dough; surface roller speed 0.15 m s^{-1}; geometry ratio 0.16.

At low reduction ratios the roller diameter does not effect the force upon the rollers (Figure 2.20). At high reduction ratios it appears that an increase in roller diameter results in an increase in the force upon the roller. As with the deformation ratio, the force on the roller appears to scale with the surface roller speed and the geometry ratio. This is illustrated in Figure 2.21.

2.6.5.3.4. Torque

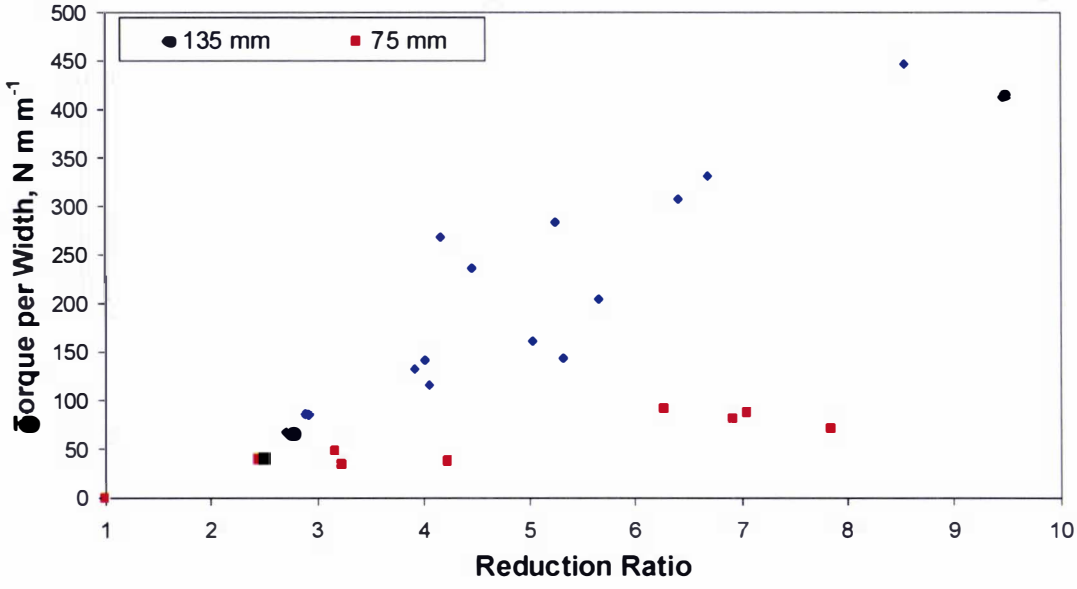

Figure 2.22 Torque, N m m^{-1} (per Width of roller), Effect of Roller Diameter: Blue diamonds are for a roller diameter of 135 mm, red squares for 75 mm. Other conditions are: *Epic* short mix dough; 19 rpm roller speed; 2mm nip gap.

The smaller the roller diameter, the smaller the torque that is measured. This is consistent with the preliminary experiments. This relationship does not scale like the deformation ratio.

2.6.5.4. Effect of Dough Properties

2.6.5.4.1. Deformation Ratio

In Figure 2.23 it can be seen that the less elastic dough made from *Halo* dough deformed more, which is expected. The Epic: short mix and Epic: long mix dough cannot be easily distinguished.

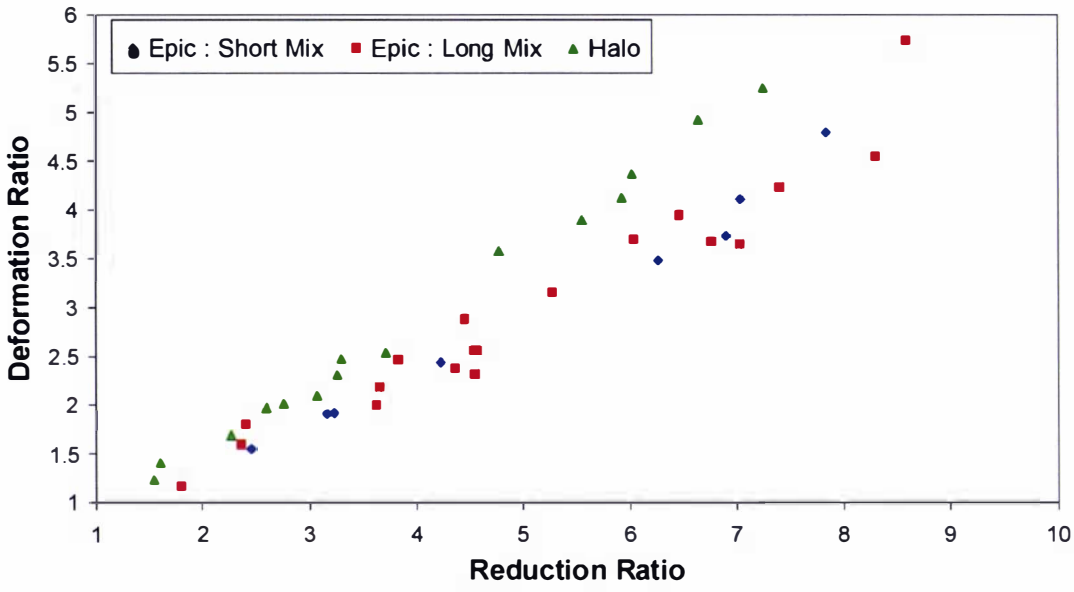

Figure 2.23 Deformation Ratio, Effect of Dough Type: Blue diamonds are for Epic: Short Mix, red squares for Epic: Long Mix, and green triangles for Halo dough. Other conditions are: 19 rpm roller speed; 2mm nip gap; and 75 mm roller diameter.

2.6.5.4.2. Exit Ratio

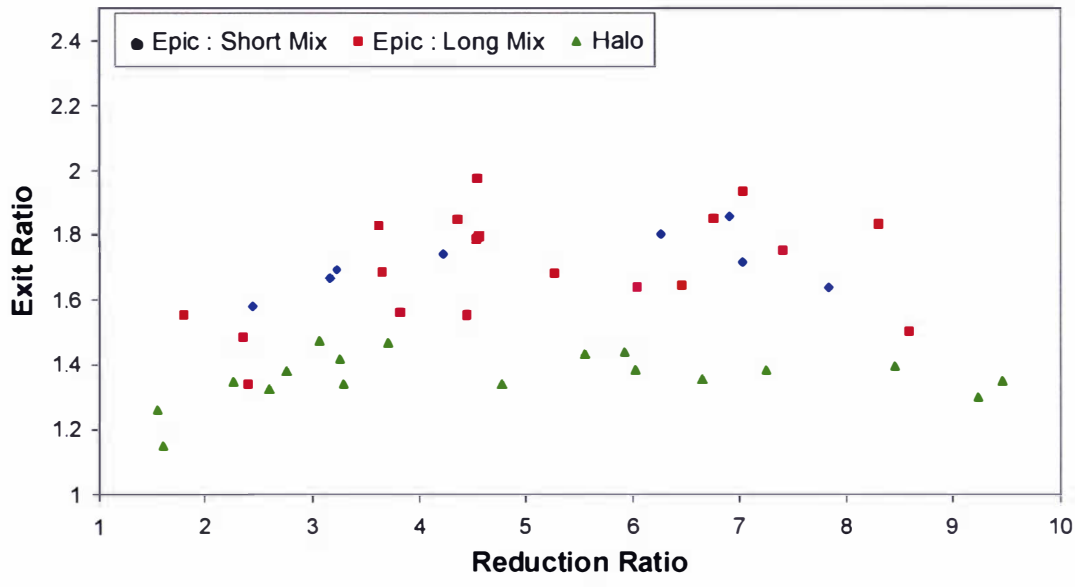

Figure 2.24 Exit Ratio, Effect of Dough Type: Blue diamonds are for Epic: Short Mix, red squares for Epic: Long Mix, and green triangles for Halo dough. Other conditions are: 19 rpm roller speed; 2mm nip gap; and 75 mm roller diameter.

Figure 2.24 demonstrates that the exit ratio is consistent with the deformation ratio, that is the less elastic *Halo* dough has a smaller exit ratio than the two epic doughs, which are quite similar to each other.

2.6.5.4.3. Force on the Roller

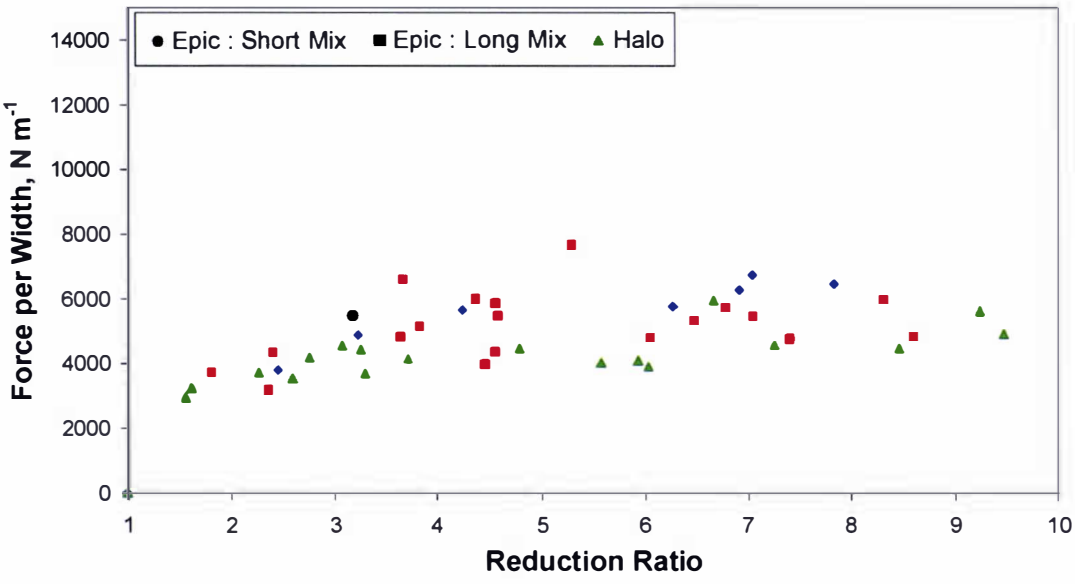

Figure 2.25 Force upon the roller, N m^{-1} (per Width of roller), Effect of Dough Type: Blue diamonds are for Epic: Short Mix, red squares for Epic: Long Mix, and green triangles for Halo dough. Other conditions are: 19 rpm roller speed; 2mm nip gap; and 75 mm roller diameter.

There is not much difference for the measured force upon the roller, at low reduction ratios, between the different dough types. At higher reduction ratios, the Halo dough exerts the least force upon the roller during sheeting. This is consistent with the earlier experiments.

2.6.5.4.4. Torque

There is no clear relationship between the dough properties and the observed torque, as shown in Figure 2.26. This is inconsistent with the preliminary experiment where dough type was an important factor in determining the torque. This is, perhaps, indicative of the difficulties in measuring the torque. It appears that the *Epic*: short mix dough may result in a smaller torque measurement, although it is not clear why this should be.

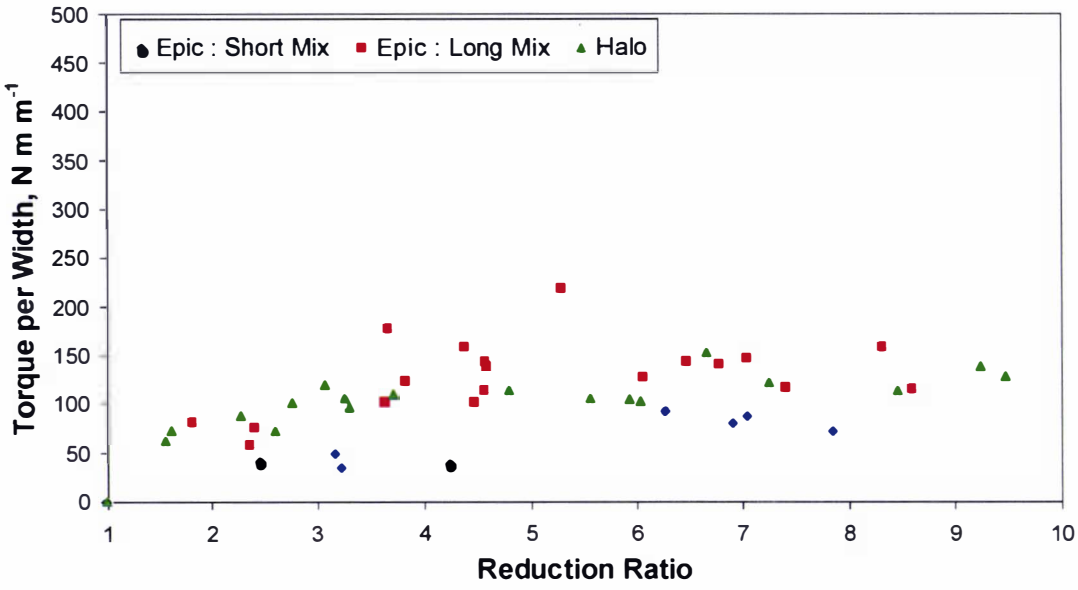

Figure 2.26 Torque, N m m^{-1} (per Width of roller), Effect of Dough Type: Blue diamonds are for Epic: Short Mix, red squares for Epic: Long Mix, and green triangles for Halo dough. Other conditions are: 19 rpm roller speed; 2mm nip gap; and 75 mm roller diameter.

2.6.6. *Summary*

The validation data experiment indicates some of the behaviours that ought to be represented in a model of a sheeting system. These include:

- an increase in the relative deformation of the sheet with increasing nip gap.
- a decrease in deformation with increasing roller speed and with increasing roller diameter.
- a similar deformation for sheeting systems built to the same geometry ratio operating at the same roller surface speed.
- an increase in force and torque on the rollers when roller diameter increases.
- less elastic doughs are more easily deformed and exert less force upon the rollers.

There is scatter in the validation data, which makes it difficult to interpret fully.

3. Dough Rheology

Rheological properties of dough are required in formulating a model of dough sheeting.

3.1. Steady State Shear Stress Measurements

Rheological properties can be measured with either a steady state system, or a dynamic system. A steady state measurement is typically performed by applying a shear stress to the test material and measuring the resultant forces and torques on the system, this data can be used to plot various viscometric functions, for example:

$$\eta(\dot{\gamma}) = -\frac{\tau_{xy}}{\dot{\gamma}_{xy}} \tag{3.1}$$

$$\Psi_1(\dot{\gamma}) = -\frac{\tau_{xx} - \tau_{yy}}{\dot{\gamma}_{xy}^2} \tag{3.2}$$

$$\Psi_2(\dot{\gamma}) = -\frac{\tau_{yy} - \tau_{zz}}{\dot{\gamma}_{xy}^2} \tag{3.3}$$

where: τ_{ij} [Pa] and $\dot{\gamma}_{ij}$ [s^{-1}] are the shear stress and strain rate respectively; $\dot{\gamma} = \left|\dot{\gamma}_{xy}\right|$ [s^{-1}]; and η [Pa s], Ψ_1 [Pa s^2] and Ψ_2 [Pa s^2] are the viscometric functions: viscosity, the first normal stress coefficient and the second normal stress coefficient, respectively. There are often instrumental difficulties in determining Ψ_1 and Ψ_2 using steady shear stress measurements.

In a parallel plate viscometer, a disk is rotated above another disk, with the test sample sandwiched between the two disks, as illustrated in Figure 3.1.

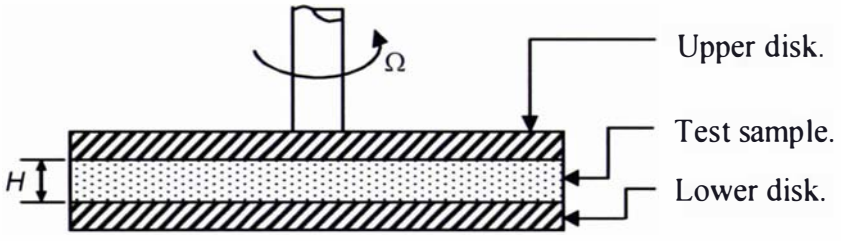

Figure 3.1 Parallel Plate Viscometer, where: Ω [rad s^{-1}] is the constant angular velocity of the upper disk; *H* [m] is the distance between the disks; *R* [m] is the radius of the disks; *T* [N m] is the torque required to maintain the rotation; *F* [N] is the force required to maintain the separation between the disks; and $\pi_{yy} = p + \tau_{yy}$ [Pa] is the downwards pressure distribution across one of the disks.

From Bird, et al. (1987):

$$\dot{\gamma}_R = \frac{R\Omega}{H} = \text{shear rate at the rim.} \tag{3.4}$$

$$\eta(\dot{\gamma}_R) = \frac{T}{2\pi R^3}\frac{1}{\dot{\gamma}_R}\left[3 + \frac{d\ln\left(\frac{T}{2\pi R^3}\right)}{d\ln(\dot{\gamma}_R)}\right] \tag{3.5}$$

$$\Psi_1(\dot{\gamma}_R) - \Psi_2(\dot{\gamma}_R) = \frac{F}{2\pi R^2}\frac{1}{\dot{\gamma}_R^2}\left[2 + \frac{d\ln\left(\frac{F}{2\pi R^2}\right)}{d\ln(\dot{\gamma}_R)}\right] \tag{3.6}$$

$$\Psi_2(\dot{\gamma}_R) = \frac{p_a - \pi_{yy}(R)}{\dot{\gamma}_R^2} \tag{3.7}$$

and p_a is the atmospheric pressure [Pa]. The parameters of a constitutive equation, and the suitability of a particular constitutive equation, can be determined by fitting the constitutive equation's predictions to the observed behaviour of the material.

3.2. Dynamic Measurements

It is, sometimes, not convenient to measure the steady stress behaviour of a material, particularly if the material's properties, such as the physical structure, change while undergoing a stress, which may mean that it is impossible to reach a steady state. In such cases it is more suitable to perform dynamic measurements, if possible.

Dynamic measurements are performed by studying the response of the test material to an oscillatory strain of frequency ω [Hz] where:

$$\gamma_{ij}(t) = \gamma_{ij,0}\exp(i\omega t) \tag{3.8}$$

$$\therefore \dot{\gamma}_{ij}(t) = i\omega\gamma_{ij}(t) \tag{3.9}$$

It is then assumed that if the strain is oscillatory, the stress is also oscillatory within the linear viscoelastic region; hence:

$$\dot{\sigma}_{ij}(t) = i\omega\sigma(t) \tag{3.10}$$

A new parameter, the complex modulus, G^* [Pa] is then defined such that:

$$\sigma_{ij}(t) = G^*\gamma_{ij}(t) \tag{3.11}$$

$$G^* = G' + iG'' \tag{3.12}$$

where G' is the shear storage modulus [Pa] and G'' the shear loss modulus [Pa].

Two other parameters η' [Pa s] and η" [Pa s] are also used in the literature to describe the response to oscillatory deformation. These are merely alternative notations that are simply related to the elements of the complex modulus (Barnes et al., 1989):

$$\eta' = \frac{G''}{\omega} \tag{3.13}$$

$$\eta'' = \frac{G'}{\omega} \tag{3.14}$$

For the parallel plate viscometer described in Figure 3.1, Bird, et al. (1987) give the following equations:

$$\gamma = \gamma_0 \exp(i\omega t) \tag{3.15}$$

$$\eta'(\omega) = -\frac{2HT_o}{\pi R^4 \omega \gamma_0} \sin\alpha \tag{3.16}$$

$$\eta''(\omega) = -\frac{2HT_o}{\pi R^4 \omega \gamma_0} \cos\alpha \tag{3.17}$$

$$\alpha = \tan^{-1}\left(\frac{G''}{G'}\right) = \tan^{-1}\left(\frac{\eta'}{\eta''}\right) \tag{3.18}$$

Again, these data can be used to determine the parameters of a constitutive equation.

3.3. The Cox-Merz rule and Laun's rule

It is convenient to have some method of converting between the more easily performed dynamic measurements and the more difficult steady state measurements. One such rule is the Cox-Merz rule, which relates the (steady state) measured apparent viscosity, $\eta(\dot{\gamma})$, to the (dynamically measured) complex viscosity, $\eta^*(\omega)$ (Bird et al., 1987):

$$\eta(\dot{\gamma}) = \sqrt{\eta'(\omega)^2 + \eta''(\omega)^2}\Big|_{\omega=\dot{\gamma}} = \eta^*(\omega)\Big|_{\omega=\dot{\gamma}} \tag{3.19}$$

A similar empiricism, relating $\Psi_1(\dot{\gamma})$, to $\eta'(\omega)$ and $\eta''(\omega)$, is Laun's rule (Bird et al., 1987):

$$\Psi_1(\dot{\gamma}) = \frac{2\eta''(\omega)}{\omega}\left[1 + \left(\frac{\eta''(\omega)}{\eta'(\omega)}\right)^2\right]^{0.7}\Bigg|_{\omega=\dot{\gamma}} \tag{3.20}$$

Ψ_2, is difficult to evaluate from dynamic measurements, but usually a suitable estimate can be obtained by the empirical relationship (Bird et al., 1987):

$$\Psi_2(\dot{\gamma}) = -0.1\Psi_1(\dot{\gamma}) \tag{3.21}$$

3.4. Dough Rheology Measurements

3.4.1. Materials

Measurements were performed on three types of dough. The doughs were made to the same recipes as those given in Section 2.6.3, except scaled to use 50 g of flour, and mixed in a 50 g MDD mixer to the same work input as the earlier doughs. Dough samples were kept in sealed containers before testing, in order to prevent drying out. A sub-sample of approximately 10 g was used for each measurement.

3.4.2. Rheometer

A controlled stress Rheometrics Scientific SR-5000 rheometer running RSI Orchestrator V643 software was used to determine dough properties. A parallel plate configuration was used. The upper plate was 40 mm in diameter. The gap between the two plates was 4 mm. Both plates had their surfaces covered in fine-grain sandpaper, in order to prevent slip. The instrument and sample were kept at 25 °C during testing and the system was kept under a sealed cup to prevent drying out. The sample was allowed to relax for 120 s after being placed in the instrument, before testing began.

3.4.3. Stress Sweep

A stress sweep was performed for each dough type, shown in Figure 3.2. The Halo dough behaved differently from the other two dough types; it was less viscous . The two Epic dough mixtures were not as distinguishable from each other: the longer mixed Epic dough was less viscous. The data shown in Figure 3.2 are consistent with the idea that dough is a shear thinning material. It is the steep, negative, linear slope that is observed for all the dough types, for strain rates greater than about 0.0002 s^{-1}, which indicates that the dough behaves as a pseudoplastic, or shear thinning, material - in these conditions. At low strain rate rates (less than 0.0002 s^{-1}) all dough types displayed a Newtonian plateau of viscosity ($\approx 2 \times 10^5$ Pa s for Halo and $\approx 10^6$ Pa s for Epic). The slight inflection in slope at the high strain rate (greater than 0.1 s^{-1}) may be an artefact of the instrument rather than a result of the dough properties.

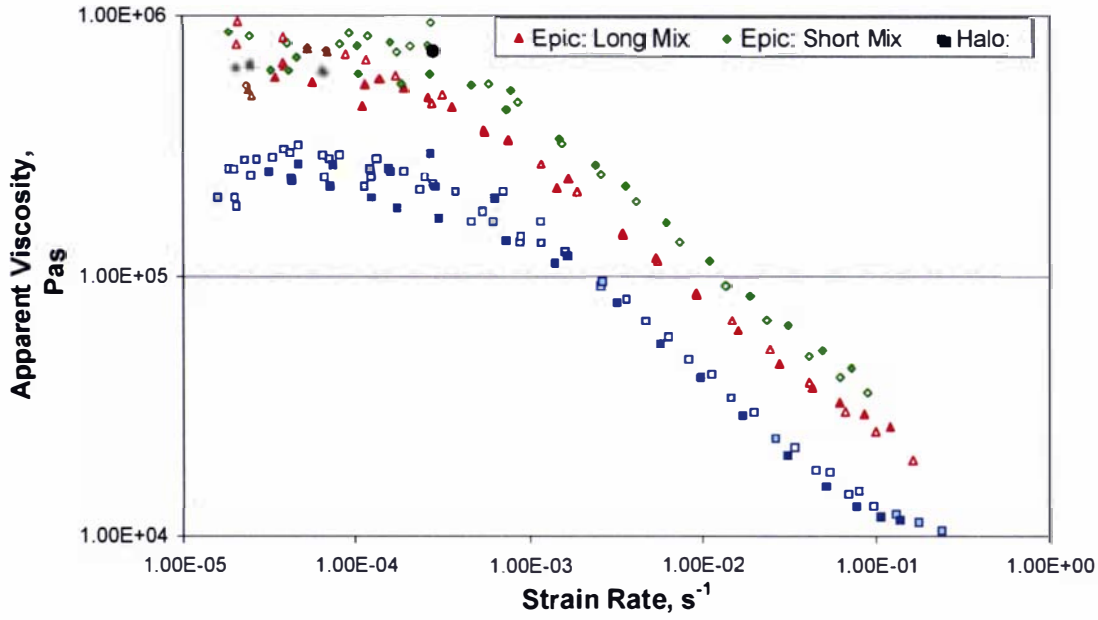

Figure 3.2 Stress Sweep, where: the red triangles are Epic Dough mixed for 17 W h kg^{-1}; the green diamonds are Epic Dough mixed for 16 W h kg^{-1}; and the blue squares are Halo Dough mixed for 9.5 W h kg^{-1}. (Filled and open symbols represent replications).

The steady state behaviour at high strain rates (as might be more realistic in a sheeting application) was not measurable. This was because the stress controlled rheometer used was not capable of applying a great enough stress to produce higher strain rates. Thus, high frequency measurements were then taken, which may be used to approximate high strain rate measurements (if the Cox-Merz rule is valid).

As mentioned in Section 1.5.4 dough properties are strongly influenced by the amount of water used in the dough recipe. Figure 3.3 demonstrates that the more water added to Epic dough mixed for 16 W h kg^{-1} the less viscous the dough. This is significant because the Halo dough (least viscous) was made according to a recipe (with regard to water content) like that which might be used in industry, while the Epic doughs were mixed with less water than would be normal. Figure 3.3 shows that when the Epic dough is mixed with 60 % water (more like an industrially useful dough), then it has a similar apparent viscosity to the Halo dough. This suggests that industrially useful doughs are likely to be very similar rheologically, because the standard methods for determining dough recipes are designed to produce doughs which will process similarly. This may be a problem in applying rheological models to dough processing.

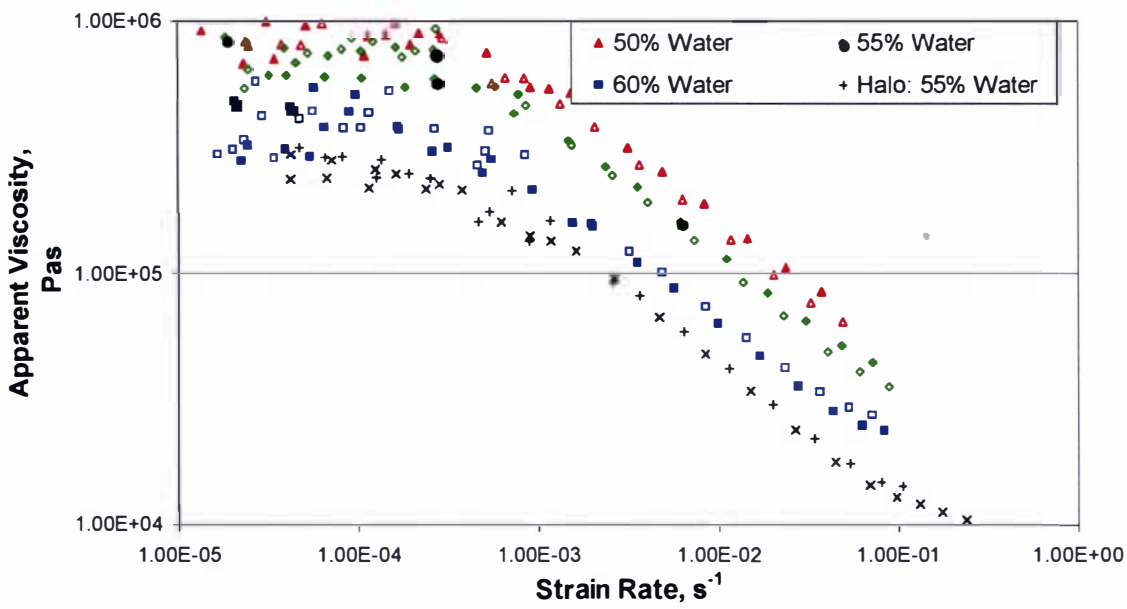

Figure 3.3 Stress Sweep, for Epic Dough mixed for 16 W h kg^{-1} where: the red triangles are 50 % water; the green diamonds are 55 % water; and the blue squares is 60 % water; for comparison the black crosses are Halo dough mixed for 9.5 W h kg^{-1}, with 55 % water.

3.4.4. *Frequency Sweep*

Frequency sweeps for the materials were conducted at a constant stress in the linear viscoelastic region for each material. Prior to the frequency sweep measurements the linear viscoelastic region was determined by measuring G' and G" as a function of the applied stress at 1 Hz. Stresses in the linear region were chosen for each material, these were: 20 Pa (for the 16 W h kg^{-1} Epic dough), 50 Pa (for the 17 W h kg^{-1} Epic dough) and 100 Pa (for the Halo dough). The resulting strain at each of the stresses was measured to be 0.08%, 0.2% and 1.4% respectively. According to Phan Than et al. (1997) the linear viscoelastic region for dough occurs for strain rates of less than 0.1 %. This is a similar order of magnitude as was found for the two Epic doughs, but the Halo dough appeared to be remain linear for slightly higher strain rates.

Figure 3.4 shows the frequency sweeps for the three doughs, plotted both as *G*' and *G*". *G*' and *G*" increased with frequency and *G*' was greater than *G*". This behaviour is typical of elastic systems. However, *G*' is less than a decade greater than *G*", rheological behaviour similar to that of "weak-gels" (Ferry, 1980).

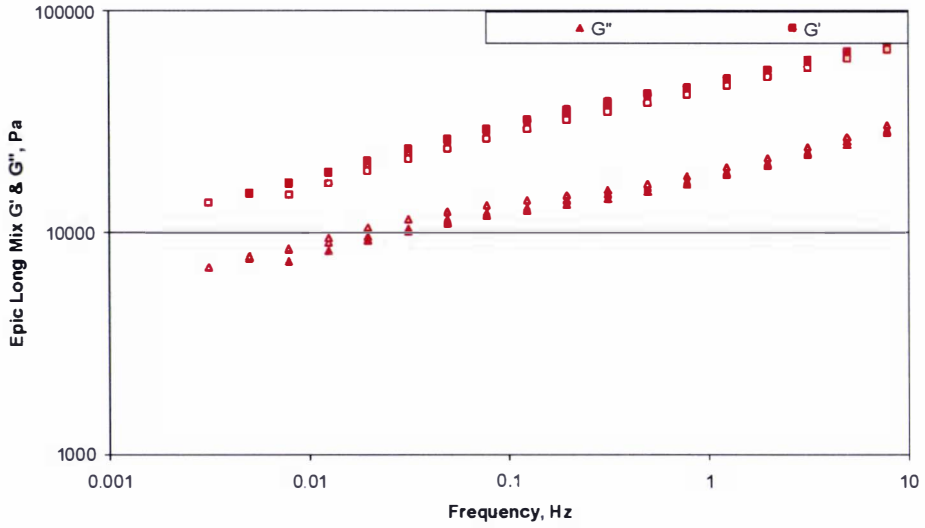

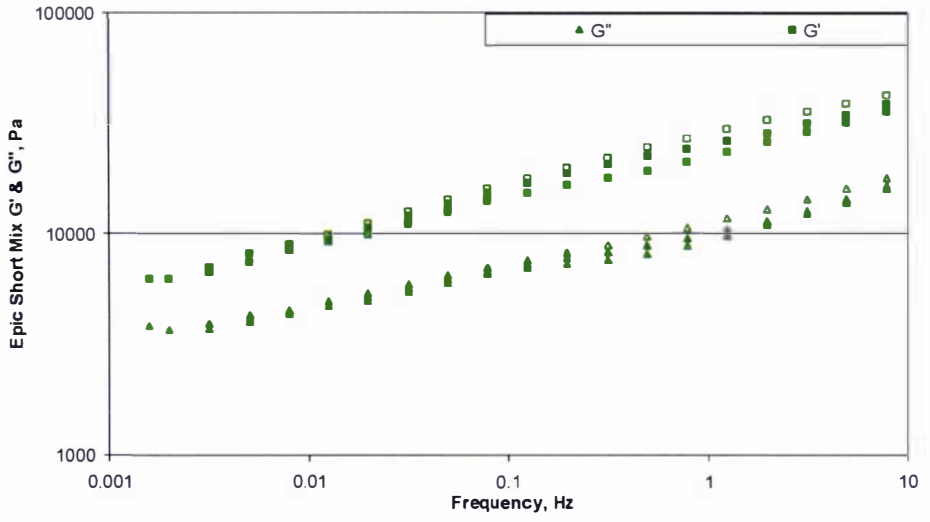

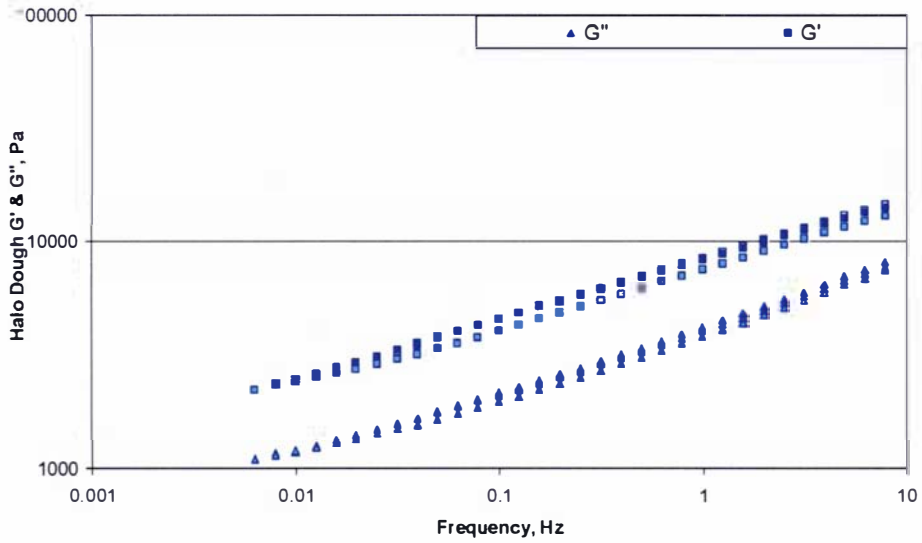

Figure 3.4 G' (squares) and G" (triangles) for the three dough types. Where: red is Epic, Long mix; green is Epic, Short mix; and blue is Halo dough.

A slight change in the slope of G'' can be observed at around 0.1 Hz and again at 1 Hz. This is more pronounced for the two Epic doughs. This may be suggestive of a relaxation time at these frequencies.

The complex elasticity G* is plotted for the three dough types in Figure 3.5. The Halo is, as for the stress sweep, clearly distinguishable by frequency sweep from the two Epic doughs. The long mixed (17 W h kg^{-1}) Epic dough was the most elastic and the Halo dough the least elastic.

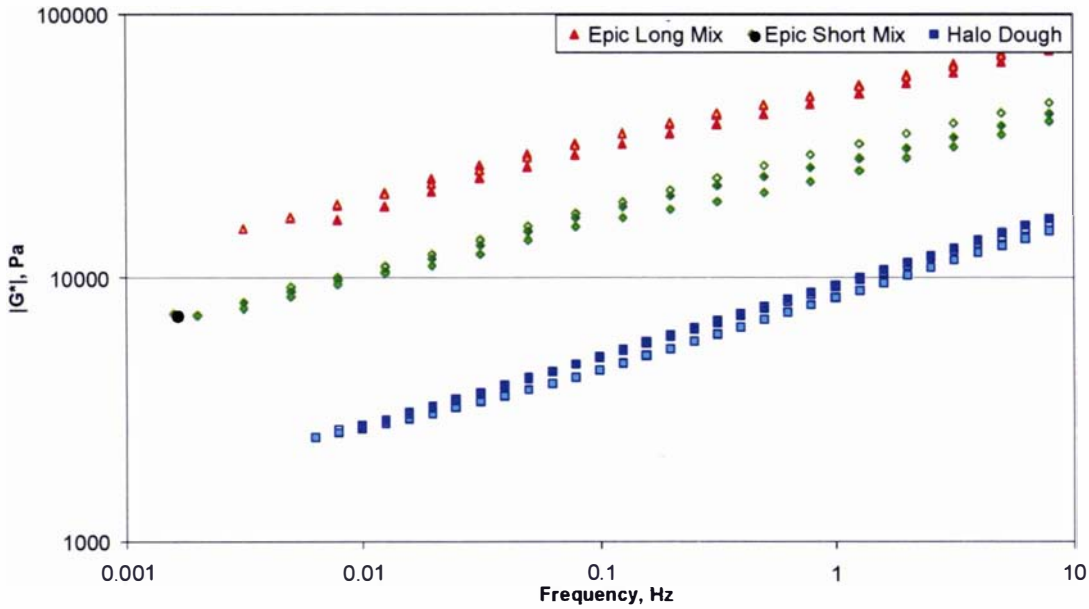

Figure 3.5 Complex Elasticity for three dough types, where: the red triangles are Epic Dough mixed for 17 W h kg^{-1}; the green diamonds are Epic Dough mixed for 16 W h kg^{-1}; and the blue squares are Halo Dough mixed for 9.5 W h kg^{-1}.

3.4.5. *Validity of the Cox-Merz rule*

Figure 3.6 shows a comparison of the apparent viscosity of the Halo dough as measured with the stress sweep, with the complex viscosity derived from the dynamic frequency sweep. According to the Cox-Merz rule (3.19), these have the same value when frequency is equal to strain rate. Clearly from Figure 3.6, the Cox-Merz rule does not apply. The agreement between dynamic and steady measurements of viscosity is closest for the Halo dough.

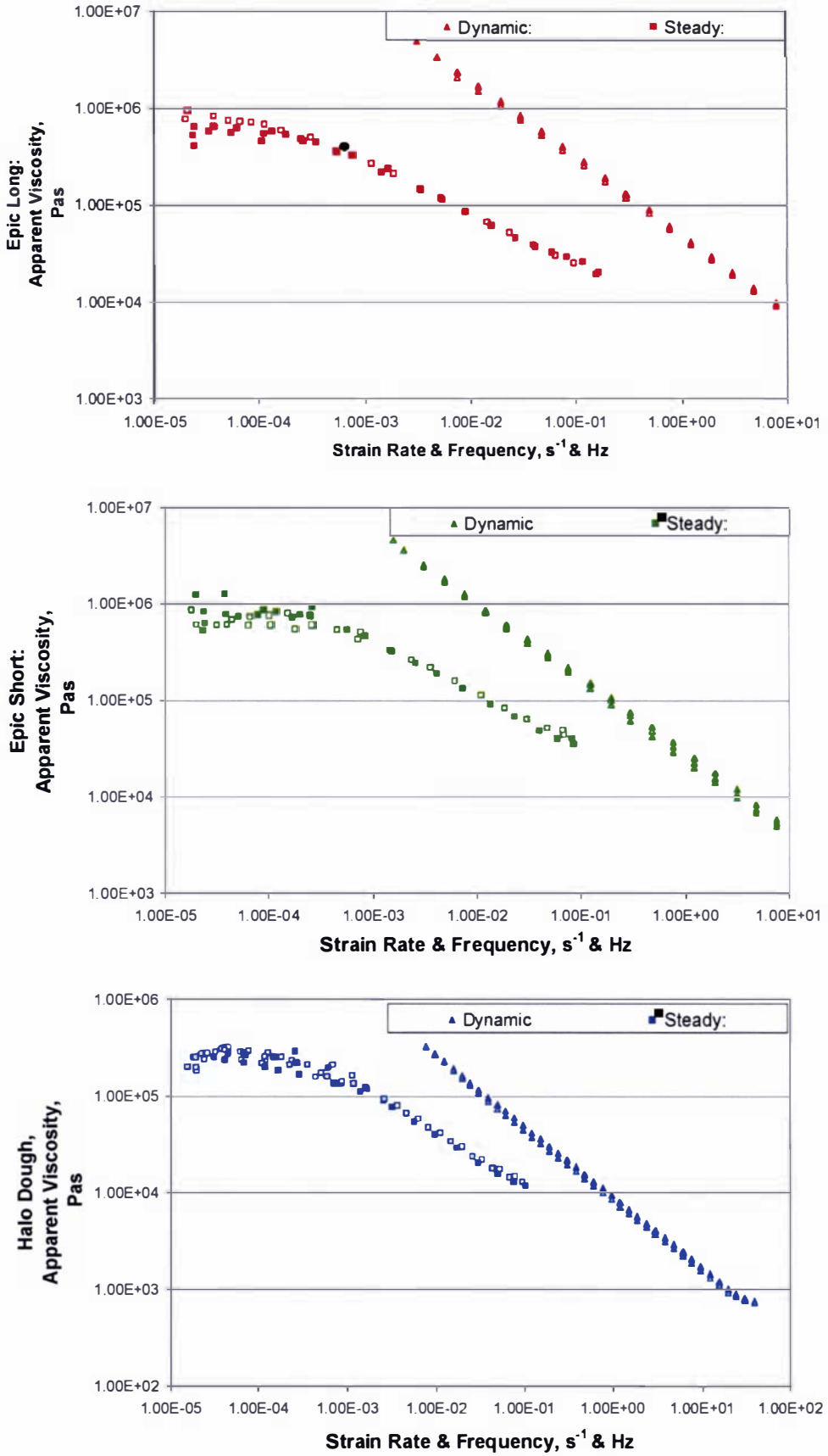

Figure 3.6 Dynamic and Steady State Apparent Viscosity, for three dough types. : red is Epic, Long mix; green is Epic, Short mix; and blue is Halo dough.

A possible reason for the discrepancy is that the dough properties are changed during the stress sweep measurements, as is suggested in Section 1.5.3. Figure 3.7 shows the steady stress sweep for Halo dough as measured with increasing stress and the stress sweep for the Halo dough measured (immediately afterwards) with the same sample with decreasing stress. The difference between the two suggests that the dough's structure (and hence properties) has changed due to the measurements. Therefore it is difficult to accurately measure steady state properties. This may explain why the Cox-Merz rule does not apply.

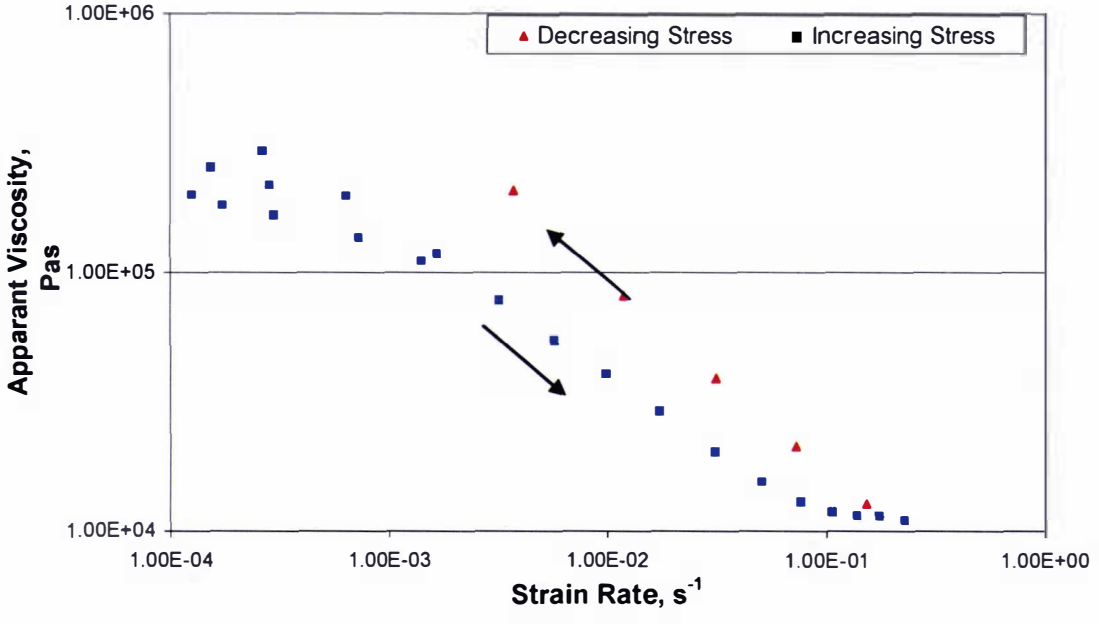

Figure 3.7 Stress Sweep: Increasing Stress compared to Decreasing Stress, where: blue squares are increasing stress; and red triangles are decreasing stress. Halo dough mixed for 9.5 W h kg^{-1}.

3.4.6. First Normal Stress Difference

Using Laun's rule (3.20), Ψ_1, can be calculated for each of the three dough materials, as shown in Figure 3.8. It should be recognised that these may not be very accurate, as the Cox Merz relationship does not apply for the dough. The first normal stress difference is lowest for the Halo dough, and highest for the longer mixed Epic dough- although the two Epic doughs are similar.

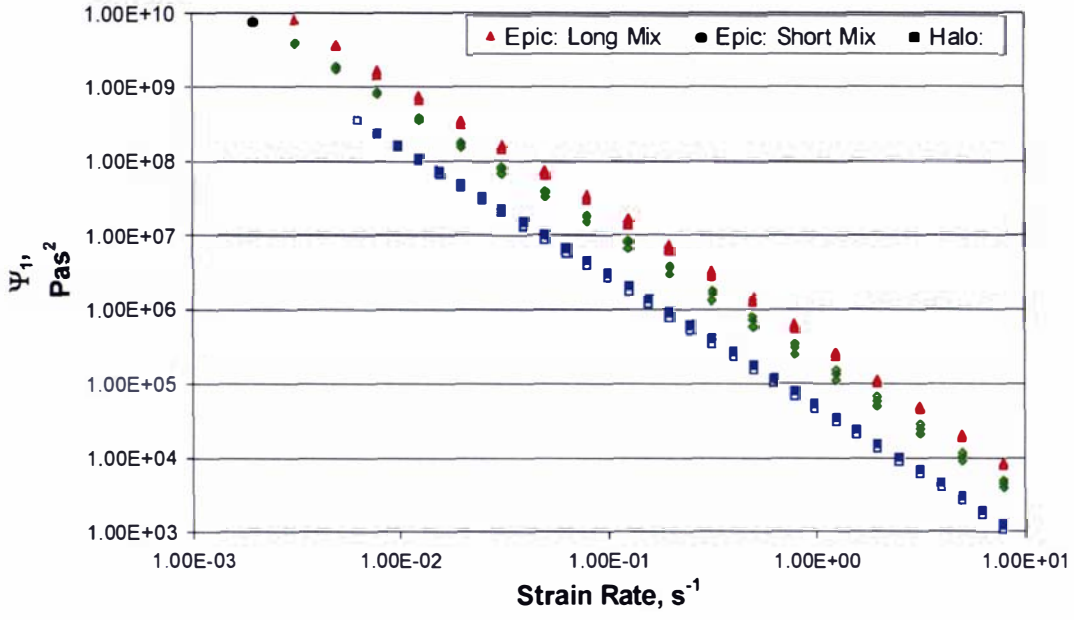

Figure 3.8 Ψ_1 calculated using Laun's Rule. Where: the red triangles are Epic Dough mixed for 17 W h kg^{-1}; the green diamonds are Epic Dough mixed for 16 W h kg^{-1}; and the blue squares are Halo Dough mixed for 9.5 W h kg^{-1}.

3.5. Constitutive Equations

For the experimentally determined rheological data to be useful, for modelling, it needs to be used to derive parameters for constitutive equations. Previously proposed constitutive equations and their parameters were discussed in Section 1.5.

The forms of the trends in Figure 3.2 to Figure 3.8 indicated that constitutive equations that included power law dependency upon the strain rate would be likely to be the most suitable. However, performing analytical calculations with power law relationships can be mathematically inconvenient. Therefore constitutive equations that do not contain a power law relationships were also investigated.

The following constitutive equations and their parameters were based on the rheological dynamic measurements made between frequencies of 0.005 Hz and 50 Hz. The fitting was performed using Sigmaplot 2000 for Windows Version 6.00. When fitting, the residuals were weighted according to the viscosity, which compensated for the large range of viscosities which were fitted. A 95 % confidence interval is given as an estimate of the error in the parameters. The "true" values of the parameters have a 95 % probability (assuming a student t distribution) of falling within the confidence interval

given. An R^2 value is also given for each fit. The closer the R^2 value is to 1 the better the fit. Some of the parameters (K in the power law relationships, for example) are not physically meaningful and their particular values are artefacts of the fitting technique. For this reason caution should be used when comparing the parameters of different samples, and particularly results from different sources.

3.5.1. Newtonian

$$\eta(\dot{\gamma}) = \eta \tag{3.22}$$

See Section 1.5.5.3.

Dough	Epic Short Mix	Epic Long Mix	Halo
η [Pa s]	$9 \times 10^3 \pm 4 \times 10^3$	$16 \times 10^3 \pm 7 \times 10^3$	$1.2 \times 10^3 \pm 0.3 \times 10^3$
R^2	0	0	0

Literature values vary between 10^2 and 10^6 Pas (Section 1.5.5.3). Figure 3.2 demonstrates that the value reported is highly dependent upon the strain rate at which the viscosity is measured. (The R^2 value of 0, is expected as the Newtonian constitutive equation is independent of $\dot{\gamma}$).

3.5.2. Power Law

$$\eta(\dot{\gamma}) = K\dot{\gamma}^{n-1} \tag{3.23}$$

See Section 1.5.5.5.

Dough	Epic Short Mix	Epic Long Mix	Halo
K [Pa s^n]	$2.70 \times 10^4 \pm 0.07 \times 10^4$	$4.99 \times 10^4 \pm 0.08 \times 10^4$	$0.91 \times 10^4 \pm 0.01 \times 10^4$
n	0.209 ± 0.009	0.203 ± 0.006	0.270 ± 0.004
R^2	0.996	0.998	0.998

Literature values vary between 0.2 and 0.4 for n and between 2×10^3 and 5×10^5 Pa s^n, for K (Section 1.5.5.5).

3.5.3. Maxwell

$$\eta^*(\omega) = \frac{\eta_1}{1+(\lambda_1\omega)^2}\sqrt{1+(\omega\lambda_1)^2} \tag{3.24}$$

See Section 1.5.5.8.

Dough	Epic Short Mix	Epic Long Mix	Halo
η_1 [Pas]	$10 \times 10^5 \pm 2 \times 10^5$	$17 \times 10^5 \pm 4 \times 10^5$	$1.1 \times 10^5 \pm 0.2 \times 10^5$
λ_1 [s]	45 ± 14	42 ± 12	13 ± 3
R^2	0.934	0.943	0.875

Typical literature values are around 10^4 Pa s, for η_1, and 15 s, for λ_1 (Section 1.5.5.8).

3.5.4. Generalised Maxwell

$$\eta^*(\omega) = \sum_n \frac{\eta_n}{1+(\lambda_n\omega)^2}\sqrt{1+(\omega\lambda_n)^2} \tag{3.25}$$

See Section 1.5.5.9.

Using a six parameter expansion, with the constraints:

$$\lambda_n > 0 \tag{3.26}$$

$$\lambda_n > \lambda_{n+1} \tag{3.27}$$

Dough	Epic Short Mix	Epic Long Mix	Halo
η_1 [Pa s]	$31 \times 10^5 \pm 14 \times 10^5$	$59 \times 10^5 \pm 25 \times 10^5$	$4.1 \times 10^5 \pm 0.6 \times 10^5$
λ_1 [s]	320 ± 180	330 ± 170	120 ± 20
η_2 [Pa s]	$10 \times 10^4 \pm 4 \times 10^4$	$20 \times 10^4 \pm 7 \times 10^4$	$1.0 \times 10^4 \pm 0.2 \times 10^4$
λ_2 [s]	9 ± 4	10 ± 3	1.7 ± 0.3
η_3 [Pa s]	$6 \times 10^3 \pm 2 \times 10^3$	$12 \times 10^3 \pm 3 \times 10^3$	$0.7 \times 10^3 \pm 0.1 \times 10^3$
λ_3 [s]	0.27 ± 0.13	0.3 ± 0.1	0.03 ± 0.01
R^2	0.996	0.998	0.996

3.5.5. CEF Equation

$$\eta(\dot{\gamma}) = K_1\dot{\gamma}^{n-1} \tag{3.28}$$

(Note this is identical to the Power Law Constitutive Equation).

Dough	Epic Short Mix	Epic Long Mix	Halo
K [Pa s^n]	$2.70 \times 10^4 \pm 0.07 \times 10^4$	$4.99 \times 10^4 \pm 0.08 \times 10^4$	$0.91 \times 10^4 \pm 0.01 \times 10^4$
n	0.209 ± 0.009	0.203 ± 0.006	0.270 ± 0.004
R^2	0.996	0.998	0.998

$$\Psi_1(\dot{\gamma}) = K_2\dot{\gamma}^{m-2} \tag{3.29}$$

Dough	Epic Short Mix	Epic Long Mix	Halo
K_2 [Pas^n]	$18.5 \times 10^4 \pm 0.8 \times 10^4$	$36 \times 10^4 \pm 1 \times 10^4$	$4.74 \times 10^4 \pm 0.08 \times 10^4$
m	0.25 ± 0.01	0.25 ± 0.01	0.230 ± 0.007
R^2	0.991	0.995	0.995

In general, it can be seen that the Halo dough is distinct from the other two doughs, which are less distinguishable from one another. As expected, power-law type expressions seem adequately to fit the data, as does the generalised Maxwell expression (with six parameters).

3.6. Summary of Dough Properties

It was possible to measure some steady state rheological properties of the three dough types. The doughs behaved as pseudoplastic materials in the strain rate of range of about 0.0002 s^{-1} to 1 s^{-1}, with a Newtonian plateau at lower strain rates. It was possible to measure some dynamic rheological properties, which indicated that dough can behave as a weak gel. These dynamic and steady state properties did not correspond to each other according to the Cox-Merz rule. This may be because the structure of the dough changes as it is measured.

The properties of Halo dough were distinguishable from those of Epic dough. It was not easy to distinguish between Epic doughs that had been mixed to give slightly different work inputs. The rheological properties were used to fit parameters for constitutive equations. In general, constitutive equations with a power-law dependency of properties upon strain rate gave better fits, as did constitutive equations with a large number of parameters, such as the Generalised Maxwell equation.

4. Modelling Approaches

Various approaches can be used to model the sheeting operation. Metal sheeting has been modelled using a friction coefficient model, and this is applied to the dough sheeting problem in this chapter. Polymer calendaring, and the existing fundamental models of dough sheeting, are solved using a continuum mechanics model in which the operation is described as a shear flow. An expansion of this type of model is developed in Chapter 5. Alternatives to the traditional continuum mechanics, a friction coefficient model and a compression model, are examined here in Chapter 4.

4.1. Friction Coefficient Model

Some models of sheet metal forming establish a maximum possible inlet size of the sheet, based on the friction coefficient between the sheet and the roller surface (Lange, 1985). This model may be applied to bread dough sheeting as well.

4.1.1. Theory

A piece of material will move if the applied force is greater than the friction force preventing movement, as illustrated in Figure 4.1.

Figure 4.1 Friction Coefficient Model Concept

The friction force preventing movement can be calculated from Coulomb's friction law, which states that:

$$F_{FR} = \mu F_N = \mu g m \qquad (4.1)$$

where: F_{FR} is the friction force [N]; μ is the friction coefficient, F_N is the normal force [N], g is the acceleration due to gravity (9.81 m s^{-2}) and m is the mass of the material [kg].

4.1.2. Experimental

A sample of dough was mixed using a 50 g dough mixer at Crop and Food Research Ltd, Palmerston North. The dough was made according to the Epic: short mix recipe, given in Chapter 2. The dough was placed on a platform made of the same material as the sheeter rollers, that is, 304 Stainless Steel with Brushed Finish #4.

The slope of the platform was increased until the dough sample started to move down the platform (Figure 4.1). From the slope, the value of μ, the friction coefficient, can be calculated (equations 4.2 to 4.4).

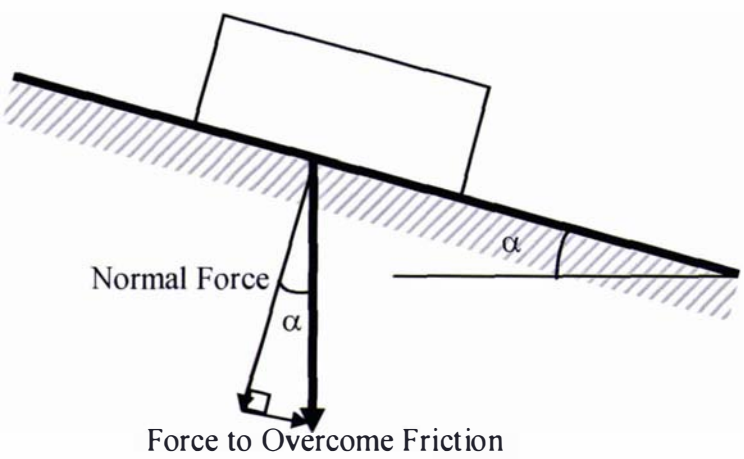

Figure 4.2 Dough sliding along platform.

$$F_{FR} = \mu F_N \tag{4.2}$$

$$mg\sin(\alpha) = \mu mg\cos(a) \tag{4.3}$$

$$\mu = \tan(\alpha) \tag{4.4}$$

4.1.3. Results

It was found that the angle, α, at which the dough began to move, was 46° ± 2°, for a thin sheet of dough (around 5mm thick) resting on the steel surface. This gives a friction coefficient of 1.04 ± 0.07. The angle for a ball or sausage shaped piece of dough was less (20° ± 2°), with a friction coefficient of 0.36 ± 0.04. Finally if the angle of the platform was lowered until the thin sheet of dough ceased to move instead of being raised until the dough began to move then the angle, α, measured was about 37°: a friction coefficient of 0.75.

4.1.4. Discussion

The difference in the values of α with shape is due to the fact that the ball and sausage shaped samples were overbalancing and tumbling down the surface rather than sliding along the surface. This was observed to happen. The values of α measured in this way are not true values.

The friction coefficient measured for the thin sheet is more suitable for application to dough sheeting, as it is a truer measurement of the friction coefficient for material sliding along a surface.

The decreased angle observed if the platform was lowered until the dough ceased to move (instead of being raised until the dough began to move) is expected. It is well known that the static friction coefficient (representing the force required to start moving a sample) is greater than the kinematic friction coefficient (representing the force required to keep a sample, already in motion, moving). The lower value observed when the platform was being lowered is the kinematic friction coefficient.

4.1.5. Application to Sheeting

One way in which measurements of the friction coefficient can be applied to sheeting is to estimate the maximum thickness of initial sheet that can be sheeted. Figure 4.3 describes the beginning of the sheeting process.

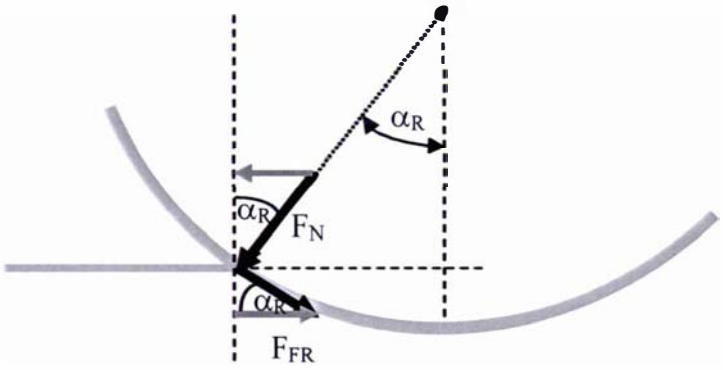

Figure 4.3 Forces acting at sheet inlet.

For the dough to be drawn into the sheeter the horizontal component of the friction force must exceed the horizontal component of the normal force.

$$\cos(\alpha_R)F_{FR} \geq \sin(\alpha_R)F_N \qquad (4.5)$$

$$F_{FR} \geq \tan(\alpha_R) F_N \tag{4.6}$$

From Coulombs Friction Law:

$$F_{FR} = \mu F_N \tag{4.7}$$

Therefore:

$$\mu \geq \tan(\alpha_R) \tag{4.8}$$

$$\alpha_R \leq \tan^{-1}(\mu) \tag{4.9}$$

The angle at which the dough contacts the roller, α_R, can be related to the reduction ratio, Θ, and the nip gap to roller radius ratio, ε^2:

$$\cos(\alpha_R) = \varepsilon^2\left(1 + \frac{1}{\varepsilon^2} - \Theta\right) \tag{4.10}$$

$$\varepsilon^2\left(1 + \frac{1}{\varepsilon^2} - \Theta\right) \geq \cos\left(\tan^{-1}(\mu)\right) \tag{4.11}$$

$$\Theta \leq \frac{1 + \varepsilon^2 - \cos\left(\tan^{-1}(\mu)\right)}{\varepsilon^2} \tag{4.12}$$

Equation (4.12) is plotted below for a value of $\mu = 1.04$. A second line is also plotted (for a value of $\mu = 2$).

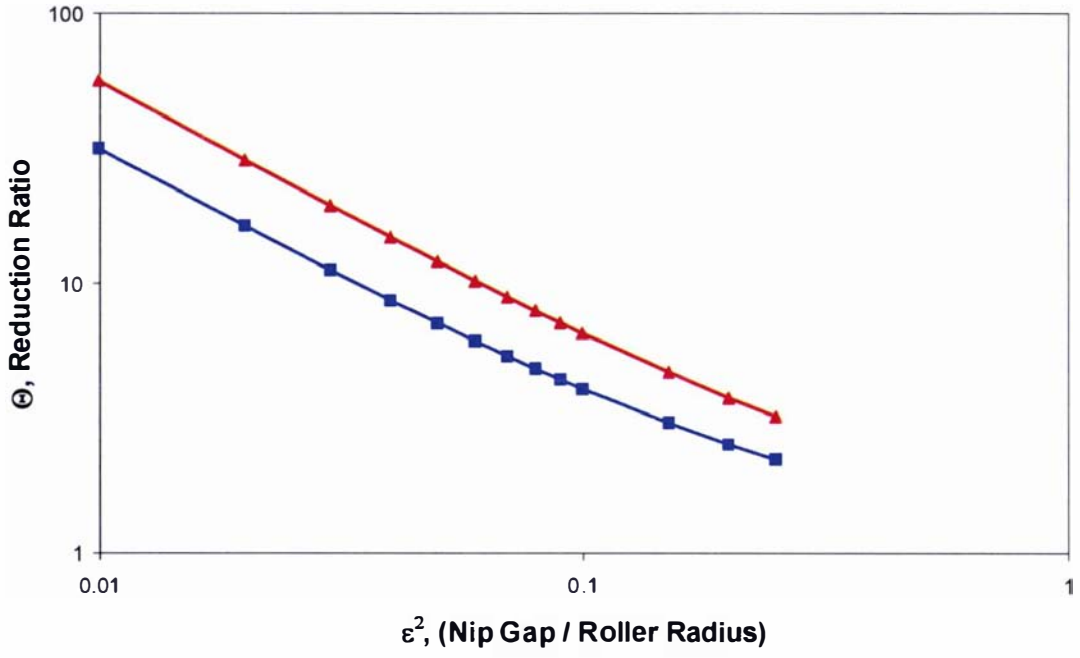

Figure 4.4 Maximum Reduction Ratio vs Epsilon. Blue squares represent a friction coefficient of 1.04, red triangles a friction coefficient of 2.

Figure 4.4 demonstrates that if the friction coefficient is increased, for example by using a rougher roller surface, then a sheet of greater initial thickness can be passed through the sheeter.

4.1.6. Validation

An attempt was made to confirm that there was a maximum reduction ratio that could be successfully sheeted. It was found that the only limit on the maximum inlet height that could be sheeted was the size of the rollers; if the sheet was larger than the nip gap plus the radius of the roller then there were difficulties sheeting. This suggests that either the friction coefficient during sheeting is greater than was measured or the model is incorrect.

It was observed that the dough recirculates behind the rollers when large inlet heights are used. Two modes were observed, which are illustrated in Figure 4.5.

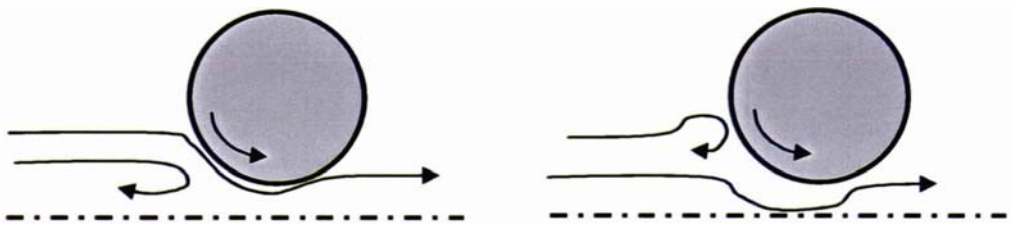

Figure 4.5 Two modes by which dough appeared to recirculate behind the rollers. a) recirculation occurs near the line of symmetry. b) recirculation occurs near (or at) the inlet surface.

The difference between the two modes lies in where the recirculation region occurs. The second mode, where the dough recirculates at the inlet surface, dominated at large inlet heights. Perhaps, the occurrence of the recirculation region allows a sheet of a larger height to be sheeted than is suggested by the friction coefficient model. This could be investigated in future work.

The maximum inlet height, according to the friction coefficient model, is close to the maximum practical limit for sheeting. It is not usual to sheet very large reductions with (relatively) small rollers. It was noticed during experimental work that large reduction ratios with small rollers often resulted in sheets that tear.

4.2. Simple Compression Model in Y Axis

4.2.1. Concept

The traditional models of dough sheeting model the sheeting operation as a shear flow in the *x-axis*. Another possibility is to consider the sheeter system as a simple compression in the *y-axis*. In this model the sheeting process consists of two steps. In the first step the dough is under a constant downwards stress. This represents the process material (dough) passing under the rollers. At a time t_1 the process material is released, that is leaves the rollers, and springs back into shape.

In this section an important concept that is used is the elongation rate, $\dot{l}$ [s^{-1}]. In this model the dough is described as being in a simple elongation (or compression). For a simple elongation:

$$\frac{\partial v}{\partial y} = \dot{l} \tag{4.13}$$

where v is the component of velocity in the y direction [m s^{-1}].

Rearranging 4.13 and integrating gives the following expression for the y velocity component (given the boundary condition that at $y = 0$, $v = 0$):

$$v = \dot{l}y \tag{4.14}$$

The y component of velocity is defined as:

$$v = \frac{\partial y}{\partial t} \tag{4.15}$$

Therefore:

$$\frac{\partial y}{y} = \dot{l}\partial t \tag{4.16}$$

$$\int \frac{dy}{y} = \int \dot{l}dt \tag{4.17}$$

$$\ln y = l + C \tag{4.18}$$

Given the boundary condition that at $t = 0$, $l = 0$ and $y = y_0$, then:

$$y = y_0 e^{l} \tag{4.19}$$

Equation 4.14 and 4.19 will be useful later.

4.2.2. Model Development

4.2.2.1. Step One: $t < t_1$

The process material is under a constant stress, σ_0, from $t = 0$ to $t = t_1$. This is the first boundary condition. The only velocity is v, the y component of the velocity. It is a simple function of the elongation rate, $\dot{l}$ (Equation 4.14). The elongation rate will be negative, as the process material is undergoing compression. At $t = 0$, $y = h_i$ and at $t = t_1$, $y = \delta$.

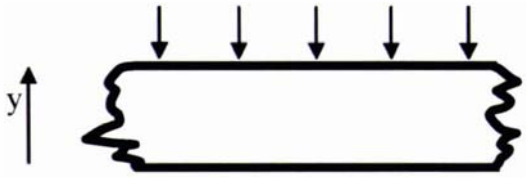

Figure 4.6 Compression Model : Step One.

4.2.2.2. Step Two: $t > t_1$

The stress is removed as the process material leaves the sheeter at the nip height, δ. The second boundary condition is that $\sigma = 0$, when $t > t_1$. Also at time t_1, the height of the process material is δ. The objective of the model is to calculate the final elongation of the process material, that is, the value of l at $t = \infty$. The exit height of the process material can be calculated from the formula (derived from Equation 4.19):

$$h = \delta e^{l(t)} \tag{4.20}$$

4.2.2.3. Constitutive Equation

In order to solve the model, it is necessary to choose a constitutive equation that describes how the process material deforms when an elongation is applied. The model will be solved using three constitutive equations: the Newtonian, the Maxwell and the Jeffrey's. These equations are used for simplicity of calculation. It should be noted, once again, that none of these constitutive equations are a realistic model of dough, although the Maxwell equation captures more of the dough's properties, than the Newtonian, and the Jeffrey's equation more than the Maxwell.

Newtonian Constitutive Equation

$$\sigma_{yy} = -\eta \dot{l}_{yy} \tag{4.21}$$

Maxwell Constitutive Equation

$$\sigma_{yy} + \lambda_1 \dot{\sigma}_{yy} = -\eta \dot{l}_{yy} \tag{4.22}$$

Using Jeffrey's Equation

$$\sigma_{yy} + \lambda_1 \dot{\sigma}_{yy} = -\eta\left(\dot{l}_{yy} + \lambda_2 \ddot{l}_{yy}\right) \tag{4.23}$$

Note: that only the $_{yy}$th components of the stress tensors are being considered.

It is also noted that the Newtonian constitutive equation is a special case of the Maxwell, when $\lambda_1 = 0$. Similarly the Maxwell constitutive equation is a special case of the Jeffrey's, when $\lambda_2 = 0$. Thus in the following solution the Jeffrey's equation will be used, and the Maxwell and Newtonian solutions simply derived at the end.

4.2.3. Model Solution

4.2.3.1. Laplace Transform

Taking the Laplace transform of the stress, and using the two boundary conditions, that at $t < t_1$, $\sigma = \sigma_0$ and at $t > t_1$, $\sigma = 0$, gives:

$$\bar{\sigma}_{yy} = \int_0^{\infty} e^{-st}\sigma_{yy}\,dt = \int_0^{t_1} e^{-st}\sigma_0\,dt + \int_{t_1}^{\infty} e^{-st}\,0\,dt = \frac{\sigma_0}{s}\left(1 - e^{-st_1}\right) \tag{4.24}$$

The Laplace transform of the Jeffrey's constitutive equation can be written as:

$$\bar{\sigma}_{yy} + \lambda_1\left(s\bar{\sigma}_{yy} - \sigma_0\right) = -\eta\left(s\bar{l}_{yy} - l_0 + \lambda_2\left(s\left(s\bar{l}_{yy} - l_0\right) - \dot{l}_0\right)\right) \tag{4.25}$$

$$\bar{\sigma}_{yy} + \lambda_1\left(s\bar{\sigma}_{yy} - \sigma_0\right) = -\eta\left(\left(s\bar{l}_{yy} - l_0\right)\left(1 + s\lambda_2\right) - \lambda_2\dot{l}_0\right) \tag{4.26}$$

Substituting (4.26) into (4.24) gives:

$$\frac{\sigma_0}{s}\left(1 - e^{-st_1}\right) - \sigma_0\lambda_1 e^{-st_1} = -\eta s\bar{l}_{yy}\left(1 + \lambda_2 s\right) + \eta l_0\left(1 + \lambda_2 s\right) + \eta\lambda_2\dot{l}_0 \tag{4.27}$$

or:

$$\bar{l}_{yy} = \frac{\sigma_0\lambda_1}{\eta s\left(1 + \lambda_2 s\right)}e^{-st_1} - \frac{\sigma_0}{\eta s^2\left(1 + \lambda_2 s\right)}\left(1 - e^{-st_1}\right) + \frac{l_0}{s} + \frac{\lambda_2\dot{l}_0}{s\left(1 + \lambda_2 s\right)} \tag{4.28}$$

or:

$$\bar{l}_{yy} = \frac{l_0}{s} + \frac{\dot{l}_0}{s\left(s + \frac{1}{\lambda_2}\right)} + \frac{\sigma_0}{\eta\lambda_2}\left(\frac{\lambda_1 e^{-st_1}}{s\left(s + \frac{1}{\lambda_2}\right)} - \frac{1 - e^{-st_1}}{s^2\left(s + \frac{1}{\lambda_2}\right)}\right) \tag{4.29}$$

Then taking the inverse Laplace transform:

$$l_{yy} = \begin{cases} l_o + \lambda_2 \dot{l}_o \left(1 - e^{-\frac{t}{\lambda_2}}\right) - \dfrac{\sigma_0}{\eta}\left(t - \lambda_2\left(1 - e^{-\frac{t}{\lambda_2}}\right)\right) & ,\forall t < t_1 \\ l_o + \lambda_2 \dot{l}_o \left(1 - e^{-\frac{t}{\lambda_2}}\right) - \dfrac{\sigma_0}{\eta}\left(t_1 - \lambda_1\left(1 - e^{\frac{t_1 - t}{\lambda_2}}\right) + \lambda_2 e^{\frac{-t}{\lambda_2}}\left(1 - e^{\frac{t_1}{\lambda_2}}\right)\right) & ,\forall t > t_1 \end{cases} \tag{4.30}$$

for the Maxwell equation:

$$l_{yy} = \begin{cases} l_o - \dfrac{\sigma_0}{\eta} t & ,\forall t < t_1 \\ l_o + \dfrac{\sigma_0}{\eta}(\lambda_1 - t_1) & ,\forall t > t_1 \end{cases} \tag{4.31}$$

for the Newtonian equation:

$$l_{yy} = \begin{cases} l_0 - \dfrac{\sigma_0}{\eta} t & ,\forall t < t_1 \\ l_0 - \dfrac{\sigma_0}{\eta} t_1 & ,\forall t > t_1 \end{cases} \tag{4.32}$$

The problem is essentially solved at this point. The elongation can be calculated, and hence the height of the dough (4.20). However an estimate of the initial stress, elongation and elongation rate is still required.

4.2.3.2. Estimation of initial stress, elongation and elongation rate

The initial stress has to be estimated. It has already been assumed that the initial stress is a constant when $t < t_1$. It can also be assumed that the elongation rate is a constant when $t < t_1$. Therefore, examining the Jeffrey's constitutive equation gives:

$$\sigma_0 = -\eta \dot{l}_0 \tag{4.33}$$

It is known that at $t = 0$, the value of $y = h_i$, the inlet height of the process material. Therefore, using (4.20), it can be seen that:

$$l_0 = \ln\left(\frac{h_i}{\delta}\right) \tag{4.34}$$

It is also known that at $t = t_1$, the value of $y = \delta$, the nip gap of the sheeting system. Therefore the elongation rate can be estimated as:

$$\dot{l}_0 \approx \frac{\ln\left(\frac{\delta}{\delta}\right) - \ln\left(\frac{h_i}{\delta}\right)}{t_1} = -\frac{1}{t_1}\ln\left(\frac{h_i}{\delta}\right) \tag{4.35}$$

and finally:

$$\sigma_0 = \frac{\eta}{t_1}\ln\left(\frac{h_i}{\delta}\right) \tag{4.36}$$

These can be substituted into the model solutions:

Jeffrey's Model

$$l_{yy} = \begin{cases} \ln\left(\frac{h_i}{\delta}\right)\left(1-\frac{t}{t_1}\right) & ,\forall t < t_1 \\ \frac{\lambda_1-\lambda_2}{t_1}\ln\left(\frac{h_i}{\delta}\right)\left(1-e^{\frac{t_1-t}{\lambda_2}}\right) & ,\forall t > t_1 \end{cases} \tag{4.37}$$

for the Maxwell equation:

$$l_{yy} = \begin{cases} \ln\left(\frac{h_i}{\delta}\right)\left(1-\frac{t}{t_1}\right) & ,\forall t < t_1 \\ \frac{\lambda_1}{t_1}\ln\left(\frac{h_i}{\delta}\right) & ,\forall t > t_1 \end{cases} \tag{4.38}$$

for the Newtonian equation:

$$l_{yy} = \begin{cases} \ln\left(\frac{h_i}{\delta}\right)\left(1-\frac{t}{t_1}\right) & ,\forall t < t_1 \\ 0 & ,\forall t > t_1 \end{cases} \tag{4.39}$$

4.2.4. Application

Figure 4.7 shows an example of deformation ratio vs time for the Jeffrey's, Maxwell and Newtonian models. Until $t > t_1$ the three models are identical, this corresponds to the period which the dough is underneath the roller. At $t = t_1$, the dough is released from under the roller. The Newtonian model undergoes no further deformation, that is the height of the dough is the gap between the rollers. This is different to the *shear* model of sheeting in which the exit height is about 1.22 times the nip gap (Middleman, 1977). The Maxwell model instantly jumps to a new height as the dough leaves the roller and the Jeffrey's model slowly increases to a (different) new height over time. The exit height which the Maxwell and Jeffrey's models predict is obviously dependent upon the values of t_1, λ_1, λ_2, h_i and δ.

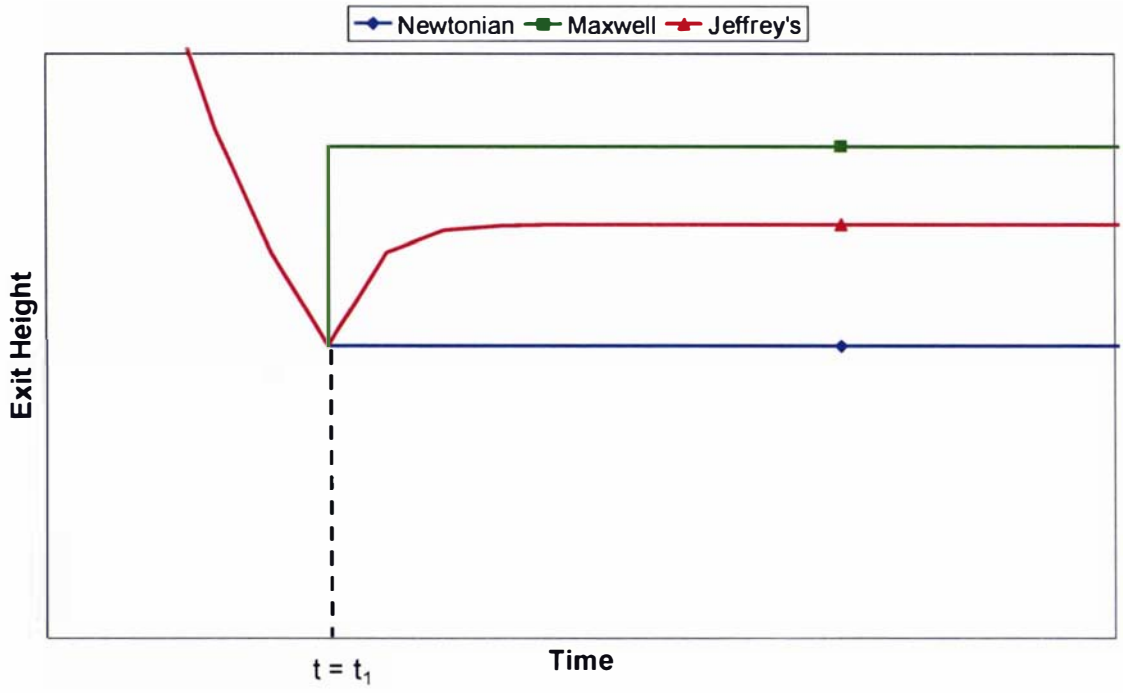

Figure 4.7 Compression Model : Newtonian (blue diamonds), Maxwell (green squares) and Jeffrey's (red triangles) model responses, for arbitrary parameters.

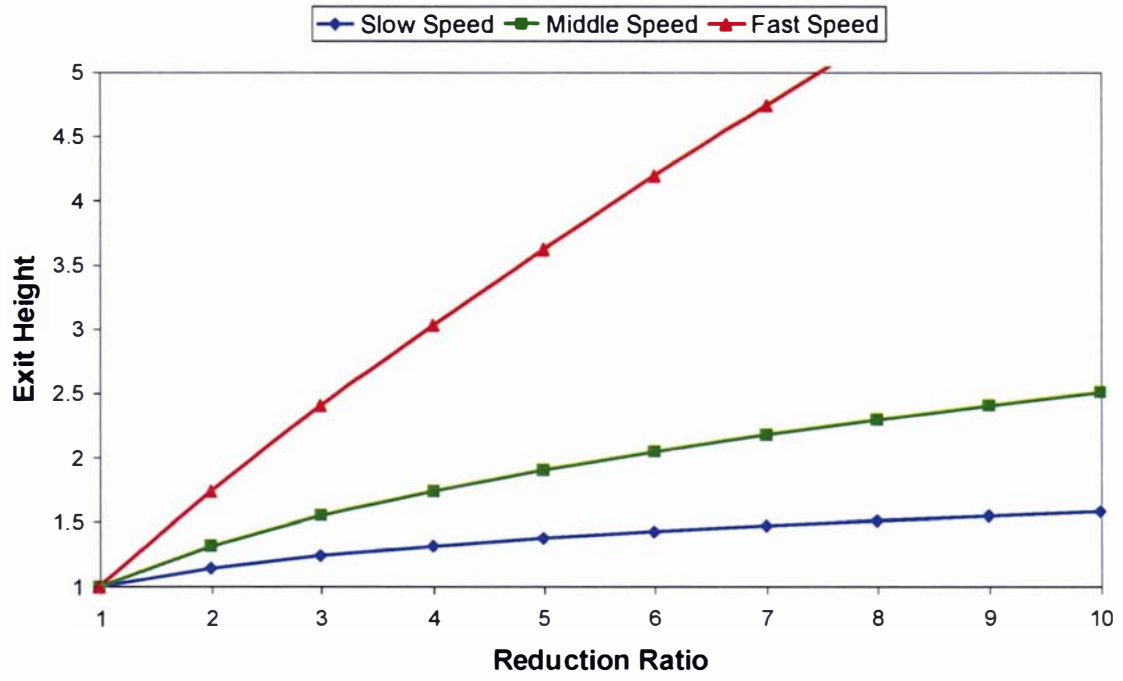

Figure 4.8 Compression Model (Jeffrey's) : Variable Speed Response.

It can also be shown (Figure 4.8) that as the speed increases (hence as t_1 decreases), the exit height increases, for the Jeffrey's model. This trend is consistent with the experimental result that the deformation ratio decreases with speed (Section 2.6.5.2.1).

4.3. Summary

The friction coefficient model suggests that there is a limit to the thickness of sheet which can be processed by a given sheeting system, although (due to the properties of the dough) this limit is not likely to be practically encountered. It was also found that other factors, for example dough tearing, may pose a bigger limit than the friction coefficient prediction, upon the maximum sheet thickness. The simple compression model captures some physical aspects of the sheeting system, for example it predicts that viscoelastic doughs will leave the sheeter with a greater thickness than a purely viscous dough. The compression model also makes the experimentally confirmed prediction that increasing roller speed will increase the height of the sheet leaving the sheeter. These two models do give a qualitative description of some aspects of the sheeting system, but neither the friction coefficient model nor the compression model completely describes the dough sheeting operation.

5. Development of a Viscoelastic Sheeting Model

5.1. Continuum Mechanics

Continuum mechanics is a paradigm that can be used to describe the velocity, pressure and temperature profiles of a system. The primary tools are mass, momentum and energy balances performed over a small, but non-zero, volume. The most important assumption is that the system can be described, in the area of interest, by smooth, differentiable functions. That is, the material properties of the system are assumed to be continuous.

Bread dough does not have a continuous structure. At even quite a coarse scale dough contains at least three regions of different properties: the gluten network, the starch solution and gas pockets. A condition for the continuum mechanics model to be valid is that the macroscopic lengths in the system being described must be significantly greater than the scale at which the material becomes non-continuous.

For the bread dough sheeting problem the smallest macroscopic length is the nip gap, $\hat{\delta}$, which could be as small as 1mm. Structural features, for example air pockets, can be seen in the bread dough at a scale of around 100 μm (Zheng, 1998). Therefore, in terms of volumes, the smallest macroscopic scale of the system is 1×10^{-9} m^3, while the structure has a scale of 1×10^{-12} m^3. As the macroscopic scale of the system under investigation is several orders of magnitude greater than the scale at which the material ceases to be continuous it is valid to use the continuum mechanics model to describe the system.

Additionally it was assumed that the problem was two dimensional, was at steady state, had neither inertial, gravitational, nor energy terms and involved an incompressible process material. The validity of these assumptions, for the dough sheeting problem, has already been discussed in Sections 1.5 and 1.6. The basic continuum mechanics

equations to describe the sheeting problem are given below (Bird et al., 1987). In these equations, and all equations used in this chapter, a variable marked with a ^ is a variable *with* dimensions. A variable without such a mark is a dimensionless variable.

$$\frac{\partial}{\partial \hat{x}}[\hat{u}]+\frac{\partial}{\partial \hat{y}}[\hat{v}]=0 \tag{5.1}$$

$$\frac{\partial}{\partial \hat{x}}[\hat{p}-\hat{p}_a]=-\left(\frac{\partial}{\partial \hat{x}}[\hat{\tau}_{xx}]+\frac{\partial}{\partial \hat{y}}[\hat{\tau}_{xy}]\right) \tag{5.2}$$

$$\frac{\partial}{\partial \hat{y}}[\hat{p}-\hat{p}_a]=-\left(\frac{\partial}{\partial \hat{x}}[\hat{\tau}_{xy}]+\frac{\partial}{\partial \hat{y}}[\hat{\tau}_{yy}]\right) \tag{5.3}$$

In order to confirm compliance with the boundary conditions it was also necessary to calculate the stress normal to the roller surface. This is given by:

$$\mathbf{T}_n^{(n)} = \hat{p}+\hat{\tau}_{xx}\sin^2(\theta)+\hat{\tau}_{yy}\cos^2(\theta)-2\hat{\tau}_{xy}\sin(\theta)\cos(\theta) \tag{5.4}$$

Finally, to allow comparison with the experimental data it was required to solve for the total upward force, $\hat{F}_y$, on the roller and the total torque, $\hat{M}$, on the roller. These are given by the following equations (whose derivations are given in Appendix B): Note: $\hat{W}$ is the width of the roller, in the $\hat{z}$ direction.

$$\frac{\sum \hat{F}_y}{\hat{W}} = \int_{\hat{x}_i}^{\hat{x}_e}\left[\hat{\tau}_{xy}\tan(\theta)-\left(\hat{p}+\hat{\tau}_{yy}\right)\right]d\hat{x} \tag{5.5}$$

$$\frac{\sum \hat{M}}{\hat{W}} = \hat{R}\int_{\hat{x}_i}^{\hat{x}_e}\left[\left(\hat{\tau}_{xx}-\hat{\tau}_{yy}\right)\sin(\theta)+\hat{\tau}_{xy}\left(\tan(\theta)\sin(\theta)-\cos(\theta)\right)\right]d\hat{x} \tag{5.6}$$

5.2. CEF Constitutive Equation

A constitutive equation, describing how the process material (dough) deforms, was required in order to solve the continuum mechanics problem. The constitutive equation relates the stress tensor, $\hat{\boldsymbol{\tau}}$, to the strain tensor, $\hat{\boldsymbol{\gamma}}$. The Criminale-Ericksen-Filbey constitutive equation (mentioned, briefly, in Chapter 3) has been used to describe viscoelastic, polymer materials in flow conditions close to steady state (Bird et al., 1987). This constitutive equation, despite not being the most realistic model possible for dough, was chosen because it is less mathematically complex than more realistic alternatives (Phan-Than et al., for example). The relative simplicity of the CEF equation means that the effect of viscoelasticty upon dough sheeting can be studied

without too many computational difficulties. Also, from a pragmatic perspective, the material property parameters for the CEF equation, unlike those for alternative constitutive equations, are easy and quick to determine with a simple rheometer. The CEF equation can be written as:

$$\hat{\boldsymbol{\tau}} = -\hat{\eta}\hat{\boldsymbol{\gamma}}_{(1)} + \tfrac{1}{2}\hat{\Psi}_1\hat{\boldsymbol{\gamma}}_{(2)} - \hat{\Psi}_2\left\{\hat{\boldsymbol{\gamma}}_{(1)} \bullet \hat{\boldsymbol{\gamma}}_{(1)}\right\} \tag{5.7}$$

Where:

$$\hat{\boldsymbol{\gamma}}_{(1)} = \hat{\dot{\boldsymbol{\gamma}}} = \nabla\hat{\mathbf{v}} + (\nabla\hat{\mathbf{v}})^t \tag{5.8}$$

$$\hat{\boldsymbol{\gamma}}_{(2)} = \frac{\partial}{\partial t}\left[\hat{\boldsymbol{\gamma}}_{(1)}\right] + \left(\mathbf{v} \bullet \nabla\hat{\boldsymbol{\gamma}}_{(1)}\right) - \left\{(\nabla\mathbf{v})^t \bullet \hat{\boldsymbol{\gamma}}_{(1)} + \hat{\boldsymbol{\gamma}}_{(1)} \bullet (\nabla\hat{\mathbf{v}})\right\} \tag{5.9}$$

It is usual to write the viscoelastic parameters, $\hat{\eta}$, $\hat{\Psi}_1$ and $\hat{\Psi}_2$, as power-law type functions of $\hat{\dot{\gamma}}$, but for this solution they were assumed to be constants. This simplified calculations whilst still allowing for the effect of viscoelasticity to be studied.

5.3. Perturbation Technique

The CEF constitutive equation 5.7 was substituted into the general continuum mechanics equations [5.1, 5.2, 5.3]:

$$\frac{\partial}{\partial\hat{x}}[\hat{u}] + \frac{\partial}{\partial\hat{y}}[\hat{v}] = 0 \tag{5.10}$$

$$\begin{aligned}\frac{\partial}{\partial\hat{x}}[\hat{p} - \hat{p}_a] = {} & \frac{\hat{\Psi}_1}{2}\left[\begin{array}{l}\dfrac{\partial\hat{u}}{\partial\hat{x}}\left(3\dfrac{\partial^2\hat{u}}{\partial\hat{x}^2} - \dfrac{\partial^2\hat{u}}{\partial\hat{y}^2}\right) + \dfrac{\partial\hat{u}}{\partial\hat{y}}\left(\dfrac{\partial^2\hat{u}}{\partial\hat{x}\partial\hat{y}} + \dfrac{\partial^2\hat{v}}{\partial\hat{x}^2}\right) + 2\dfrac{\partial\hat{v}}{\partial\hat{x}}\dfrac{\partial^2\hat{u}}{\partial\hat{x}\partial\hat{y}} \\ -\hat{u}\left(\dfrac{\partial^3\hat{u}}{\partial\hat{x}^3} + \dfrac{\partial^3\hat{u}}{\partial\hat{x}\partial\hat{y}^2}\right) - \hat{v}\left(\dfrac{\partial^3\hat{u}}{\partial\hat{y}^3} + \dfrac{\partial^3\hat{u}}{\partial\hat{x}^2\partial\hat{y}}\right)\end{array}\right] \\ & + 2\hat{\Psi}_2\left[4\frac{\partial\hat{u}}{\partial\hat{x}}\frac{\partial^2\hat{u}}{\partial\hat{x}^2} + \left(\frac{\partial\hat{u}}{\partial\hat{y}} + \frac{\partial\hat{v}}{\partial\hat{x}}\right)\left(\frac{\partial^2\hat{u}}{\partial\hat{x}\partial\hat{y}} + \frac{\partial^2\hat{v}}{\partial\hat{x}^2}\right)\right] \\ & + \hat{\eta}\left[\frac{\partial^2\hat{u}}{\partial\hat{y}^2} + \frac{\partial^2\hat{u}}{\partial\hat{x}^2}\right]\end{aligned} \tag{5.11}$$

$$\begin{aligned}\frac{\partial}{\partial\hat{y}}[\hat{p} - \hat{p}_a] = {} & \frac{\hat{\Psi}_1}{2}\left[\begin{array}{l}\dfrac{\partial\hat{v}}{\partial\hat{y}}\left(3\dfrac{\partial^2\hat{v}}{\partial\hat{y}^2} - \dfrac{\partial^2\hat{v}}{\partial\hat{x}^2}\right) + \dfrac{\partial\hat{v}}{\partial\hat{x}}\left(\dfrac{\partial^2\hat{v}}{\partial\hat{x}\partial\hat{y}} + \dfrac{\partial^2\hat{u}}{\partial\hat{y}^2}\right) + 2\dfrac{\partial\hat{u}}{\partial\hat{y}}\dfrac{\partial^2\hat{v}}{\partial\hat{x}\partial\hat{y}} \\ -\hat{v}\left(\dfrac{\partial^3\hat{v}}{\partial\hat{y}^3} + \dfrac{\partial^3\hat{v}}{\partial\hat{x}^2\partial\hat{y}}\right) - \hat{u}\left(\dfrac{\partial^3\hat{v}}{\partial\hat{x}^3} + \dfrac{\partial\hat{v}}{\partial\hat{x}\partial\hat{y}^2}\right)\end{array}\right] \\ & + 2\hat{\Psi}_2\left[4\frac{\partial\hat{v}}{\partial\hat{y}}\frac{\partial^2\hat{v}}{\partial\hat{y}^2} + \left(\frac{\partial\hat{v}}{\partial\hat{x}} + \frac{\partial\hat{u}}{\partial\hat{y}}\right)\left(\frac{\partial^2\hat{v}}{\partial\hat{x}\partial\hat{y}} + \frac{\partial^2\hat{u}}{\partial\hat{y}^2}\right)\right] \\ & + \hat{\eta}\left[\frac{\partial^2\hat{v}}{\partial\hat{y}^2} + \frac{\partial^2\hat{v}}{\partial\hat{x}^2}\right]\end{aligned} \tag{5.12}$$

In order to establish compliance with inlet and exit boundary conditions, and to calculate the force and torque exerted on the rollers, it was also necessary to calculate the stress components:

$$\hat{\tau}_{yy} = -2\hat{\eta}\frac{\partial \hat{v}}{\partial \hat{y}} - \hat{\Psi}_1\left[2\left(\frac{\partial \hat{v}}{\partial \hat{y}}\right)^2 + \frac{\partial \hat{v}}{\partial \hat{x}}\left(\frac{\partial \hat{v}}{\partial \hat{x}} + \frac{\partial \hat{u}}{\partial \hat{y}}\right) - \hat{v}\frac{\partial^2 \hat{v}}{\partial \hat{y}^2} - \hat{u}\frac{\partial^2 \hat{v}}{\partial \hat{y}\partial \hat{x}}\right] - \hat{\Psi}_2\left[4\left(\frac{\partial \hat{v}}{\partial \hat{y}}\right)^2 + \left(\frac{\partial \hat{v}}{\partial \hat{x}} + \frac{\partial \hat{u}}{\partial \hat{y}}\right)^2\right] \tag{5.13}$$

$$\hat{\tau}_{xy} = -\hat{\eta}\left(\frac{\partial \hat{v}}{\partial \hat{x}} + \frac{\partial \hat{u}}{\partial \hat{y}}\right) - \frac{\hat{\Psi}_1}{2}\left[2\frac{\partial \hat{u}}{\partial \hat{y}}\frac{\partial \hat{v}}{\partial \hat{y}} + 2\frac{\partial \hat{v}}{\partial \hat{x}}\frac{\partial \hat{u}}{\partial \hat{x}} - \hat{u}\left(\frac{\partial^2 \hat{v}}{\partial \hat{x}^2} + \frac{\partial^2 \hat{u}}{\partial \hat{y}\partial \hat{x}}\right) - \hat{v}\left(\frac{\partial^2 \hat{v}}{\partial \hat{y}\partial \hat{x}} + \frac{\partial^2 \hat{u}}{\partial \hat{y}^2}\right)\right] \tag{5.14}$$

$$\hat{\tau}_{xx} = -2\hat{\eta}\left(\frac{\partial \hat{u}}{\partial \hat{x}}\right) - \hat{\Psi}_1\left[2\left(\frac{\partial \hat{u}}{\partial \hat{x}}\right)^2 + \frac{\partial \hat{u}}{\partial \hat{y}}\left(\frac{\partial \hat{v}}{\partial \hat{x}} + \frac{\partial \hat{u}}{\partial \hat{y}}\right) - \hat{u}\frac{\partial^2 \hat{u}}{\partial \hat{x}^2} - \hat{v}\frac{\partial^2 \hat{u}}{\partial \hat{y}\partial \hat{x}}\right] - \hat{\Psi}_2\left(4\left(\frac{\partial \hat{u}}{\partial \hat{x}}\right)^2 + \left(\frac{\partial \hat{v}}{\partial \hat{x}} + \frac{\partial \hat{u}}{\partial \hat{y}}\right)^2\right) \tag{5.15}$$

These equations were too complicated to simply solve. Therefore a perturbation technique was employed (Nayfeh, 1981; Simmonds & Mann, 1986).

The perturbation technique involves rewriting each of the dependent variables in the equation ($\hat{p}, \hat{u}, \hat{v}, \hat{\tau}_{yy}, \hat{\tau}_{xy}, \hat{\tau}_{xx}$) as a series in terms of a perturbation variable, ε. The equations are then rearranged so that terms are collected together by order of ε. This was intended to give a set of, hopefully, simpler equations, one for each order of ε, which are then solved sequentially, converging upon the "true" solution of the original equations.

5.4. Dimensionless Form

The first step in the perturbation technique was to rewrite the variables in dimensionless forms, which are given below. Some additional detail about how these dimensionless forms were derived is given in Appendix B.

$$\hat{x} = x\sqrt{\hat{\delta}\hat{R}} \tag{5.16}$$

$$\hat{y} = y\hat{\delta} \tag{5.17}$$

$$\hat{u} = u.\hat{u}_r \tag{5.18}$$

$$\hat{v} = v.\hat{u}_r \sqrt{\frac{\hat{\delta}}{\hat{R}}} \tag{5.19}$$

$$\hat{p} - \hat{p}_a = \frac{P\hat{u}_r\hat{\eta}}{\hat{\delta}} \sqrt{\frac{\hat{R}}{\hat{\delta}}} \tag{5.20}$$

$$\hat{\eta} = \hat{\eta}\eta \tag{5.21}$$

$$\hat{\Psi}_1 = \Psi_1 \frac{\hat{\eta}\hat{\delta}}{\hat{u}_r} \tag{5.22}$$

$$\hat{\Psi}_2 = \Psi_2 \frac{\hat{\eta}\hat{\delta}}{\hat{u}_r} \tag{5.23}$$

$$\hat{\tau}_{nn} = \mathrm{T}_{nn} \frac{\hat{\eta}\hat{u}_r}{\hat{\delta}} \tag{5.24}$$

where:

$$P = P_0 + \varepsilon P_1 + \varepsilon^2 P_2 + \ldots \tag{5.25}$$

$$u = u_0 + \varepsilon u_1 + \varepsilon^2 u_2 + \ldots \tag{5.26}$$

$$v = v_0 + \varepsilon v_1 + \varepsilon^2 v_2 + \ldots \tag{5.27}$$

$$\mathrm{T}_{nn} = \mathrm{T}_{nn0} + \varepsilon \mathrm{T}_{nn1} + \varepsilon^2 \mathrm{T}_{nn2} + \ldots \tag{5.28}$$

and:

$$\varepsilon = \sqrt{\frac{\hat{\delta}}{\hat{R}}} \tag{5.29}$$

Equations 5.5 and 5.6 can also be written in a dimensionless form, given that:

$$\tan(\theta) = \varepsilon x + \varepsilon^3 \frac{x^3}{2} + \ldots \tag{5.30}$$

$$\cos(\theta) = 1 - \varepsilon^2 \frac{x^2}{2} + \ldots \tag{5.31}$$

$$\sin(\theta) = \varepsilon x + \ldots \tag{5.32}$$

$$\frac{\sum \hat{F}_y}{W} = \frac{\hat{\eta}\hat{u}_r}{\varepsilon^2} \frac{\sum F_y}{W} \tag{5.33}$$

$$\frac{\sum \hat{M}}{W} = \frac{\hat{\eta}\hat{R}\hat{u}_r}{\varepsilon} \frac{\sum M}{W} \tag{5.34}$$

$$\frac{\sum F_y}{W} = \int_{x_i}^{x_e} [P_0]dx + \varepsilon \int_{x_i}^{x_e} [P_1 + \mathrm{T}_{yy,0}]dx + \varepsilon^2 \int_{x_i}^{x_e} [P_2 + \mathrm{T}_{yy,1} + x\mathrm{T}_{xy,0}]dx + \ldots \tag{5.35}$$

$$\begin{aligned} \frac{\sum M}{W} = {} & \int_{x_i}^{x_e} [-\mathrm{T}_{xy,0}]dx + \varepsilon \int_{x_i}^{x_e} [x(\mathrm{T}_{xx,0} - \mathrm{T}_{yy,0}) - \mathrm{T}_{xy,1}]dx \\ & + \varepsilon^2 \int_{x_i}^{x_e} \left[x(\mathrm{T}_{xx,1} - \mathrm{T}_{yy,1}) - \mathrm{T}_{xy,2} + \left(1 + \frac{x^2}{2}\right)\mathrm{T}_{xy,0} \right] dx + \ldots \end{aligned} \tag{5.36}$$

For the perturbation solution to be valid, the value of the perturbation variable, ε, must be less than 1. For the dough sheeting problem the nip gap, $\hat{\delta}$, may range from 1 mm to 5 mm, while the roller radius, $\hat{R}$, may range from 25 mm to 135 mm. This means that ε may range from 0.44 to 0.09. As this range is below 1 it is valid to use the perturbation technique. However, it should be noted that in the case where the nip gap is large, or the rollers small, then ε is close to 1, and the perturbation solution may be less accurate.

5.5. Perturbation Equations

The dimensionless forms of the variables were substituted into equations 5.10 to 5.15. These can be grouped by order of ε. The first three orders are given below:

5.5.1. Zeroth Order

$$\frac{\partial u_0}{\partial x}+\frac{\partial v_0}{\partial y}=0 \tag{5.37}$$

$$\frac{\partial P_0}{\partial x}=\eta\frac{\partial^2 u_0}{\partial^2 y} \tag{5.38}$$

$$\frac{\partial P_0}{\partial y}=0 \tag{5.39}$$

$$T_{yy,0}=-\Psi_2\left(\frac{\partial u_o}{\partial y}\right)^2 \tag{5.40}$$

$$T_{xy,0}=-\eta\frac{\partial u_o}{\partial y} \tag{5.41}$$

$$T_{xx,0}=-(\Psi_1+\Psi_2)\left(\frac{\partial u_o}{\partial y}\right)^2 \tag{5.42}$$

5.5.2. First Order

$$\frac{\partial u_1}{\partial x}+\frac{\partial v_1}{\partial y}=0 \tag{5.43}$$

$$\frac{\partial P_1}{\partial x}=\eta\frac{\partial^2 u_1}{\partial^2 y}+\frac{\Psi_1}{2}\left(\frac{\partial^2 u_0}{\partial x\partial y}\frac{\partial u_0}{\partial y}-\frac{\partial^2 u_0}{\partial y^2}\frac{\partial u_0}{\partial x}-u_0\frac{\partial^3 u_0}{\partial x\partial y^2}-v_0\frac{\partial^3 u_0}{\partial y^3}\right)+2\Psi_2\frac{\partial^2 u_0}{\partial x\partial y}\frac{\partial u_0}{\partial y} \tag{5.44}$$

$$\frac{\partial P_1}{\partial y}=2\Psi_2\frac{\partial u_0}{\partial y}\frac{\partial^2 u_0}{\partial y^2} \tag{5.45}$$

$$T_{yy,1} = -2\eta\frac{\partial v_0}{\partial y} - 2\Psi_2\frac{\partial u_o}{\partial y}\frac{\partial u_1}{\partial y} \tag{5.46}$$

$$T_{xy,1} = -\eta\frac{\partial u_1}{\partial y} + \frac{\Psi_1}{2}\left(2\frac{\partial u_o}{\partial x}\frac{\partial u_0}{\partial y} + u_0\frac{\partial^2 u_o}{\partial x\partial y} + v_0\frac{\partial^2 u_o}{\partial y^2}\right) \tag{5.47}$$

$$T_{xx,1} = -2\eta\frac{\partial u_0}{\partial x} - 2(\Psi_2 + \Psi_1)\frac{\partial u_o}{\partial y}\frac{\partial u_1}{\partial y} \tag{5.48}$$

5.5.3. Second Order

$$\frac{\partial u_2}{\partial x} + \frac{\partial v_2}{\partial y} = 0 \tag{5.49}$$

$$\frac{\partial P_2}{\partial x} = \eta\left(\frac{\partial^2 u_2}{\partial^2 y} + \frac{\partial^2 u_0}{\partial x^2}\right) + \frac{\Psi_1}{2}\left(\begin{array}{l}\frac{\partial^2 u_0}{\partial x\partial y}\frac{\partial u_1}{\partial y} - \frac{\partial^2 u_0}{\partial y^2}\frac{\partial u_1}{\partial x} - u_0\frac{\partial^3 u_1}{\partial x\partial y^2} - v_0\frac{\partial^3 u_1}{\partial y^3} \\ + \frac{\partial^2 u_1}{\partial x\partial y}\frac{\partial u_0}{\partial y} - \frac{\partial^2 u_1}{\partial y^2}\frac{\partial u_0}{\partial x} - u_1\frac{\partial^3 u_0}{\partial x\partial y^2} - v_1\frac{\partial^3 u_0}{\partial y^3}\end{array}\right) + 2\Psi_2\left(\frac{\partial^2 u_1}{\partial x\partial y}\frac{\partial u_0}{\partial y} + \frac{\partial^2 u_0}{\partial x\partial y}\frac{\partial u_1}{\partial y}\right) \tag{5.50}$$

$$\frac{\partial P_2}{\partial y} = \eta\frac{\partial^2 v_0}{\partial y^2} + 2\Psi_2\left(\frac{\partial u_1}{\partial y}\frac{\partial^2 u_0}{\partial y^2} + \frac{\partial u_0}{\partial y}\frac{\partial^2 u_1}{\partial y^2}\right) \tag{5.51}$$

$$T_{yy,2} = -2\eta\frac{\partial v_1}{\partial y} + \Psi_1\left(v_0\frac{\partial^2 v_0}{\partial y^2} + u_0\frac{\partial^2 v_0}{\partial x\partial y} - \frac{\partial u_0}{\partial y}\frac{\partial v_0}{\partial x} - 2\left(\frac{\partial v_0}{\partial y}\right)^2\right) - 2\Psi_2\left(\frac{\partial u_o}{\partial y}\frac{\partial u_2}{\partial y} + \frac{\partial u_o}{\partial y}\frac{\partial v_0}{\partial x} + \frac{1}{2}\left(\frac{\partial u_1}{\partial y}\right)^2 + 2\left(\frac{\partial v_0}{\partial y}\right)^2\right) \tag{5.52}$$

$$T_{xy,2} = -\eta\left(\frac{\partial u_2}{\partial y} + \frac{\partial v_0}{\partial x}\right) + \frac{\Psi_1}{2}\left(\begin{array}{l}2\left(\frac{\partial u_o}{\partial x}\frac{\partial u_1}{\partial y} + \frac{\partial u_o}{\partial y}\frac{\partial u_1}{\partial x}\right) + u_0\frac{\partial^2 u_1}{\partial x\partial y} + u_1\frac{\partial^2 u_0}{\partial x\partial y} \\ + v_0\frac{\partial^2 u_1}{\partial y^2} + v_1\frac{\partial^2 u_0}{\partial y^2}\end{array}\right) \tag{5.53}$$

$$T_{xx,2} = -2\eta\frac{\partial u_1}{\partial x} - (\Psi_1 + \Psi_2)\left(\frac{\partial u_0}{\partial y}\frac{\partial v_0}{\partial x} + 2\frac{\partial u_0}{\partial y}\frac{\partial u_2}{\partial y} + \left(\frac{\partial u_1}{\partial y}\right)^2 + 2\left(\frac{\partial u_0}{\partial x}\right)^2\right) - \Psi_2\left(2\left(\frac{\partial u_0}{\partial x}\right)^2 + \frac{\partial u_0}{\partial y}\frac{\partial v_0}{\partial x}\right) + \Psi_1\left(v_0\frac{\partial^2 u_0}{\partial x\partial y} + u_0\frac{\partial^2 u_0}{\partial x^2}\right) \tag{5.54}$$

5.6. Boundary Conditions

The boundary conditions for the problem also had to be rewritten in terms of the dimensionless variables. The boundary conditions were explained in Section 1.6.6.

Additional details of how these boundary conditions were made dimensionless can be found in Appendix B.

5.6.1. No Slip at the Roller Surface

At the roller surface, $\hat{h}$, the dough velocity is equal to the roller velocity, $\hat{u}_r$.

$$\text{at } y = h = 1 + \frac{x^2}{2} + \varepsilon^2 \frac{x^4}{8} + \ldots, \tag{5.55}$$

$$u = u_0 + \varepsilon u_1 + \varepsilon^2 u_2 + \ldots = 1 - \varepsilon^2 \frac{x^2}{2} - \varepsilon^4 \frac{x^4}{8} + \ldots \tag{5.56}$$

$$v = v_0 + \varepsilon v_1 + \varepsilon^2 v_2 + \ldots = x \tag{5.57}$$

5.6.2. Line of Symmetry

At $\hat{y} = 0$, there is a line of symmetry, which means: $\hat{v} = 0$ and $\frac{\partial \hat{u}}{\partial \hat{y}} = 0$.

This boundary condition was simply rewritten:

$$\text{at } y = 0, \tag{5.58}$$

$$\frac{\partial u}{\partial y} = \frac{\partial u_0}{\partial y} + \varepsilon \frac{\partial u_1}{\partial y} + \varepsilon^2 \frac{\partial u_2}{\partial y} + \ldots = 0 \tag{5.59}$$

$$v = v_0 + \varepsilon v_1 + \varepsilon^2 v_2 + \ldots = 0 \tag{5.60}$$

5.6.3. Inlet Condition

At the point of inlet $(\hat{x}_i, \hat{h}_i)$, there is a free surface, at which the total stress on the roller surface is equal to zero.

$$\text{at } y = h_i = 1 + \frac{x_i^2}{2} + \varepsilon^2 \frac{x_i^4}{8} + \ldots \text{and } x = x_i, \tag{5.61}$$

$$p_0 + \varepsilon\left(p_1 + \mathrm{T}_{yy,0}\right) + \varepsilon^2\left(p_2 + \mathrm{T}_{yy,1} - 2x\mathrm{T}_{xy,0}\right) + \ldots = 0 \tag{5.62}$$

5.6.4. Outlet Condition

At the point of outlet $(\hat{x}_e, \hat{h}_e)$, there is a free surface, at which the total stress on the roller surface is equal to zero.

$$\text{at } y = x_e = 1 + \frac{x_e^2}{2} + \varepsilon^2 \frac{x_e^4}{8} + \ldots \text{and } x = x_e, \tag{5.63}$$

$$p_0 + \varepsilon\left(p_1 + \mathrm{T}_{yy,0}\right) + \varepsilon^2\left(p_2 + \mathrm{T}_{yy,1} - 2x\mathrm{T}_{xy,0}\right) + \ldots = 0 \tag{5.64}$$

5.6.5. Conservation of Mass

At any value of $\hat{x}$ the integral of the horizontal velocity component by $\hat{y}$, from $\hat{y}=0$ to $\hat{y}=\hat{h}$, is equal to a constant. Assuming that the exit velocity profile is flat, and obeying the outlet boundary condition, then the constant is equal to $\hat{u}_e\hat{h}_e$

$$\forall x \tag{5.65}$$

$$\begin{aligned} u_e h_e &= 1+\frac{x_e^{\,2}}{2}-\varepsilon^2\frac{x_e^{\,2}}{8}\left(x_e^{\,2}+4\right)-\ldots \\ &= \int_0^h u\,dy \\ &= \int_0^{1+\frac{x^2}{2}} u_0\,dy+\varepsilon\int_0^{1+\frac{x^2}{2}} u_1\,dy+\varepsilon^2\left(\int_0^{\frac{x^4}{8}} u_0\,dy+\int_0^{1+\frac{x_e^{\,2}}{2}} u_2\,dy\right)+\ldots \end{aligned} \tag{5.66}$$

5.7. Equation Solution

The perturbation equations [5.37 to 5.54] were then solved. The details of this solution are given in Appendix B. Below are the solutions, grouped by order of ε. (Note that the second order solutions of T_{yy} and T_{xx} have been omitted as they are not required for a second order solution of the exit height, upwards force and torque).

5.7.1. Zeroth Order Solution

$$u_0=\frac{3x_e^{\,2}-x^2+4}{2\left(x^2+2\right)}-\frac{6y^2\left(x_e-x\right)\left(x_e+x\right)}{\left(x^2+2\right)^3} \tag{5.67}$$

$$v_0=\frac{3xy\left(x_e^{\,2}+2\right)}{\left(x^2+2\right)^2}-\frac{4xy^3\left(3x_e^{\,2}-2x^2+2\right)}{\left(x^2+2\right)^4} \tag{5.68}$$

$$P_0=-\eta\frac{3}{8}\left(\begin{array}{l}\dfrac{x\left(10x_e^{\,2}+4\right)+x^3\left(3x_e^{\,2}-2\right)}{\left(x^2+2\right)^2}-\dfrac{x_i\left(10x_e^{\,2}+4\right)+x_i^{\,3}\left(3x_e^{\,2}-2\right)}{\left(x_i^{\,2}+2\right)^2} \\ +\dfrac{3x_e^{\,2}-2}{\sqrt{2}}\left(\tan^{-1}\left(\dfrac{x}{\sqrt{2}}\right)-\tan^{-1}\left(\dfrac{x_i}{\sqrt{2}}\right)\right)\end{array}\right) \tag{5.69}$$

$$T_{yy,0}=-144\Psi_2 y^2\frac{\left(x_e-x\right)^2\left(x_e+x\right)^2}{\left(x^2+2\right)^6} \tag{5.70}$$

$$T_{xy,0}=12\eta y\frac{\left(x_e-x\right)\left(x_e+x\right)}{\left(x^2+2\right)^3} \tag{5.71}$$

$$T_{xx,0} = -144(\Psi_1 + \Psi_2)y^2 \frac{(x_e - x)^2 (x_e + x)^2}{(x^2 + 2)^6} \tag{5.72}$$

5.7.2. First Order Solution

$$u_1 = 0 \tag{5.73}$$

$$v_1 = 0 \tag{5.74}$$

$$\begin{aligned} P_1 = {} & 144\Psi_2 y^2 \frac{(x_e + x)^2 (x_e - x)^2}{(x^2 + 2)^6} \\ & - 3\Psi_1 \frac{(x_i - x_e)(x_i + x_e)}{({x_i}^2 + 2)^4} ({x_i}^2 - 3{x_e}^2 - 4) \\ & + 3\Psi_1 \frac{(x - x_e)(x + x_e)}{(x^2 + 2)^4} (x^2 - 3{x_e}^2 - 4) \end{aligned} \tag{5.75}$$

$$T_{yy,1} = \frac{24\eta x y^2 (3{x_e}^2 - 2x^2 + 2)}{(x^2 + 2)^4} - \frac{6\eta x ({x_e}^2 + 2)}{(x^2 + 2)^2} \tag{5.76}$$

$$T_{xy,1} = -\frac{12\Psi_1 xy}{(x^2 + 2)^7} \begin{bmatrix} y^2 (48{x_e}^4 - {x_e}^2 (80x^2 - 32) + 32x^2 (x^2 - 1)) \\ -6{x_e}^4 (x^4 + 4x^2 + 4) + 6{x_e}^2 (x^6 + 2x^4 - 4x^2 - 7) \\ -x^8 + 4x^6 + 24x^4 + 16x^2 - 16 \end{bmatrix} \tag{5.77}$$

$$T_{xx,1} = \frac{6\eta x ({x_e}^2 + 2)}{(x^2 + 2)^2} - \frac{24\eta x y^2 (3{x_e}^2 - 2x^2 + 2)}{(x^2 + 2)^4} \tag{5.78}$$

5.7.3. Second Order Solution

$$\begin{aligned} u_2 = {} & \frac{2y^4}{(x^2 + 2)^5} (3{x_e}^2 (7x^2 - 2) - 2(5x^4 - 13x^2 + 2)) \\ & + \frac{3y^2}{10(x^2 + 2)^4} \begin{pmatrix} 5{x_e}^4 (x^2 + 2) - {x_e}^2 (27x^4 + 52x^2 - 64) \\ -2(21x^4 + 68x^2 - 8) \end{pmatrix} \\ & - \frac{1}{40(x^2 + 2)^2} \begin{pmatrix} 15{x_e}^4 (x^2 + 2) - 6{x_e}^2 (x^4 - 4x^2 - 22) \\ -8(2x^4 + 11x^2 - 1) \end{pmatrix} \end{aligned} \tag{5.79}$$

$$\begin{aligned} v_2 = {} & \frac{24xy^5}{5(x^2 + 2)^6} (2{x_e}^2 (7x^2 - 6) - 5x^4 + 24x^2 - 12) \\ & + \frac{3xy^3}{5(x^2 + 2)^5} \begin{pmatrix} 5{x_e}^4 (x^2 + 2) - 2{x_e}^2 (9x^4 + 8x^2 - 69) \\ -4(7x^4 + 20x^2 - 28) \end{pmatrix} \\ & - \frac{3xy}{20(x^2 + 2)^3} (5{x_e}^4 (x^2 + 2) + 8{x_e}^2 (2x^2 + 9) - 8(x^2 - 8)) \end{aligned} \tag{5.80}$$

$$p_2 = \frac{3\eta}{\sqrt{2}}\left(\tan^{-1}\left(\frac{x}{\sqrt{2}}\right)-\tan^{-1}\left(\frac{x_i}{\sqrt{2}}\right)\right)\left(\frac{3x_e^{\,4}+15x_e^{\,2}-50}{32}-\frac{3x_e^{\,2}-10}{10}\right)$$
$$-12\eta x y^2\frac{3x_e^{\,2}-2x^2+2}{\left(x^2+2\right)^4}+3\eta x_i\frac{3x_e^{\,2}x_i^{\,2}+10x_i^{\,2}+22x_e^{\,2}+52}{10\left(x_i^{\,2}+2\right)^2}$$
$$-3\eta x\frac{3x_e^{\,2}x^2+30x^2-8x_e^{\,2}+32}{10\left(x^2+2\right)^2}$$
$$+3\eta\left(x_i-x\right)x_e^{\,4}\frac{\left(\begin{array}{l}xx_i^{\,3}\left(3x^2+10\right)-2x_i^{\,2}\left(x^2+6\right)\\+2xx_i\left(5x^2+14\right)-4\left(3x^2+10\right)\end{array}\right)}{32\left(x^2+2\right)^2\left(x_i^{\,2}+2\right)^2} \qquad (5.81)$$
$$+3\eta\left(x_i-x\right)\frac{\left(\begin{array}{l}2\left(\begin{array}{l}\left(xx_i^{\,5}-8\right)\left(39x^4+112x^2+100\right)\\-2x_i^{\,4}\left(61x^4+184x^2+156\right)+16xx_i^{\,3}\left(7x^4+19x^2+18\right)\\-16x_i^{\,2}\left(23x^4+66x^2+56\right)+4xx_i\left(25x^4+72x^2+76\right)\end{array}\right)\\+x_e^{\,2}\left(\begin{array}{l}\left(xx_i^{\,5}-8\right)\left(15x^4+48x^2+68\right)\\-2x_i^{\,4}\left(21x^4+56x^2+60\right)+16xx_i^{\,3}\left(3x^4+11x^2+18\right)\\-16x_i^{\,2}\left(7x^4+18x^2+24\right)+4xx_i\left(17x^4+72x^2+108\right)\end{array}\right)\end{array}\right)}{32\left(x^2+2\right)^3\left(x_i^{\,2}+2\right)^3}$$

$$T_{yy,2} = \ldots\text{not required} \qquad (5.82)$$

$$T_{xy,2} = 3\eta y\frac{\left(\begin{array}{l}x_e^{\,4}\left(10x^2+20\right)-x_e^{\,2}\left(27x^4+52x^2-124\right)\\-20x^6-102x^4-216x^2+56\end{array}\right)}{5\left(x^2+2\right)^4} \qquad (5.83)$$
$$-12\eta y^3\frac{21x^2x_e^{\,2}-6x_e^{\,2}-10x^4+26x^2-4}{\left(x^2+2\right)^5}$$

$$T_{xx,2} = \ldots\text{not required} \qquad (5.84)$$

5.8. Solution for Force and Torque

Substituting the solutions of equations 5.67 to 5.84 into equations 5.35 and 5.36, gave the solution for the force and torque on the roller.

5.9. Numerical Solution for Exit Distance

The only unknown in the equations now is the exit distance, x_e. This was determined by numerically solving the outlet boundary condition represented by Equation (5.64), for different candidate values of x_e, until an x_e value that satisfies the boundary condition was found. The numerical calculations were performed using MATLAB.

The following is an example graph of the stress on the roller vs candidate values of x_e. It can be seen that there is a value of x_e for which the stress on the roller is equal to zero, and is perturbed slightly depending upon the order of solution used.

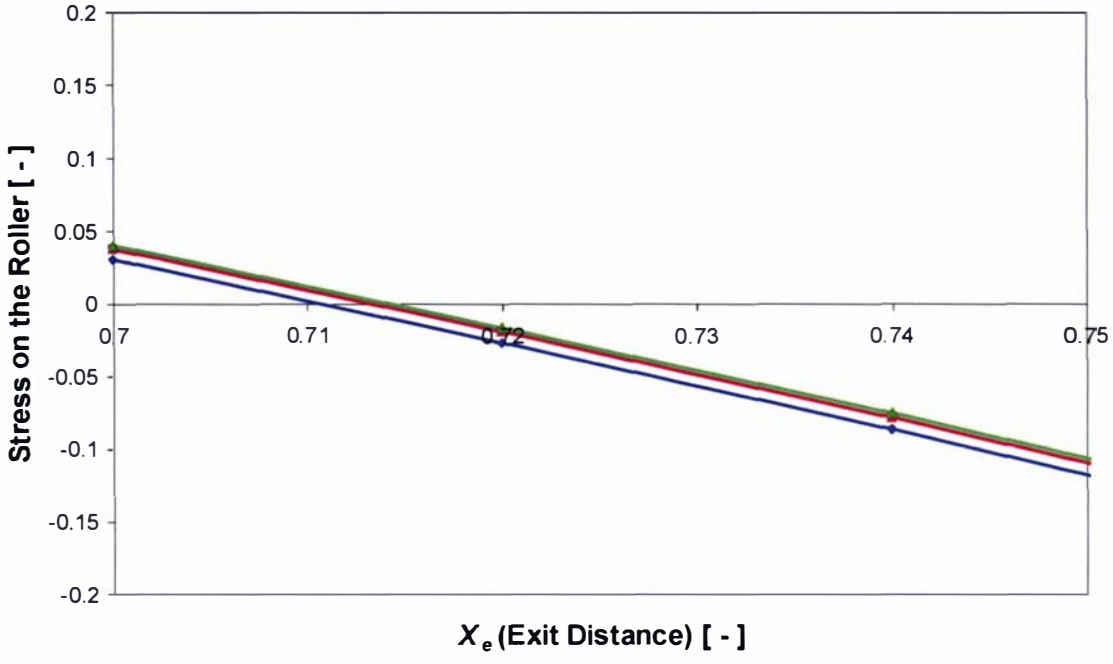

Figure 5.1 Stress on the roller vs candidate values of x_e. = 0^{th} order, = 1^{st} order, and = 2^{nd} order.

5.10. Implementation of the Solution

The solution was implemented using a program written in MATLAB. To perform the numerical solution of x_e, for a particular sheeting condition, and to then calculate the value of the torque and upward force took on average less than 0.1 s, when the calculations were performed with a Intel Pentium iii, 866 MHz processor, with 256 MB RAM running Win2K, with MATLAB version 6.0.0.88 R12. Such a fast computation means that the solution could be suitable to be implemented as part of a real time control system.

5.11. Sensitivity of Solution

The dimensionless solution of this description of the sheeting system is dependent upon the value of the two dimensionless variables that describe the geometry of the sheeting system: x_i, the inlet distance, and ε, the perturbation parameter. The solution is also

dependent upon two dimensionless variables that describe the dough properties: Ψ_1 and Ψ_2, the first and second normal stress coefficients, respectively. The following graphs (Figures 5.2 to 5.5) show plots of the second order solution for two representative sheeting outcomes. Note that these are dimensionless outcomes to which their dimensioned equivalents are related in a complicated manner. For example, Figure 5.3 suggests that as the dimensionless geometry ratio (ε), increases the dimensionless force on the roller will exponentially increase. This would not be true of the *dimensioned* force upon the roller which (although proportional to the dimensionless force) is inversely proportional to ε^2 (Equation 5.33).

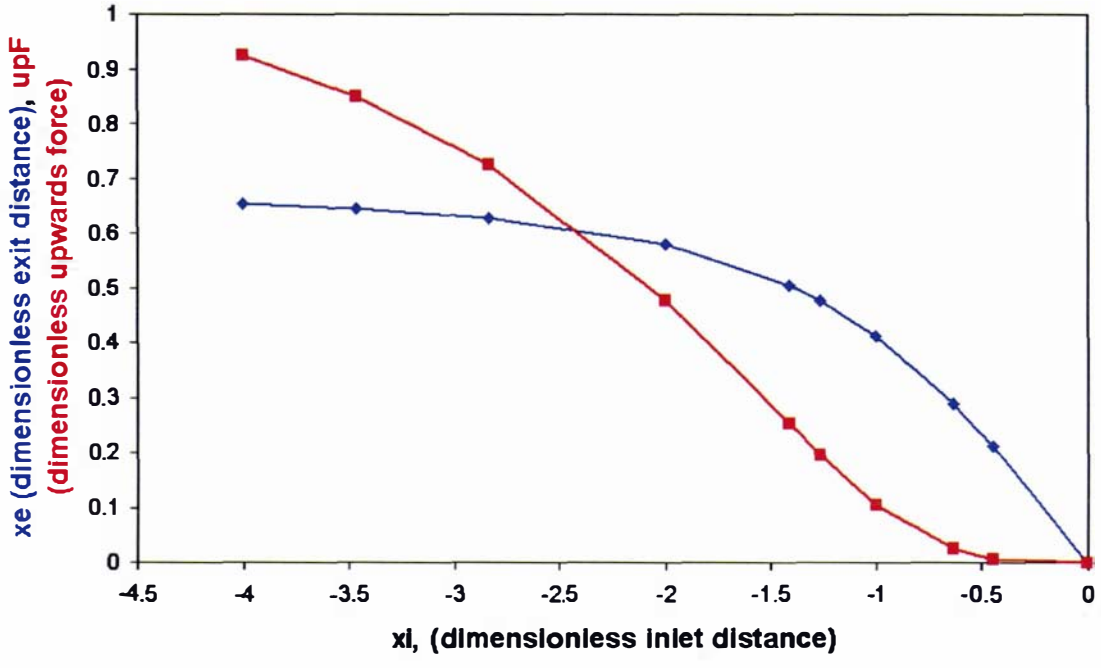

Figure 5.2 Sensitivity of Solutions to x_i (dimensionless inlet distance). Blue diamonds correspond to the (dimensionless) exit distance. Red squares correspond to the (dimensionless) upwards force upon the roller. $\varepsilon = 0.01$, $\Psi_1 = 0$, $\Psi_2 = 0$.

Figure 5.2 demonstrates the sensitivities of the solution for the (dimensionless) exit distance, x_e, and the solution for the (dimensionless) upward force on the roller, to changes in the (dimensionless) inlet distance. The inlet distance is negative because the zero of the x-coordinate is at the nip, between the two rollers. As the inlet distance increases in magnitude, the inlet sheet increases in thickness. This results in a greater exit distance (and therefore height) and also a greater upward force upon the roller.

Figure 5.3 demonstrates the sensitivities of the solution for the (dimensionless) exit distance, x_e, and solution for the (dimensionless) upward force on the roller, to changes

in the value of ε. As ε increases, both the exit distance and the upward force on the roller increase.

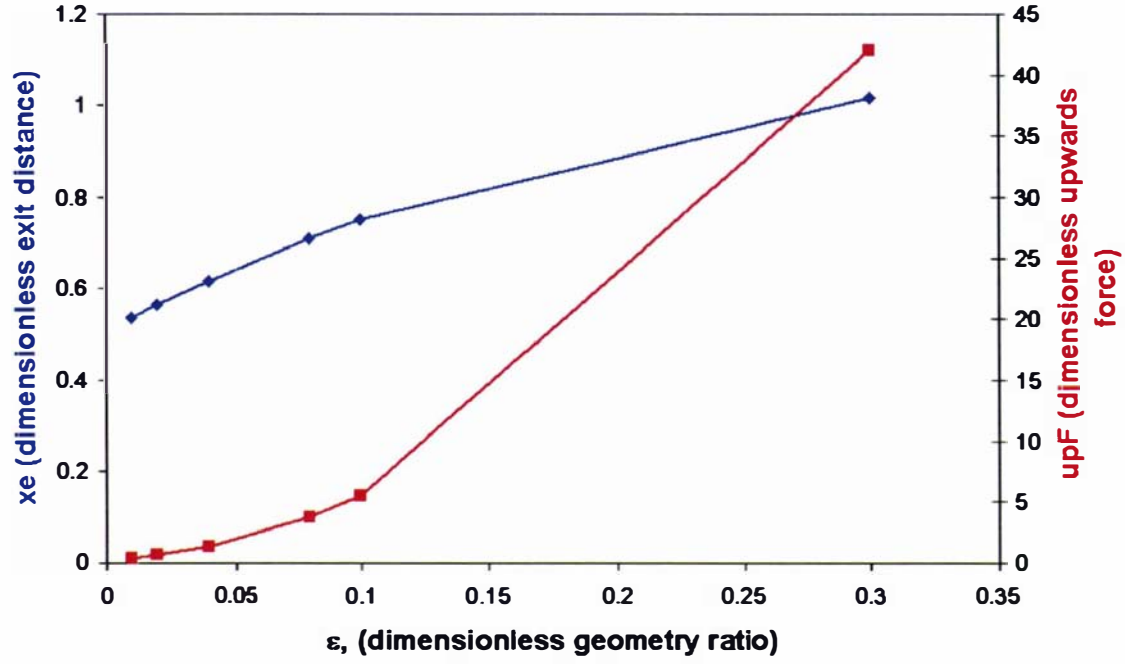

Figure 5.3 Sensitivity of Solutions to ε (dimensionless geometry ratio). Blue diamonds correspond to the (dimensionless) exit distance. Red squares correspond to the (dimensionless) upwards force upon the roller. $x_i = -1.41$, $\Psi_1 = 100$, $\Psi_2 = 0$.

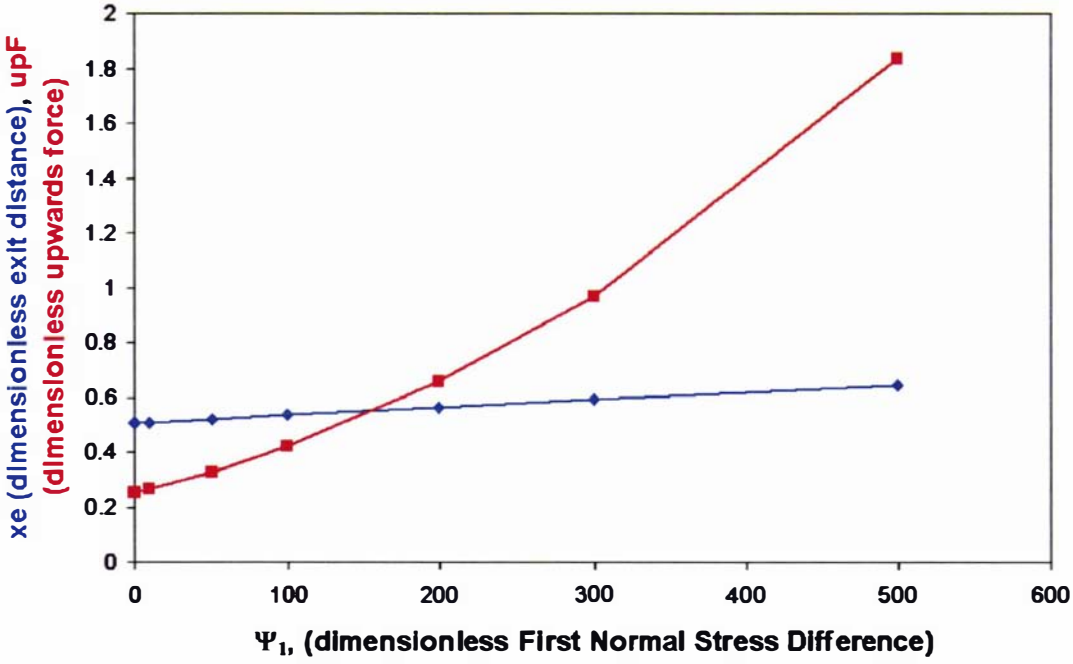

Figure 5.4 Sensitivity of Solutions to Ψ_1 (dimensionless First Normal Stress Difference). Blue diamonds correspond to the (dimensionless) exit distance. Red squares correspond to the (dimensionless) upwards force upon the roller. $x_i = -1.41$, $\varepsilon = 0.01$, $\Psi_2 = 0$.

Figure 5.4 demonstrates the sensitivities of the solution for the (dimensionless) exit distance, x_e, and solution for the (dimensionless) upward force on the roller to changes in the (dimensionless) value of Ψ_1. As Ψ_1 increases the upward force increases. The exit distance also increases with Ψ_1, but seems to be quite insensitive to small changes in Ψ_1. This is a problem as it suggests that a more elastic dough will not leave the sheeting system at a significantly greater height than a less elastic dough, which is contradictory to the results of validation experiments.

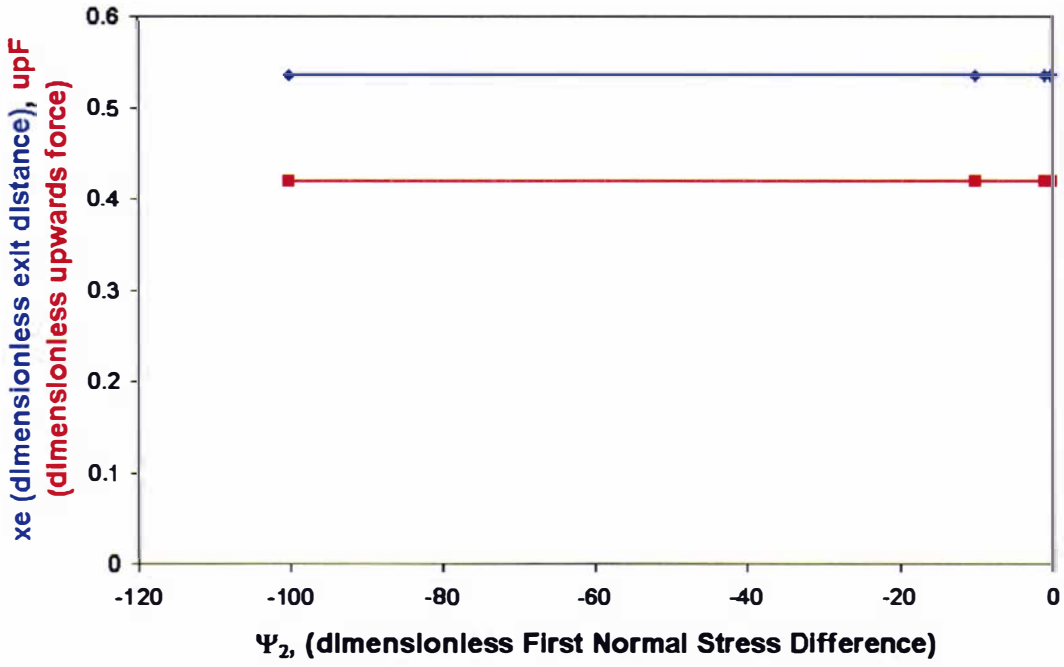

Figure 5.5 Sensitivity of Solutions to Ψ_2 (dimensionless Second Normal Stress Difference). Blue diamonds correspond to the (dimensionless) exit distance. Red squares correspond to the (dimensionless) upwards force upon the roller. $x_i = -1.41$, $\varepsilon = 0.01$, $\Psi_1 = 100$.

Figure 5.5 indicates that the sheeting outcomes are insensitive to changes in Ψ_2. This is because although Ψ_2 appears as a variable in the perturbation solutions it is cancelled out in the sheeting outcome solutions. The insensitivity of solutions to Ψ_2 means that the unreliability of measurements of Ψ_2 will not be significant.

6. Discussion

6.1. Geometry Parameters

In order to apply the 2nd order model developed in Chapter 5, the geometry of the sheeting system under study needs to be described. The model uses a number of dimensionless parameters for this purpose, the forms of which were given by equations (5.16) to (5.36). Table 2.10 gave the details of the sheeting geometry and sheeting conditions used in the validation experiments. An important, dimensionless, geometric parameter is ε, the perturbation variable, which varied between 0.11 and 0.38 in the validation experiments. Another important geometric parameter is the reduction ratio (and the corresponding inlet distance). The reduction ratio ranged from around 2 to 10 in the validation experiments. The roller speed is required to obtain the dimensionless forms of the material parameters Ψ_1 and Ψ_2. The roller speed varied from 6 to 35 rpm.

6.2. Material Parameters

The parameters of the process material, dough, are also required in order to examine the model. The model uses the CEF constitutive equation (Equation (5.7)) to describe the dough. In Section 3.5.5 the CEF parameters of the three doughs used in the validation experiments (Epic, short mixed; Epic, long mixed; and Halo) were determined, as given below:

$$\hat{\eta}(\dot{\gamma}) = K_1 \dot{\gamma}^{n-1} \tag{6.1}$$

Dough	Epic Short Mix	Epic Long Mix	Halo
K [Pas^n]	$2.70 \times 10^4 \pm 0.07 \times 10^4$	$4.99 \times 10^4 \pm 0.08 \times 10^4$	$0.91 \times 10^4 \pm 0.01 \times 10^4$
n	0.209 ± 0.009	0.203 ± 0.006	0.270 ± 0.004
R^2	0.996	0.998	0.998

$$\hat{\Psi}_1(\dot{\gamma}) = K_2 \dot{\gamma}^{m-2} \tag{6.2}$$

Dough	Epic Short Mix	Epic Long Mix	Halo
K_2 [Pas^n]	$18.5 \times 10^4 \pm 0.8 \times 10^4$	$36 \times 10^4 \pm 1 \times 10^4$	$4.74 \times 10^4 \pm 0.08 \times 10^4$
m	0.25 ± 0.01	0.25 ± 0.01	0.230 ± 0.007
R^2	0.991	0.995	0.995

In the model, the parameters of the CEF constitutive equation were approximated by constants, instead of power-law functions of the strain rate. In order to estimate the constants, an estimate of the value of the strain rate, $\dot{\gamma}$, was made.

$$\dot{\gamma} \approx \frac{\hat{u}_r}{\hat{\delta}} \tag{6.3}$$

where: $\hat{u}_r$ is the tangential speed of the roller, [ms^{-1}]; $\hat{\delta}$ is the nip gap, [m].

Therefore:

$$\hat{\eta} = K_1 \left(\frac{\hat{u}_r}{\hat{\delta}} \right)^{n-1} \tag{6.4}$$

$$\hat{\Psi}_1 = K_2 \left(\frac{\hat{u}_r}{\hat{\delta}} \right)^{m-2} \tag{6.5}$$

or in dimensionless forms:

$$\eta = 1 \tag{6.6}$$

$$\Psi_1 = \frac{K_2}{K_1} \left(\frac{\hat{u}_r}{\hat{\delta}} \right)^{m-n} \tag{6.7}$$

and from equation (3.21).

$$\Psi_2 = -0.1\Psi_1 \tag{6.8}$$

6.3. Exit Height Comparison

It was found from the experimental data that the exit height of the sheet was around twice the nip gap (that is, the exit ratio was around 2 ± 0.5). The exit height increased with the inlet height (reduction ratio); increased with greater roller speeds; increased with larger diameter rollers; decreased with increasing nip gap; was constant for a given ratio of nip gap and roller diameter, and constant surface speed of the rollers (ε); and varied by dough type, being lowest for the Halo dough.

The exit height predictions of the model, illustrated in Figure 6.1, are poor. The model's predictions of the exit ratio are about 1.2, regardless of changes in sheeting conditions. In this respect the model predictions are no better than the Newtonian prediction of 1.225, proposed by Middleman (1977). The only feature captured by the model is a variation with reduction ratio. Clearly, modelling the dough sheeting problem using the CEF equation to account for elasticity does not result in an accurate prediction of the exit height.

a)

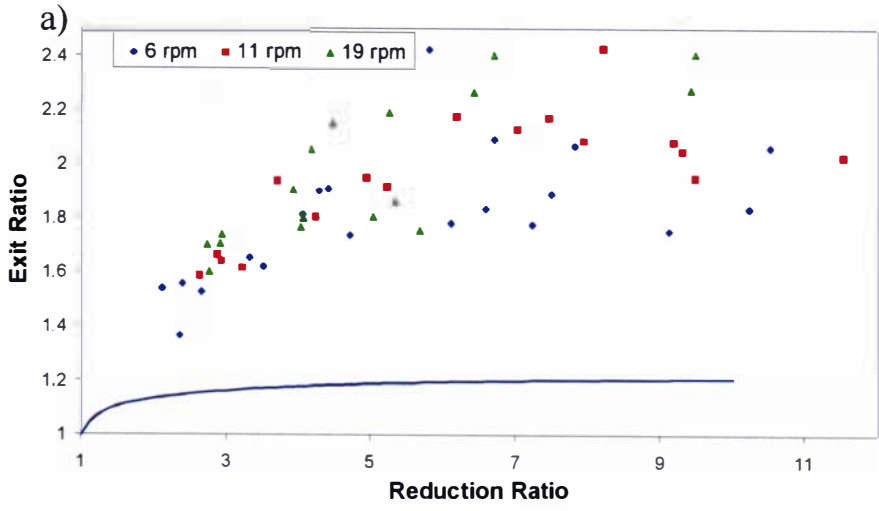
6 rpm
11 rpm
19 rpm
Exit Ratio
Reduction Ratio
2.4
2.2
2
1.8
1.6
1.4
1.2
1
1
3
5
7
9
11

b)

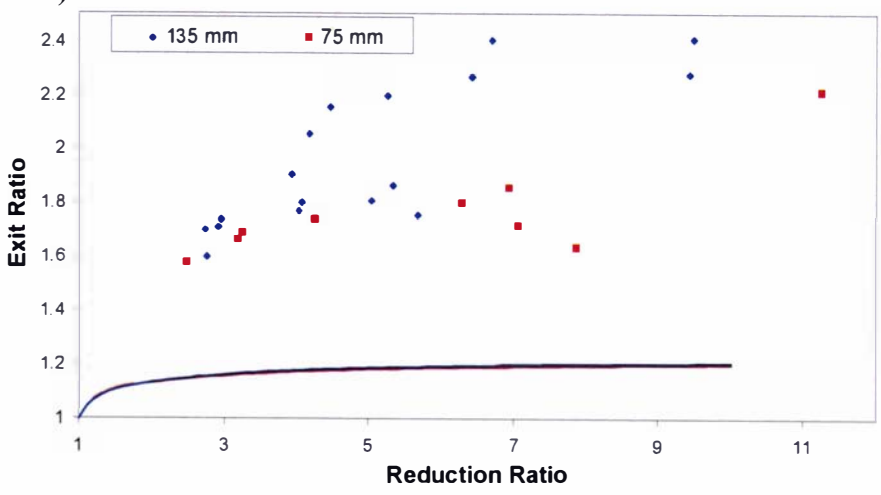
135 mm
75 mm
Exit Ratio
Reduction Ratio
2.4
2.2
2
1.8
1.6
1.4
1.2
1
1
3
5
7
9
11

c)

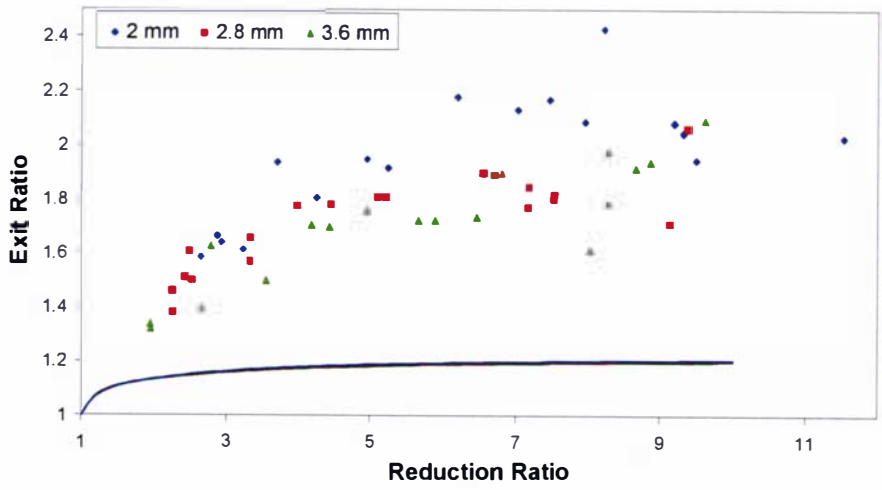
2 mm
2.8 mm
3.6 mm
Exit Ratio
Reduction Ratio
2.4
2.2
2
1.8
1.6
1.4
1.2
1
1
3
5
7
9
11

d)

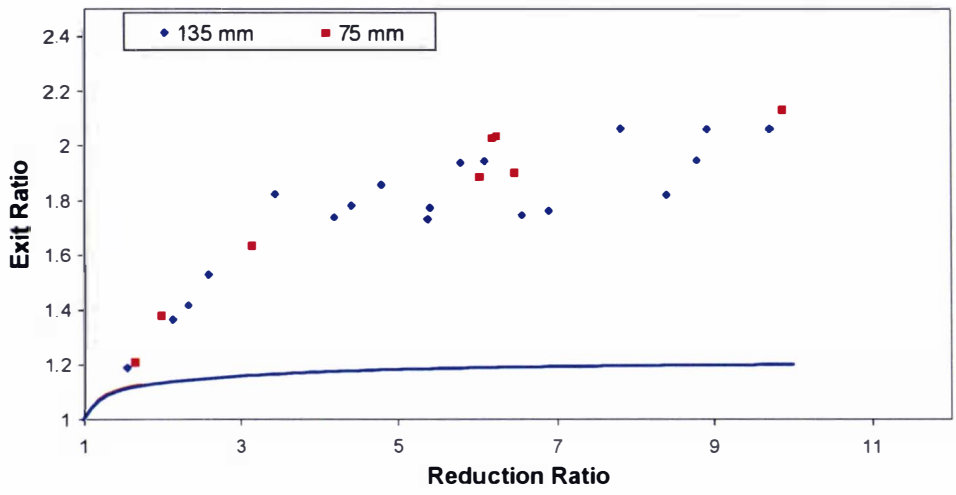

e)

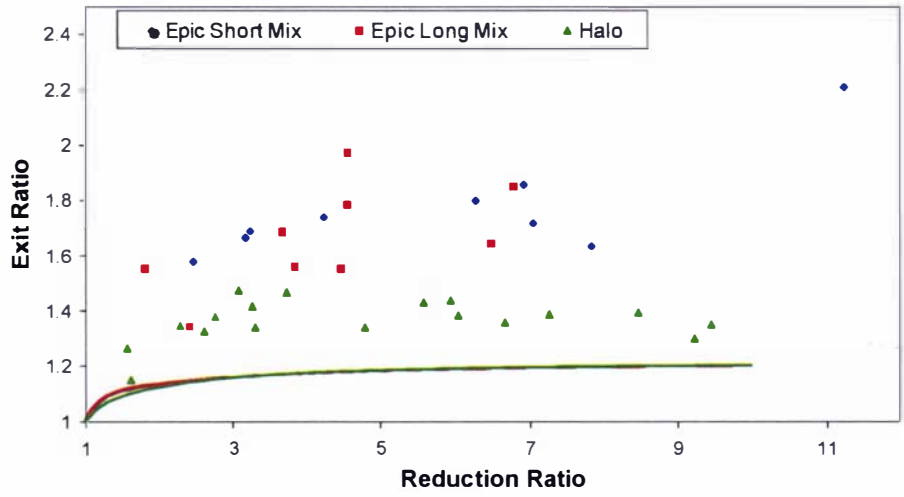

Figure 6.1 Model predictions for the Exit Ratio. The points are experimental points, the lines are predictions (as they are very similar, the prediction lines may be difficult to differentiate). a) Varying Roller Speed, for Epic Short Mixed Dough, 135 mm radius roller, 2.8 mm nip gap. b) Varying Roller Radius, for Epic Short Mixed Dough, 2 mm nip gap, 19 rpm roller speed. c) Varying Nip Gap, for Epic Short Mixed Dough, for Epic Short Mixed Dough, 135 mm radius roller, 11 rpm roller speed. d) Epic Short Mixed Dough with a constant ε ratio (0.16) and a constant surface speed (0.27 ms^{-1}). e) Varying Dough Type, for 75 mm radius roller, 2 mm nip gap, 19 rpm roller speed.

One possible problem is the values chosen to represent the CEF model parameters (K_1, K_2, n, m). For example, in Section 3.4.5 it was shown that if steady state measurements were used to estimate the viscosity of the dough, then lower values would be obtained. However, the insensitivity of the model to the CEF parameters demonstrated by Figure 6.1 e) suggests this is not the source of inaccuracy.

A possible problem with the perturbation solution technique is that an unaccounted for, higher order term may have a significant influence. In order to simplify the algebraic work, the perturbation technique was used to remove elements of the problem, which are successively returned as the order of the solution is increased. The solutions given are the 2nd order solutions of the problem. Perhaps at the 3rd, 4th or higher order an important missing factor would be returned to the model. For example, the exit height solution is, up to 2nd order, independent of the value of Ψ_2 (because all the Ψ_2 terms cancel each other out in the exit height solution).

The perturbation technique is protected somewhat from such an error because each order contains a higher order factor of the perturbation parameter (ε); that is, the 2nd order solution contains a factor of ε^2, the 3rd order solution a factor of ε^3 etc. As long as ε is small ($<< 1$), then the correction made with each successive higher order solution should be decreasingly small. Unfortunately, ε is relatively close to 1 ($\varepsilon \approx 0.1$ to 0.4).

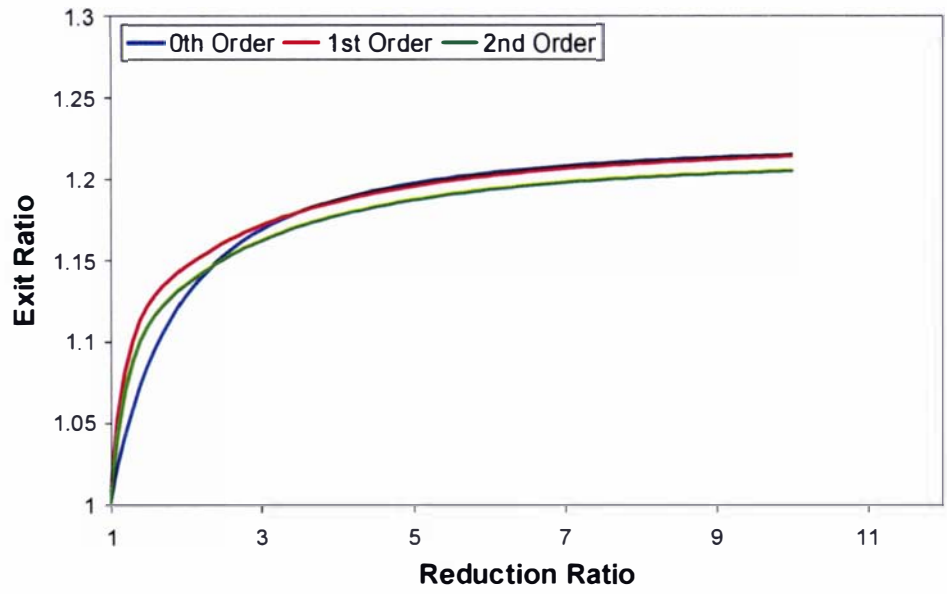

Figure 6.2 Exit ratio solutions by order. For Epic Short Mixed Dough, 135 mm radius roller, 2.8 mm nip gap, 11 rpm roller speed.

In Figure 6.2, the exit ratio solution for a particular sheeting condition is plotted for different orders of solution. The 1st order solution is a small perturbation upon the 0th order solution, which is consistent with an appropriate perturbation scheme. The 2nd order solution for small reduction ratios (<2) is a small perturbation upon the 1st order.

However, Figure 6.2 also shows that at higher reduction ratios the 2nd order solution is a greater perturbation upon the 1st order, than the 1st is upon the 0th. Such behaviour is indicative of a possible problem with the perturbation scheme.

In Figure 6.1 c), the nip gap is changing for a constant roller radius. This means that the nip gaps of 2, 2.8 and 3.6 mm are equivalent to ε values of 0.12, 0.14 and 0.16, respectively. The fact that none of the sheeting situations are well modelled suggests that the value of ε is not itself the cause of the model inaccuracy. Indeed, the largest ε value is (marginally) the best modelled, which is the opposite of what would be expected if large values of ε were causing the model mismatch.

It is therefore more likely that a significant feature of the problem is not represented by the lower order solutions. Possibly, this could be confirmed by successively solving for higher solutions until the feature was found. Unfortunately this is impractical, firstly because there is no criteria (except exhaustion) for stopping such a procedure, as the "significant feature" might always lie in the next highest order. The second problem is that as the solution order increases, the problem becomes exponentially more complex to solve. (Avoiding complexity was, after all, the point of using the perturbation technique).

Zheng and Tanner (1988) calculated the free surface of a viscoelastic sheet *after* it separated from the roller surfaces. They found that a maximum of about 5% swelling occurred as the material left the sheeter, in a similar phenomena to die swell (Bird et al. 1987). A 5% swelling would not account for the discrepancy observed here in exit height.

An alternative is that the problem might lie, not with the solution method, but with the assumptions upon which the model is based. Rheological models of bread dough more accurate that the CEF equation are available (Phan-Thien et al., 1997). However, such constitutive equations are very complicated to apply to the sheeting problem, both mathematically and in terms of the difficulty in measuring appropriate parameters. Another assumption, which may have introduced significant error, is the assumption that that the dough is incompressible, which as discussed in Section 1.5.2 is incorrect.

The source of compressibility in dough is air pockets which are formed during processes like mixing. This suggests that the less mixing a dough experiences, then the less compressible it will be. Figure 6.1e) indicates that the Halo dough is the best modelled of the three dough types. This was consistent with the assumption of incompressibility being the cause of modelling inaccuracy as the Halo dough was mixed for the shortest time (a period of 95 s) and is therefore possibly the least compressible, while the Epic doughs were both mixed for over 135 s each (Section 2.6.3).

6.4. Upward Force Predictions

a)

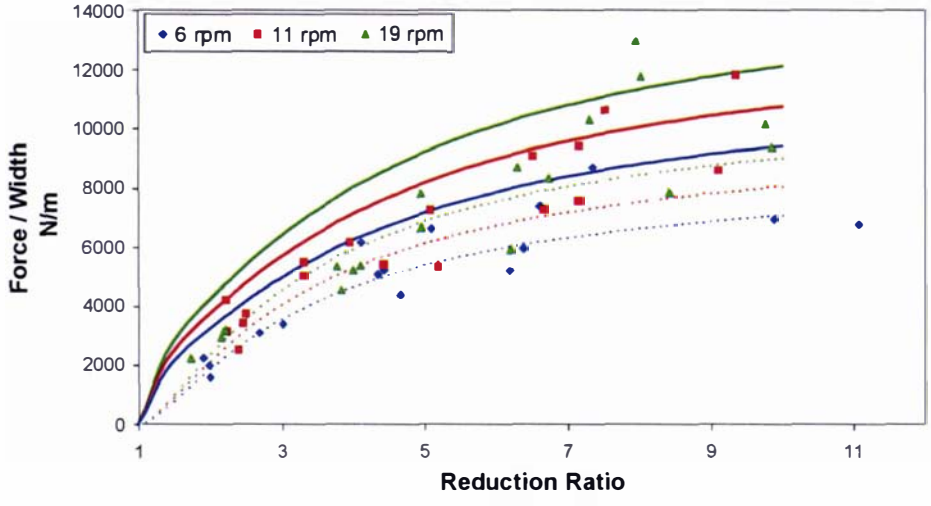

b)

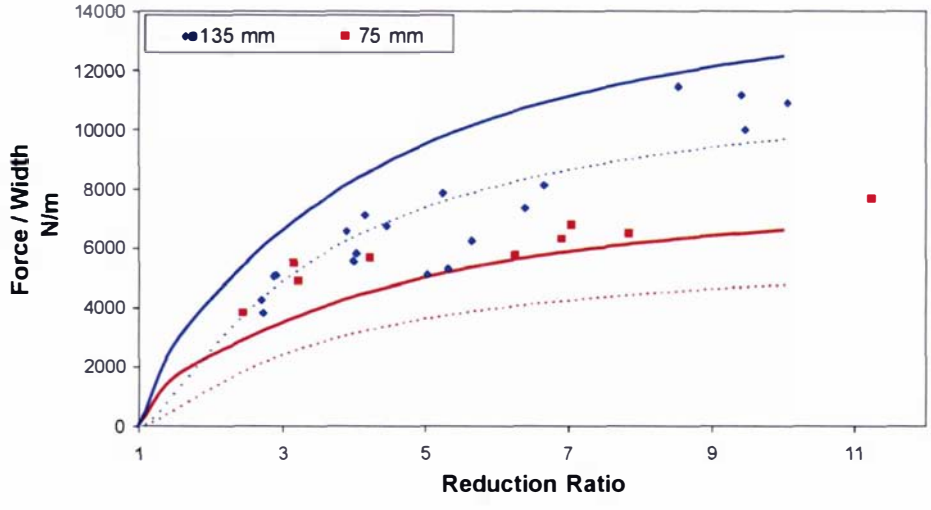

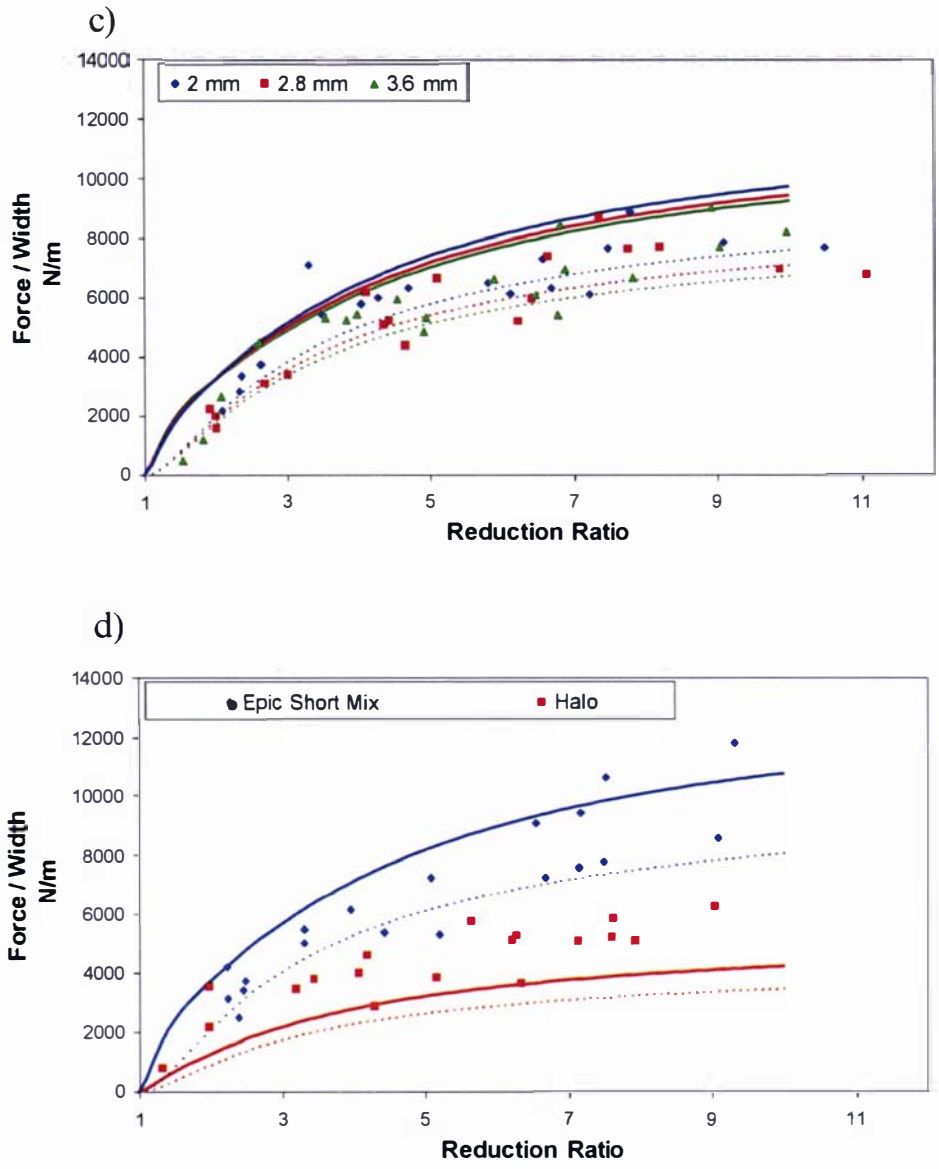

Figure 6.3 Model predictions for the Upward Force per unit width. The points are the experimental data, the solid lines are the CEF model predictions, the dotted lines are Newtonian model predictions. a) Varying Roller Speed, for Epic Short Mixed Dough, 135 mm radius roller, 2.8 mm nip gap. b) Varying Roller Radius, for Epic Short Mixed Dough, 2 mm nip gap, 19 rpm roller speed. c) Varying Nip Gap, for Epic Short Mixed Dough, for Epic Short Mixed Dough, 135 mm radius roller, 6 rpm roller speed. d) Varying Dough Type, for 135 mm radius roller, 2.8 mm nip gap, 11 rpm roller speed.

It was found from the experimental data that the upward force per unit width, on the rollers, ranges between about 2,000 and 10,000 Nm^{-1}. It was found that the upward force per unit width increased slightly with reduction ration; increased with roller speed; increased with roller diameter; and varied with dough type, Halo dough giving the lowest. The upward force per unit width, was quite insensitive to changes in the nip gap.

Figure 6.3 demonstrates that the upward force per unit width, predictions of the CEF model are close to the experimental results. The CEF model results are also compared with those of a Newtonian model based upon Middleman (1977). The Newtonian model used here differs from that of Middleman's by having a finite inlet height (and hence a dependence upon reduction ratio). Equation 6.4 was used to determine the viscosity for the Newtonian model; thus the viscosity despite being "constant" is dependent upon the sheeting conditions, in the same way that the CEF model is.

In general, the CEF prediction of the upward force per unit width, is greater than the Newtonian prediction, for a particular sheeting condition, with the experimental data scattered between the predictions. Both sets of predictions have a similar dependency upon reduction ratio. Both models show appropriate trends with respect to roller speed, roller diameter and dough type. Both models are insensitive to changes in the nip gap (which is consistent with the experimental measurements).

Due to the large variation in the experimental data it is difficult to judge which model (CEF or Newtonian) best represents the observations. During the design of a sheeting system, it may be better to use the CEF model, as it will predict a larger and possibly more realistic force experienced by the roller.

Figure 6.3 d) demonstrates that the solution is sensitive to the values that are chosen for the CEF parameters. Figure 6.3 d) and Figure 6. 4 suggest that the variation due to rheological properties (i.e. dough type) which is predicted by the CEF model is in fact too great. In both of these figures, there is an experimentally observed difference between the short mixed Epic dough and the halo dough. This trend of this difference is reflected in the CEF model predictions, but the model considerably under-predicts the magnitude of the Halo dough results. Figure 6.4 demonstrates that, similarly, the magnitude of the long mixed Epic dough results is considerably over-predicted by model.

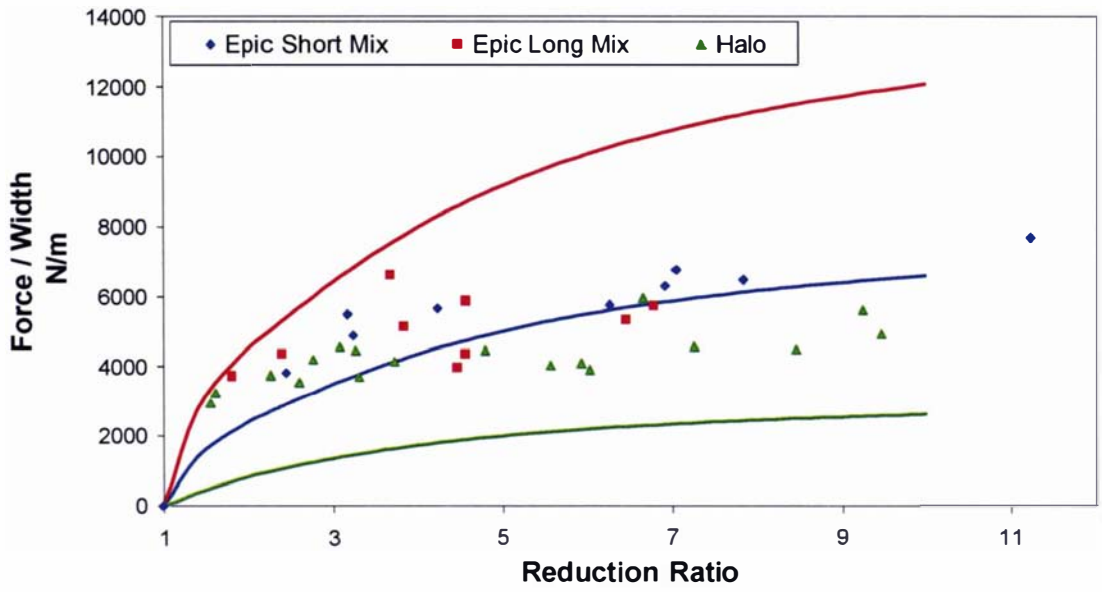

Figure 6.4 Model predictions for the Upward Force per unit width. For three dough types. (The points are the experimental data, the solid lines are the CEF model predictions). Sheeting conditions are: 75 mm radius roller, 2 mm nip gap, 19 rpm roller speed.

The over sensitivity of the model to rheology properties, means that the three dough types display more similar rheological behaviours (to each other) when sheeted than they do in the rheological instruments which were used to determine their model properties. A possible solution to this problem is to use a specialised instrument, which simulates the sheeting process, to measure the dough properties. However, such an approach does not aid in a fundamental understanding of the processes that occur in the sheeting process, as discussed in Section 1.5.4.

A use of the force predictions is to estimate the distortion that a roller might undergo during a sheeting operation (as illustrated in Figure 6.5).

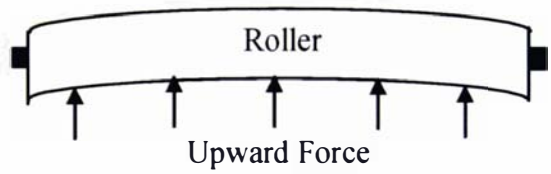

Figure 6.5 Roller Distortion (Not to Scale).

From Shigley and Mischke (2001), the distortion experienced by the roller (assuming the roller can be approximated by a fixed beam) is given by the equation:

$$\Delta\hat{y} = \frac{\hat{W}^4}{384GI}\frac{\sum \hat{F}_y}{\hat{W}} \tag{6.9}$$

where: $\hat{W}$ = the width of the roller, [m]; G = the modulus of Elasticity (of the roller material), [Pa]; I = the 2nd moment of inertia of the roller; $\frac{\sum \hat{F}_y}{\hat{W}}$ = the total force/per unit area, experienced by the roller.

For a cylindrical roller:

$$I = \frac{\pi \hat{R}^4}{4} \tag{6.10}$$

Thus given that the approximate force experienced by the rollers varies between 1,000 and 10,000 Nm^{-1}, E for 303 stainless steel is about 193 GPa, the roller radius between 135 and 75 mm, and that the roller width is about 1 m, then the approximate distortion of the roller should be 5×10^{-8} to 5×10^{-6} m. Such a small distortion is unlikely to be significant and hence is not responsible for the discrepancy between modelled and observed exit height. The small distortion also suggests that stainless steel is a significantly over designed material (from a structural perspective) with which to construct the rollers of a dough sheeter.

6.5. Torque Predictions

It was found from the experimental data that the torque per unit width, on the rollers, ranged between about 100 and 500 N. It was found that the torque per unit width: increased with reduction ratio; increased with roller speed; increased with roller diameter; and varied with dough type, Halo dough being the least. Like the force per unit width, measurements the torque per unit width measurements were insensitive to changes in nip gap.

The CEF model predictions for the torque per unit width, are compared in Figure 6.6 to both the experimental data and a Newtonian model based upon Middleman (1977) (the same model used in the upwards force comparisons).

a)

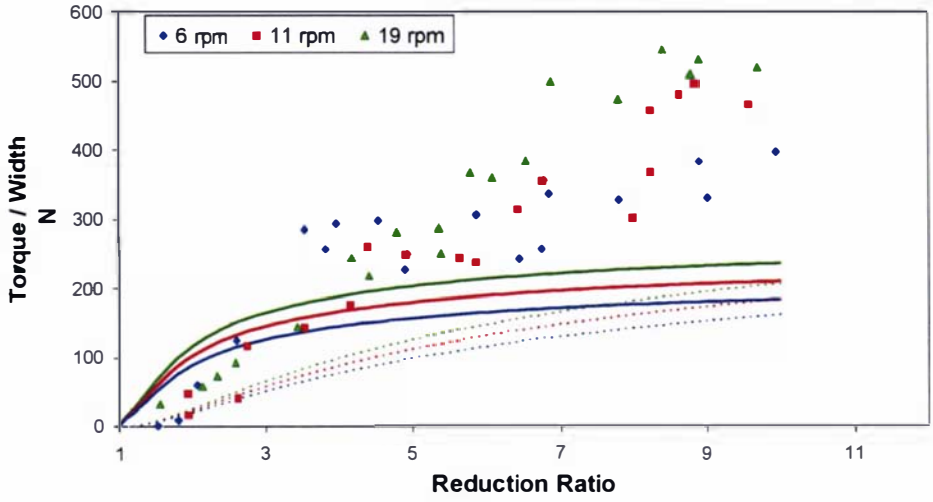
6 rpm
11 rpm
19 rpm
Torque / Width
N
600
500
400
300
200
100
0
1
3
5
7
9
11
Reduction Ratio

b)

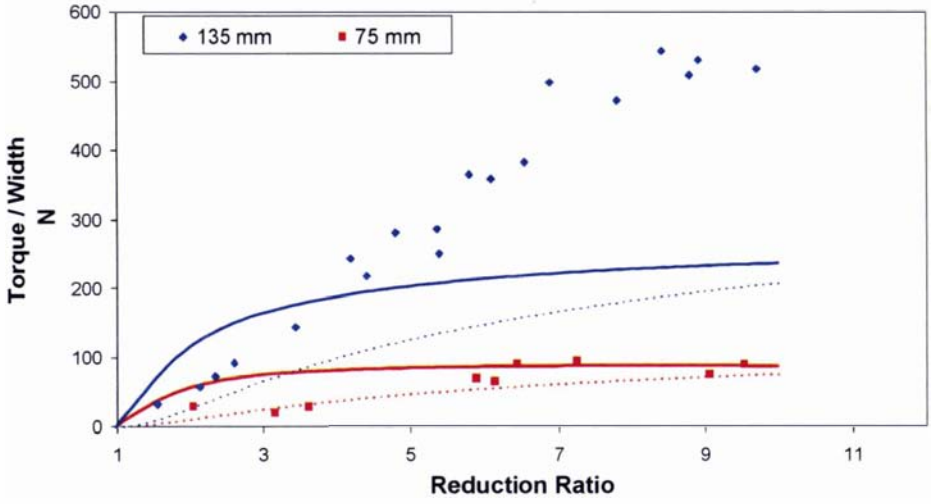
135 mm
75 mm
Torque / Width
N
600
500
400
300
200
100
0
1
3
5
7
9
11
Reduction Ratio

c)

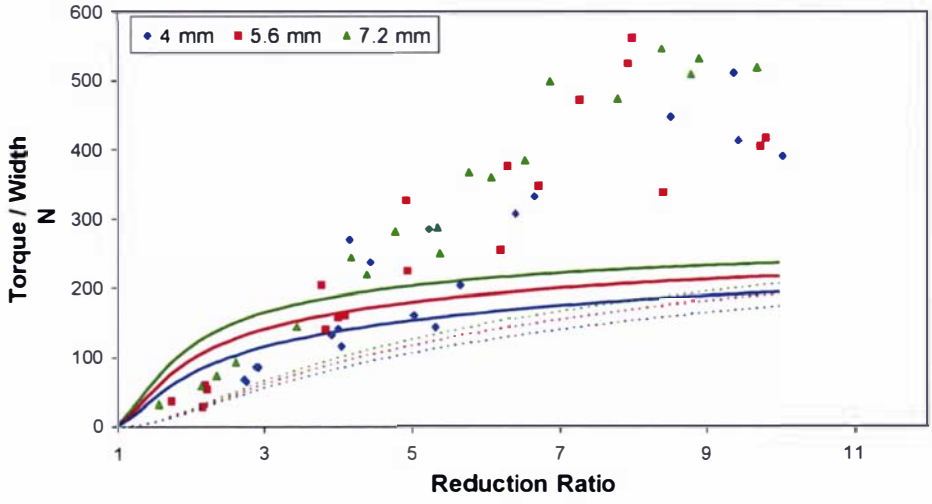
4 mm
5.6 mm
7.2 mm
Torque / Width
N
600
500
400
300
200
100
0
1
3
5
7
9
11
Reduction Ratio

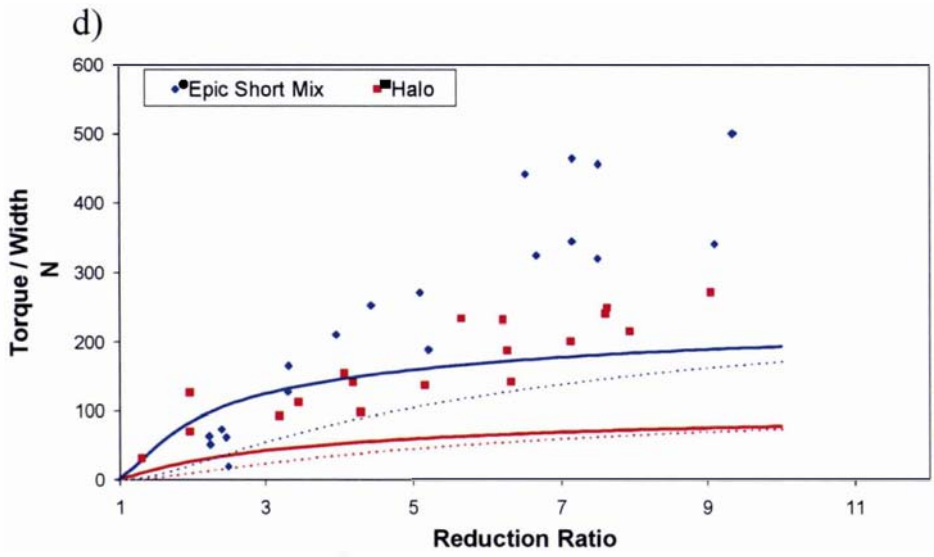

Figure 6.6 Model predictions for the torque per unit width. The points are the experimental data, the solid lines are the CEF model predictions, the dotted lines are Newtonian model predictions. a) Varying Roller Speed, for Epic Short Mixed Dough, 135 mm radius roller, 3.6 mm nip gap. b) Varying Roller Radius, for Epic Short Mixed Dough, 3.6 mm nip gap, 19 rpm roller speed. c) Varying Nip Gap, for Epic Short Mixed Dough, for Epic Short Mixed Dough, 135 mm radius roller, 6 rpm roller speed. d) Varying Dough Type, for 135 mm radius roller, 2.8 mm nip gap, 11 rpm roller speed.

As with the upward force, the CEF model predicts a greater magnitude of torque per unit width, than the Newtonian model. The predictions from both models are considerably lower in magnitude than the experimental observations, although the trends of the responses to changes in sheeting conditions are correct.

6.6. Pressure Profile

The model can also be used to plot the pressure profile that occurs in the dough during sheeting. Figure 6.7 shows the predicted pressure profiles for several sheeting conditions.

In all cases, illustrated in Figure 6.7, the pressure peaks near, but slightly to the left (inlet side) of the nip gap. There is also a slight pressure gradient in the y direction, with higher pressures occurring away from the rollers, near the line of symmetry. The region of highest pressure is, therefore, likely to be near the line of symmetry and slightly to the inlet side of the nip gap.

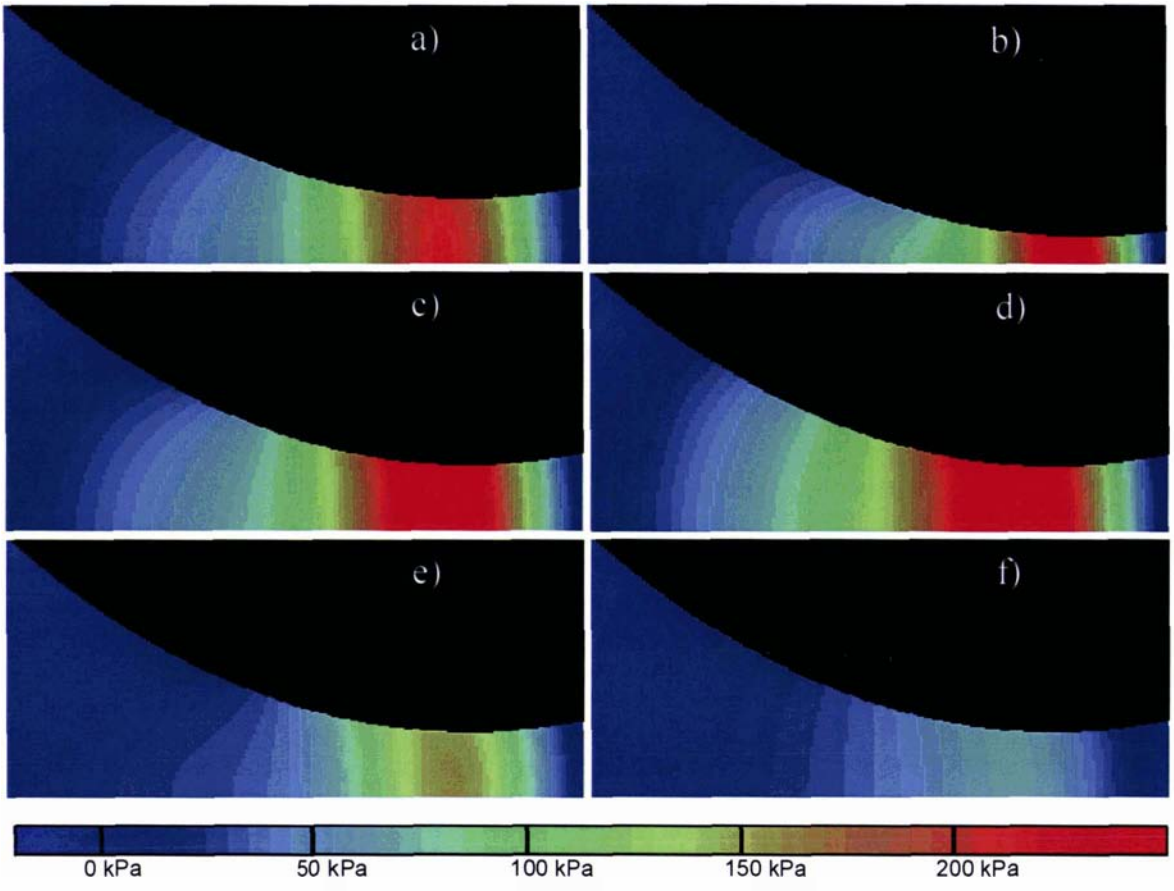

Figure 6.7 Pressure Profiles for Varying Sheeting Conditions, upper half of dough (assuming symmetry boundary). Black shadow represents roller position. Dough is travelling left to right. Pressure scale indicated above. x and y dimensions are approximate, only. a) Epic Short Mixed Dough, 135 mm radius roller, 3.6 mm nip gap, 6 rpm roller speed, and a reduction ratio of 4; b) Epic Short Mixed Dough, 135 mm radius roller, 3.6 mm nip gap, 6 rpm roller speed, and a reduction ratio of 10; c) Epic Short Mixed Dough, 135 mm radius roller, 3.6 mm nip gap, 19 rpm roller speed, and a reduction ratio of 4; d) Epic Short Mixed Dough, 135 mm radius roller, 2 mm nip gap, 6 rpm roller speed, and a reduction ratio of 4; e) Epic Short Mixed Dough, 75 mm radius roller, 3.6 mm nip gap, 6 rpm roller speed, and a reduction ratio of 4; f) Halo Dough, 135 mm radius roller, 3.6 mm nip gap, 6 rpm roller speed, and a reduction ratio of 4.

By comparing each of the individual pressure profiles to the base case of Figure 6. 7a), the effect of the sheeting conditions can be determined. Figure 6. 7b) demonstrates that changing the reduction ratio from a value of 4 to a value of 10 results in a greater (redder) pressure in the region of the nip. Furthermore, the red region of high pressure is smaller (relative to total area under the roller). Likewise increasing the roller speed (Figure 6. 7c)) increases the size of the high pressure in the nip region. Figure 6. 7d) shows that decreasing the nip gap (from 3.6 mm to 2 mm) increases the size of the high pressure region. Decreasing the nip gap also widens the region of high pressure slightly towards the inlet. Figure 6. 7e) demonstrates that decreasing the size of the roller radius (from 135 mm to 75 mm) results in a marked decrease in the pressure in the nip gap.

Finally, Figure 6. 7f) shows that changing the dough type (from Epic: short mixed to Halo) also has a large effect, dramatically lowering pressure in the nip gap.

The variation in nip gap pressure (increasing with increasing roller speed and roller radius and decreasing with increasing nip gap) is consistent with the behaviour of the upward force measurements, which the model predicts are largely dependent upon the pressure. The change observed in the pressure profile when the dough type varies is also consistent with the upwards force behaviour. The increase in upwards force, observed as the reduction ratio increases, can be explained by considering the fact that as the reduction ratio increases, a greater proportion of the surface area of the dough comes into contact with the roller, thereby exerting a greater integral force upon the roller.

Finally, Figure 6.8 shows a comparison between the CEF model developed here, and a Newtonian model. The CEF model predicts a greater maximum pressure. For the Newtonian model the point of maximum pressure is considerably closer to the inlet than it is for the CEF model.

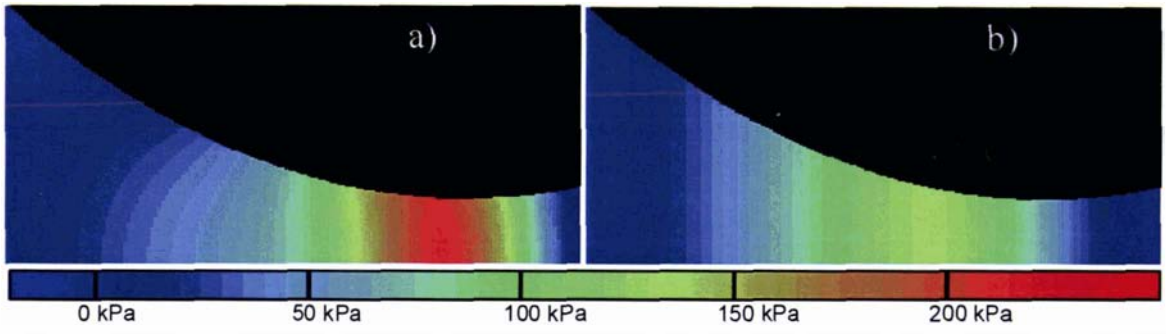

Figure 6.8 Pressure Profiles for CEF and Newtonian models. Sheeting Conditions are: Epic: Short Mixed Dough, 135 mm radius roller, 3.6 mm nip gap, 6 rpm roller speed, and a reduction ratio of 4. a) CEF model; b) Newtonian model.

6.7. Velocity Profile

In Figure 6.9, the velocity profiles for a number of representative sheeting conditions are plotted. The velocity profiles were determined using the equations given in Section 5.7.

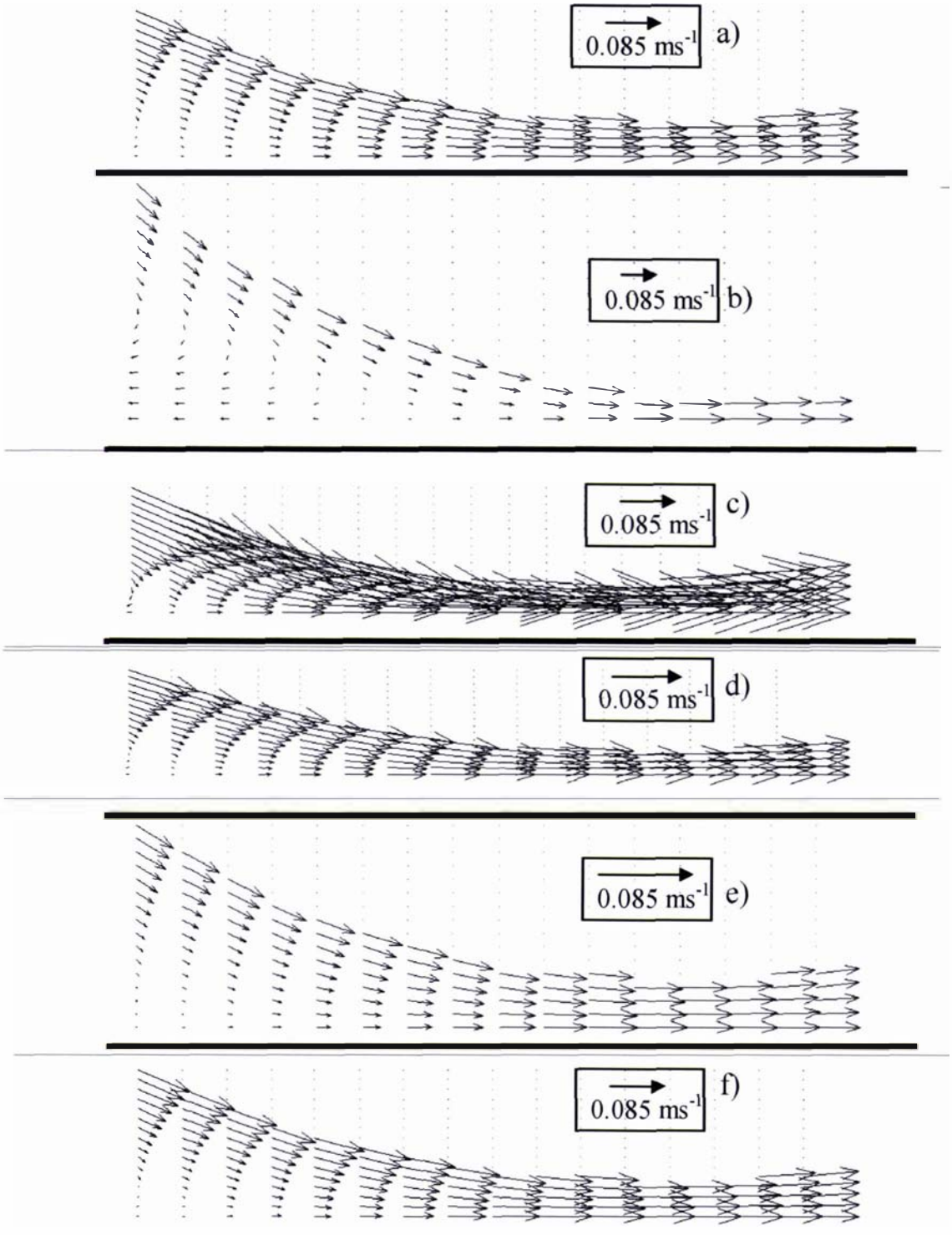

Figure 6.9 Velocity Profiles for Varying Sheeting Conditions, upper half of dough (assuming symmetry boundary). x and y dimensions are approximate. a) Epic Short Mixed Dough, 135 mm radius roller, 3.6 mm nip gap, 6 rpm roller speed, and a reduction ratio of 4; b) Epic Short Mixed Dough, 135 mm radius roller, 3.6 mm nip gap, 6 rpm roller speed, and a reduction ratio of 10; c) Epic Short Mixed Dough, 135 mm radius roller, 3.6 mm nip gap, 19 rpm roller speed, and a reduction ratio of 4; d) Epic Short Mixed Dough, 135 mm radius roller, 2 mm nip gap, 6 rpm roller speed, and a reduction ratio of 4; e) Epic Short Mixed Dough, 75 mm radius roller, 3.6 mm nip gap, 6 rpm roller speed, and a reduction ratio of 4; f) Halo Dough, 135 mm radius roller, 3.6 mm nip gap, 6 rpm roller speed, and a reduction ratio of 4.

All cases are consistent with the boundary conditions, that is: at the roller surface the dough velocity is equal to the tangential surface speed of the roller, and at the line symmetry the direction of movement is horizontal. As with the pressure profiles, comparing the individual plots to the base case of Figure 6.9a) demonstrates the effect upon the velocity profile of changing sheeting conditions.

Figure 6.9b) demonstrates that increasing the reduction ratio results in an increase in the size of the re-circulation region, which is practically non-existent in the base case. It may appear that the magnitude of the velocities in Figure 6.9b) are diminished, particularly with respect to the velocity at the roller surface. However, this is not the case, as the scales in the two plots are different; the resolution of Figure 6.9b) is smaller, in order to accommodate the increased size of the region under the roller. In fact, the velocities close to the roller surface in Figure 6.9a) and Figure 6.9b) are identical.

Figure 6.9c) demonstrates that increasing the roller velocity increases the velocities within the dough. Roller velocity does not seem to effect the formation of the re-circulation region. Figure 6.9d) demonstrates that changing the nip gap seems to have no effect upon the re-circulation region. Figure 6.9e) illustrates the elementary fact that if the roller speed (in rpm) is unchanged while the roller diameter is decreased, then the velocities within the dough will decrease. Finally, Figure 6.9f) shows that the properties of the dough have no influence on the shape of the velocity profiles. This is expected from an inspection of the relevant equations in section 5.7; these do not contain the dough property parameters of η, Ψ_1 or Ψ_2.

An application for which velocity profile information can be used is to determine the conditions under which re-circulation will occur. In Figure 6.10, a typical velocity profile where re-circulation is occurring has been drawn. (The area of re-circulation is shaded for clarity). Examining the horizontal velocity along the axis of symmetry (at which $y = 0$), it can be seen that to the right of point x_r the horizontal velocity component is positive. To the left of x_r, where re-circulation is occurring, the horizontal velocity component is negative and at the point x_r the horizontal velocity component is equal to zero. Clearly, if point x_r lay, for a particular sheeting condition, between the inlet and exit distances (x_i and x_e, respectively) then re-circulation would be observed.

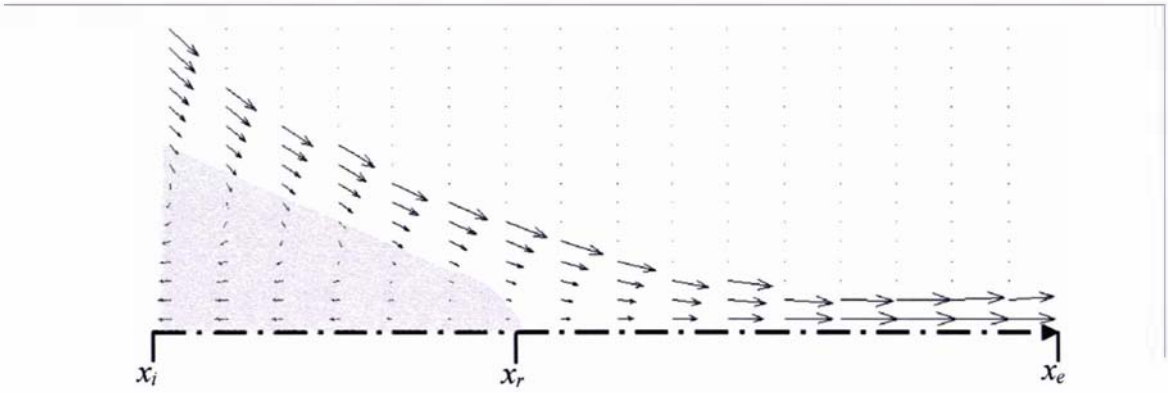

Figure 6.10 Velocity Profile, where re-circulation is occurring. Distance x_r is the point at which re-circulation begins. x_i and x_e are the inlet and exit distances, respectively. x and y dimensions are only approximate. For clarity the approximate area of re-circulation has been shaded.

The value of x_r can be calculated from the equations for the horizontal velocity components.

$$\text{When } x = x_r,\ 0 = u_0 + \varepsilon u_1 + \varepsilon^2 u_2\big|_{y=0} \tag{6.11}$$

Substituting in equations (5.67, 5.73, and 5.79) for the horizontal velocity components, and solving for x_r gives:

$$x_r = -\frac{1}{2}\sqrt{\frac{\left[\begin{array}{l}\varepsilon^2\left(15x_e^{\,4}+24x_e^{\,2}-88\right)-60x_e^{\,2}-40 \\ -\sqrt{3}\sqrt{\begin{array}{l}\varepsilon^4\left(75x_e^{\,8}+480x_e^{\,6}+1008xe^4+1472x_e^{\,2}+2752\right) \\ -\varepsilon^2\left(600x_e^{\,6}-3120x_e^{\,4}-4480x_e^{\,2}-1280\right) \\ +1200x_e^{\,4}+4800x_e^{\,2}+4800\end{array}}\end{array}\right]}{\varepsilon^2\left(3x_e^{\,2}+8\right)-10}} \tag{6.12}$$

This model shows that the point at which re-circulation occurs is dependent upon only on the exit distance, x_e, and the geometry ratio, ε.

Figure 6.11 shows a plot of the ratio of inlet thickness to nip gap at which re-circulation should be observed (the reduction ratio). If the reduction ratio for a certain sheeting condition is greater than the re-circulation ratio then re-circulation should be observed. If it is lower then re-circulation will not occur. The figure demonstrates that for most practical sheeting arrangements of ε, the re-circulation ratio is between 3.5 and 4. This value is consistent with the work of Morgenstern and Ross, 1998. The re-circulation increases with x_e, the exit distance. The values of x_e chosen here are typical of the, possibly unrealistically, small range of possible values that the model predicts, as discussed in Section 6.3.

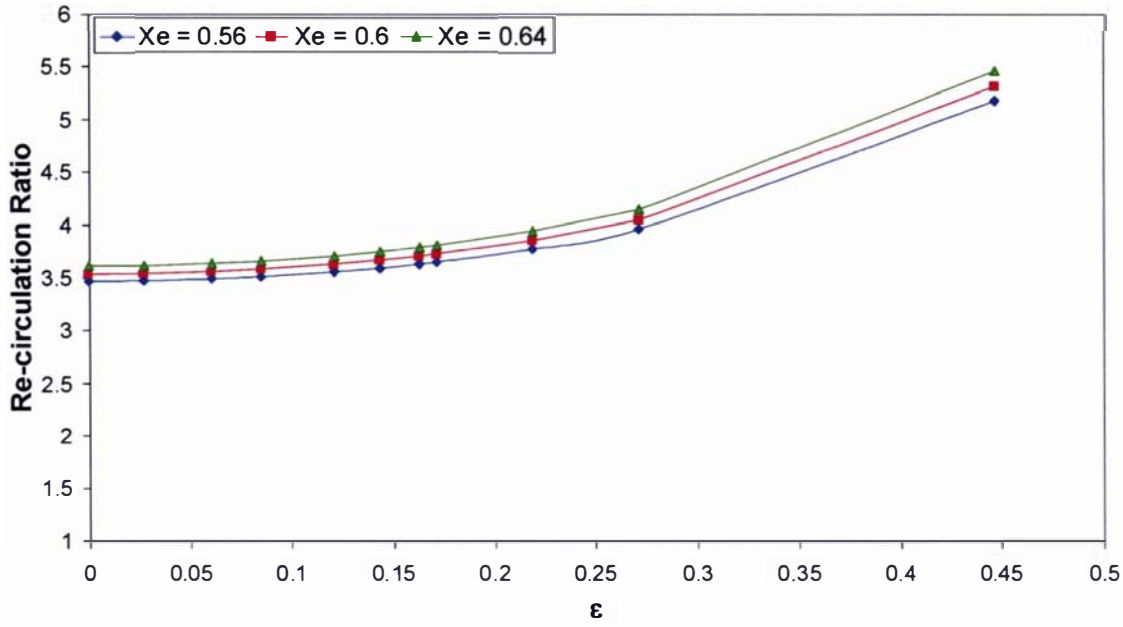

Figure 6.11 Ratio of inlet height to nip gap at which re-circulation occurs, for different values of ε.

It is surprising that the formation of the re-circulation region (or indeed any particular velocity profile) is independent of the dough properties (except in so far as the exit distance is very weakly influenced by dough properties), and solely dependent upon the geometry. Perhaps this represents a shortcoming in the model.

7. Conclusion

A model of the behaviour of bread dough during the dough sheeting operation has been developed. This operation is an important part of bread dough manufacture, performing shaping, laminating and development functions.

The operation was simply modelled using friction coefficient and compression models. These models were not accurate, although they did capture some physical characteristics of the system. A more detailed continuum mechanics model was also developed to describe the dough sheeting system. Although clearly neither final nor comprehensive, this model has increased the understanding of the bread dough sheeting process.

The model is a fundamental, continuum mechanics model, which differs from previous models in its choice of constitutive equation and in the use of the perturbation solution technique. A constitutive equation is used to describe the dough's deformation properties, and the chosen equation was the Criminale-Ericksen-Filby (CEF) equation. This equation was chosen because of its capability of representing viscoelastic materials in conditions close to steady state and, its relative simplicity. Despite the simplicity of the CEF equation some difficulties were encountered in measuring the properties of the dough adequately with available instruments. The CEF equation allows the model to demonstrate some of the effects of the processing material's rheological properties upon sheeting outcomes, for example the force on the roller.

A reasonably realistic description of the geometry of the problem was used in this model. Important assumptions made by the model were that:

- the process was two dimensional, with variation occurring in the length and height under the sheeting rollers, but with no variation in the direction of the width of the rollers;
- the process is isothermal;
- it is not subject to inertial or gravitational effects;
- the process is symmetrical about the centre line between the rollers;
- dough is incompressible;
- slip does not occur on the roller surfaces.

These assumptions were justified by appeals to the literature and preliminary calculations of the orders of magnitude of effects. The assumption that dough is incompressible is probably the most likely assumption to require modification in the future development of this model.

The method by which the model was solved was different from methods used in developing some other models of the process. A perturbation technique was used for the solution. In this technique the equations for the system are written in terms of a small dimensionless perturbation parameter, $\varepsilon \left(= \sqrt{\delta / R}\right)$, which is then set to be of value zero. The model is solved for this case, and the solution (the zero order solution) is then used to solve the case in which ε is non-zero but higher order terms (ε^2, ε^3...) remain set at a value of zero. This solution (first order) is then used to solve for the second order solution and so on; in each sequential solution the next successive order of ε is set to non-zero. Thus the solution is perturbated about ε and converges upon the "true" solution to the original system of equations. The perturbation solution technique was employed because the set of perturbated solutions, although algebraically complex, are computationally simple. Computational simplicity means that the model output can be quickly generated using a desktop PC and therefore might be more useful as a real time guide in designing and re-tooling efforts than alternative methods, for example finite element techniques, which can take a number of hours to solve even with sophisticated computers.

It was found that the model could be used to predict the exit height, force and torque on the rollers and the velocity and pressure profiles in the dough during the sheeting process. The exit height predictions made were the least accurate in comparison with measurements made on a pilot plant sheeter. This might be due to the neglect of compressibility in the model. The force and torque measurements were better predicted than the exit height ratio, although not perfectly predicted, and the velocity and pressure profiles were consistent with other work. Model predictions could be applied, for example, to estimating the deflection of the rollers or to predicting the conditions under which re-circulation might occur.

The variance between the model predictions and the experimental measurements could be due to problems with the model and / or the experiments. Both model and experiments were adversely affected by the fact that the properties of dough change during processing, that is they are history dependent. This resulted in difficulties both measuring dough properties (for the model) and performing the experimental measurements with doughs of consistent properties. A possible solution, and goal for future work, is to use a more realistic constitutive equation to describe the dough properties, for example the Phan-Thien-Tanner equation (Phan-Thien et. al., 1997). A potential problem with this approach would be that the model might become too complex to solve. Even if such a model could be solved swiftly computationally, performing measurements upon dough, to determine the parameters of a more realistic constitutive equation, is likely to increase the total handling time of the model beyond what is appropriate for use in a production environment.

It would also be interesting to measure the sheeting behaviour of simpler materials, such as conventional polymers, with more easily measurable rheological properties, and then compare this behaviour to that predicted by the model. Such work could aid in determining whether the problems encountered in using the model accurately to predict dough's sheeting behaviour, are due to the difficulties in adequately describing the dough or to a fundamental problem with the model itself.

Other possible goals for future work include challenging the assumptions of the model, for example compressibility, and comparing this solution of the dough sheeting model to that developed with another solution method, for example a finite element technique.

8. References

Anderssen, RS, Gras, PW, MacRitchie, F, "Linking mathematics to data from the testing of wheat-flour dough", *Chemistry in Australia,* **Sept,** (1997) 3-5.

Bagley, EB, Christianson, DD, Martindale, JA, "Uniaxial Compression of a Hard Wheat Flour Dough: Data Analysis using the Upper Convected Maxwell Model", *Journal of Texture Studies,* **19,** (1988) 289-305.

Bagley, EB, Christianson, DD, Trebacz, DL, "The computation of viscosity and relaxation time of doughs from Biaxial Extension data", *Journal of Texture Studies,* **21,** (1990) 339-354.

Barnes, HA, Hutton, JF, Walters, K, An Introduction to Rheology, Elsevier Science, 1989.

Barney, JE, Pollock HB, Bolze, "A Study of the relationship between Viscoelastic Properties and the Chemical Nature of Wheat Gluten and Glutenin", *Cereal Chemistry*, **42**, (1965) 215-236.

Bhattacharya, M, "Slit rheometer studies of wheat flour dough", *Journal of Texture studies,* **24,** (1993) 391-409.

Bird, RB, Armstrong, RC, Hassager, O, Dynamics of Polymeric Liquids, 2nd ed, John Wiley and Sons,1987.

Bloksma, AH, "Dough structure Dough Rheology and Baking Quality", *Cereal Foods World,* **35,** (1990) 237-244.

Bloksma, AH, "Rheology of Wheat Flour Doughs", *Journal of Texture Studies,* **3,** (1972) 3-17.

Campbell, GM, Rielly, CD, Fryer, PJ, Sadd, PA, "Aeration of Bread Dough During Mixing: Effect of mixing dough at reduced pressure.", *Cereal Foods World,* **43,** (1998) 163-167.

Campos, DT, Steffe, JF, NG, PKW, "Rheological Behaviour of Undeveloped and Developed Wheat Dough", *Cereal Chemistry,* **74,** (1997) 489-494.

Castell-Perez, ME, Steffe, JF, "Viscoelastic properties of dough", Viscoelastic Properties of Foods, ELSEVIER, 1992.

Chong, JS, "Calendering Thermoplastic Materials", *Journal of Applied Polymer Science,* **12,** (1968) 191-212.

Dus, SJ, Kokini, JL, "Prediction of the non-linear viscoelastic properties of a hard wheat flour dough using the Bird-Carreau constitutive model", *Journal of Rheology,* **34,** (1990) 1069-1084.

Eliasson AC, Larsson K, Cereals in Breadmaking: A molecular colloidal approach, Marcel Dekker, New York, 1993

Faubion, JM, Hoseney, RC, "The Viscoelastic Properties of Wheat Flour Doughs", Dough Rheology and Baked Product Texture, Chapman, 1989.

Ferry, JD Viscoelastic Properties of Polymers, 3rd Edition ,John Wiley and Sons, 1980.

Finston, M, "Thermal Effects in Calendering Viscous Fluids", *Journal of Applied Mechanics,* **18,** (1951) 12-18.

French, FD, Fish, AR, " High Speed Mechanical Dough Development", *Bakers Digest,* **55**, (1981) 80-82.

Gaskell, RE, "The Calendering of Plastic Materials", *Journal of Applied Mechanics,* **17,** (1950) 334-336.

Gorton, L, "Stressing Sheeting", *Baking and Snack,* **June,** (1997) 34-39.

Hibberd GE, Parker NS, "Measurement of the Fundamental Rheological Properties of Wheat Flour Doughs", *Cereal Chemistry*, **52**, (1975) 2r-23r

Keentok M, Newberry MP, Gras P, Bekes F, Tanner RI, "The Rheology of Bread Made from Four Commercial Flours", *Rheol. Acta*, **41**, (2002) 173-179

Kilborn, RH, Preston, KR, "A Dough Sheeting and Molding Property Indicator", *Cereal*

Chemistry, **59,** (1982) 171-174.

Kilborn, RH, Tipples, KH, "Implications of Mechanical Development of Bread Dough by Means of Sheeting Rolls", *Cereal Chemistry,* **51,** (1974) 648-657.

Kiparissides, C, Vlachopouplos, J, "Finite Element Analysis of Calendering", *Polymer Engineering and Science,* 16, (1976) 712-719.

Lange K, Handbook of Metal Forming, McGraw Hill, Inc, 1985.

Larsson, H, Eliasson, A, "Phase Separation of Wheat Flour Dough studied by Ultracentrifugation and stress relaxation. (I & II)", *Cereal Chemistry,* **73,** (1996) 18-24, 25-31.

Launay, B, "A Simplified Non-Linear Model for Describing the Viscoelastic Properties of Wheat Flour Doughs at Hugh Shear Strains.", *Cereal Chemistry,* **67,** (1990) 25-31.

Launay, B, Bure, J, "Application of a viscometric method to the study of wheat flour doughs", *Journal of Texture Studies,* **4,** (1973) 82-101.

Levine, L, "Models for Dough Compressibility in Sheeting", *Cereal Foods World,* **43,** (1998) 629-634.

Levine, L, Corvalan, CM, Campanella, OH, Okos, MR, "A Model Describing the Calendering of Finite Width Sheets", *Chemical Engineering Science,* **57**, (2002) 643-650

Levine, L, Drew, BA, "Rheological and Engineering aspects of the sheeting and laminating of Doughs", Dough Rheology and Baked Product Texture, Chapman, 1989, 513-555.

Levine, L, Levine, S, "A premliminary investigation of the Deformation of Cereal Pellets by Flaking Rolls.", *Cereal Foods World,* **42,** (1997) 444-451.

Mackey, KL, Ofoli, RY, "Rheological Modelling of corn starch doughs of low to intermediate moisture", *Journal of Food Science,* **55,** (1990) 417-423.

Menjvar, JA, "Fundamental Aspects of Dough Rheology", Dough Rheology and Baked

Product Texture, Chapman, 1989.

Middleman, S, Fundamentals of Polymer Processing, McGraw Hill Ltd, 1977.

Mitsoulis, E, Vlachopouplos, J, Mirza, FA, "Calendering analysis without the lubrication approximation", *Polymer Engineering and Science,* **25,** (1985) 6-18.

Montgomery, DC, Design and Analysis of Experiments, 4th ed, John Wiley and Sons, 1997.

Morgan, RG, Steffe, JF, Ofoli, RY, "A generalised visocosity model for the extrusion of protein doughs", *Journal of Food Process Engineering,* **11,** (1989) 55-78.

Morgenstern, M, Newberry, MP, Holst, SE, "Extensional Properties of Dough Sheets", *Cereal Chemistry,* **73,** (1996) 478-482.

Morgenstern, M, Ross, M, "Sheeting of Dough", *Research Bulletin, Crop & Food,* **3 Winter,** (1998).

Morgenstern, M, Zheng, H, Ross, M, Campanella, OH, "Rheological properties of sheeted wheat flour Dough measured with large deformations", *Submited Int. J. Food Properties Feb 1999,* (1999).

Morgenstern, MP, Wilson AJ, Ross M, Al-Hakkak F, "The Importance of Visco-Elasticity in Sheeting of Wheat Flour Dough", (2000), ICEF8.

Nayfeh AH, Introduction to Perturbation Techniques, John Wiley & Sons, Inc, 1981.

Phan-Thien, N, Safari-Ardi, M, Morales-Patino, A, Srinivasa Rao, PN, "Oscillatory and Simple Shear Flows of a flour-water dough: A Constitutive Equation", *Rheol. Acta.,* **36,** (1997) 38-48.

Raghavan, CV, Chand, N, Srichandan Babu, R, Srinivasa Rao, PN, "Modeling the Power Consumption during sheeting of doughs for tradional indian foods.", *Journal of Food Process Engineering,* **18,** (1995) 397-415.

Raghavan, CV, Srichandan Babu, R, Chand, N, Srinivasa Rao, PN, "Response Surface Analysis of Power Consumption of Dough Sheeting as a Function of Gap, Reduction

Ratio, Water, Salt and Fat", *Journal of Food Science Technology*, 33, (1996) 313-321.

Rahman, S, Food Properties Handbook, CRC Press, 1995.

Sharma, N, Hanna, MA, Chen, YR, "Flow Behaviour of Wheat Flour-Water Dough Using a Capillary Rheometer: 1: Effect of Capillary Geometry", *Cereal Chemistry,* **70,** (1993) 59-63.

Shigley JE, Mischke CR, Mechanical Engineering Design, 6th Edition, McGraw Hill Inc, 2001.

Simmonds JG, & Mann JE, A First Look at Perturbation Theory, Robert E. Kreiger Publishing Co., Inc, 1986.

Tanner, RI, Engineering Rheology, Clarendon Press, 1985.

U.S. Department of Agriculture, Agricultural Research Service, USDA Nutrient Database for Standard Reference, Release 15, 2002, Nutrient Data Laboratory Home Page, http://www.nal.usda.gov/fnic/foodcomp

Walker, CE, Hazelton, JL, "Dough Rheological Test", *Cereal Foods World*, **41**, (1996) 23-28.

Wang, CF, Kokini, JL, "Prediction of the non-linear Viscoelastic properties of Gluten Doughs", *Journal of Food Engineering,* **25,** (1995b) 297-309.

Wang, CF, Kokini, JL, "Simulation of the non-linear rheological properties of gluten dough using the wagner constitutive model", *Journal of Rheology,* **39,** (1995a) 1465-1482.

Zheng, H, Rheological Properties of Wheat Flour Dough, Master's Thesis, Massey University, New Zealand, 1998.

Zheng, R, Tanner RI, "A numerical analysis of calendering", *Journal of Non-Newtonian Fluid Mechanics*, **28**, (1998) 149-170

9. Appendix A: Experimental Details

This appendix contains additional detail about the experimental work.

9.1 Calibration of Measurement Devices

9.1.1. Motor Torque Load Cell

A Precision Transducer, ASB 125 kg, load cell was used to measure the torque, T, on the motor that turned the lower roller. The load cell was calibrated by hanging a series of weights (Wt) on a lever bar a known distance (Dt) from the roller shaft (as shown in Figure A.1). The calibration was performed dynamically, with the roller rotating, and the digital output (for a particular torque) was averaged over a 20s period. This eliminated errors due to asymmetry in either the roller or the shaft.

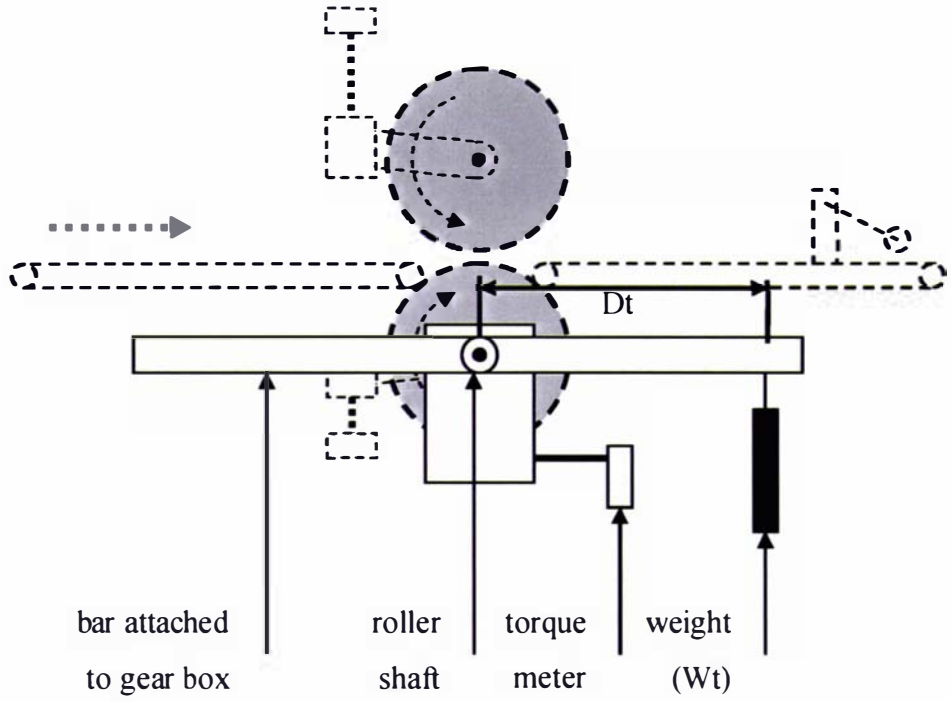

Figure A.1 Motor Torque Load Cell Calibration (diagram not to scale).

There was no significant variation in the digital output due to the direction or speed of the rollers.

On the calibration curve (Figure A.2) negative torques result from weights hung on the outlet side of the sheeter, while positive torques result from weights hung on the inlet side of the sheeter.

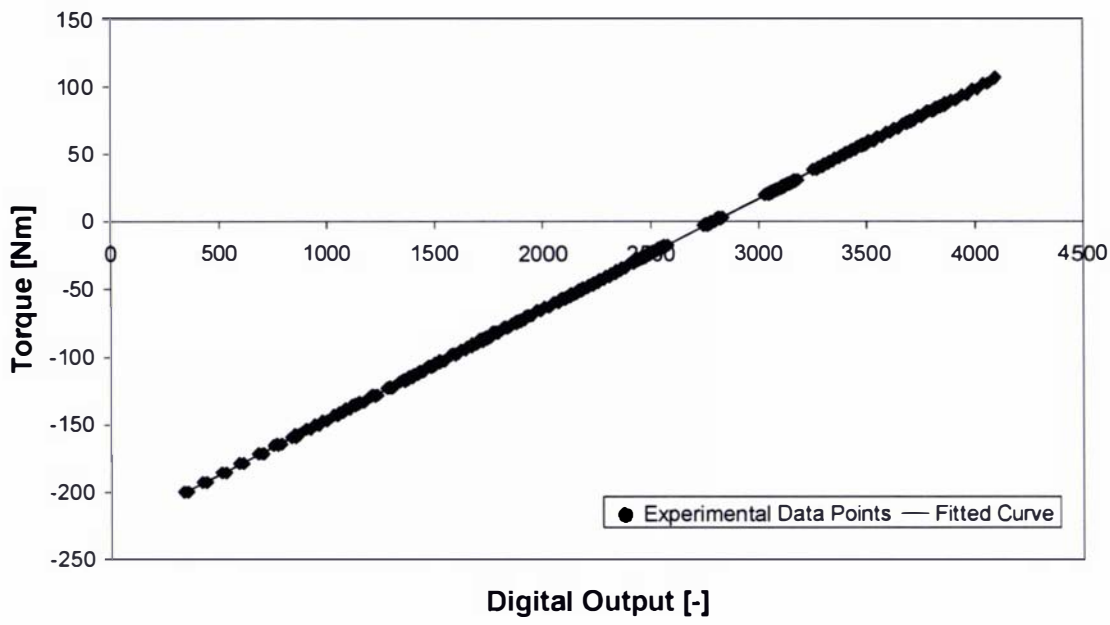

Figure A.2 Motor Torque Load Cell Calibration Curve

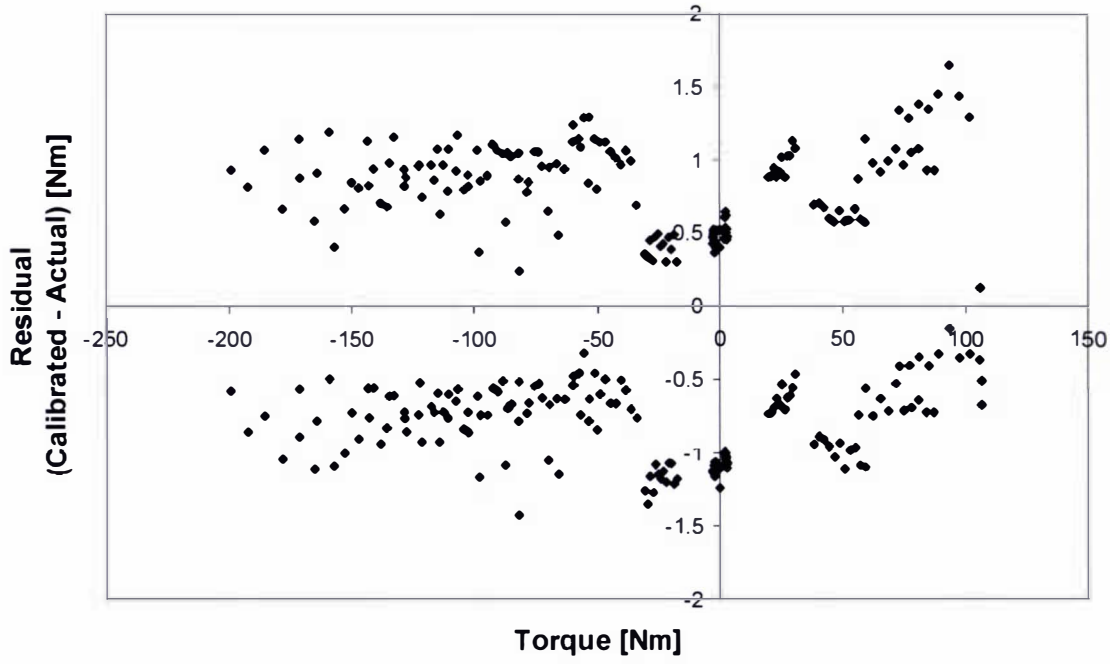

Figure A.3 Motor Torque Load Cell Calibration Residuals

The equation of the calibration curve was:

$$T = 0.0814(DS) - 227 \qquad \text{(A.1)}$$

where, DS = the digital signal. The R^2 value of the curve is 1.000.

The residuals of the calibration data are shown in Figure A.3. The residuals are distributed about zero, confirming the linear relationship. The accuracy of the torque calibration was about ± 1.5 N m.

9.1.2. Downward Force Load Cell

The downward force load cell measureed the total force exerted downwards (F) on the lower roller, as the dough was passed through the sheeter. A Precision Transducers, Model LPX, 1000 kg, load cell was used and was calibrated by hanging a series of weights (Wt) from the roller and recording the digital output (as shown in Figure A.4). Although in practice forces of 400-500 N are observed in sheeting, only masses corresponding to forces of up to 150 N were hung from the roller. It was assumed that the load cell remained linear beyond this range and into the sheeting range.

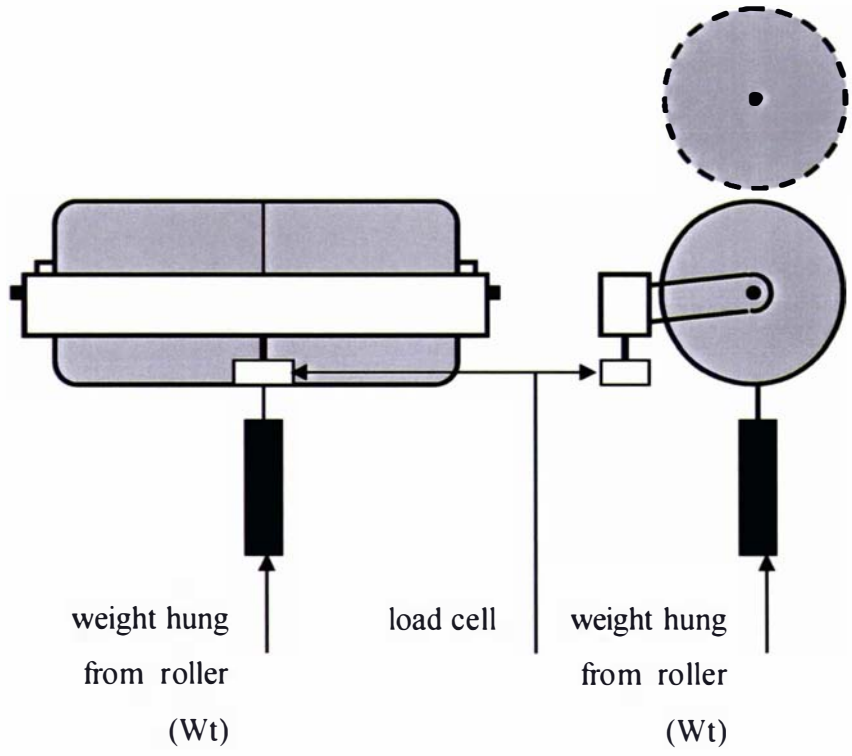

Figure A.4 Downward Force Load Cell Layout

The calibration curve shown in Figure A.5 was used to calibrate the digital output of the downward force load cell. The equation of the calibration curve was:

$$F = 2.0817(DS) - 892 \qquad \text{(A.2)}$$

where, DS = the digital signal. The R^2 value of the curve is 1.000.

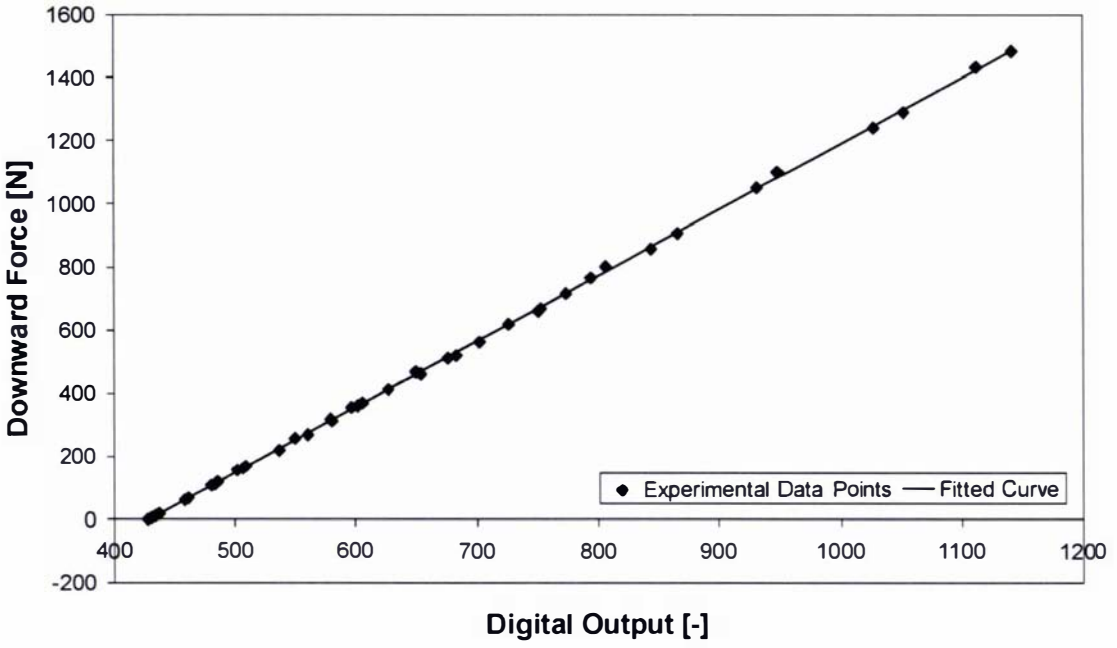

Figure A.5 Downward Force Load Cell Calibration Curve

The residuals of the calibration data are shown in Figure A.6. The residuals are distributed about zero, confirming the linear relationship. The accuracy of the force calibration was about ± 15 N.

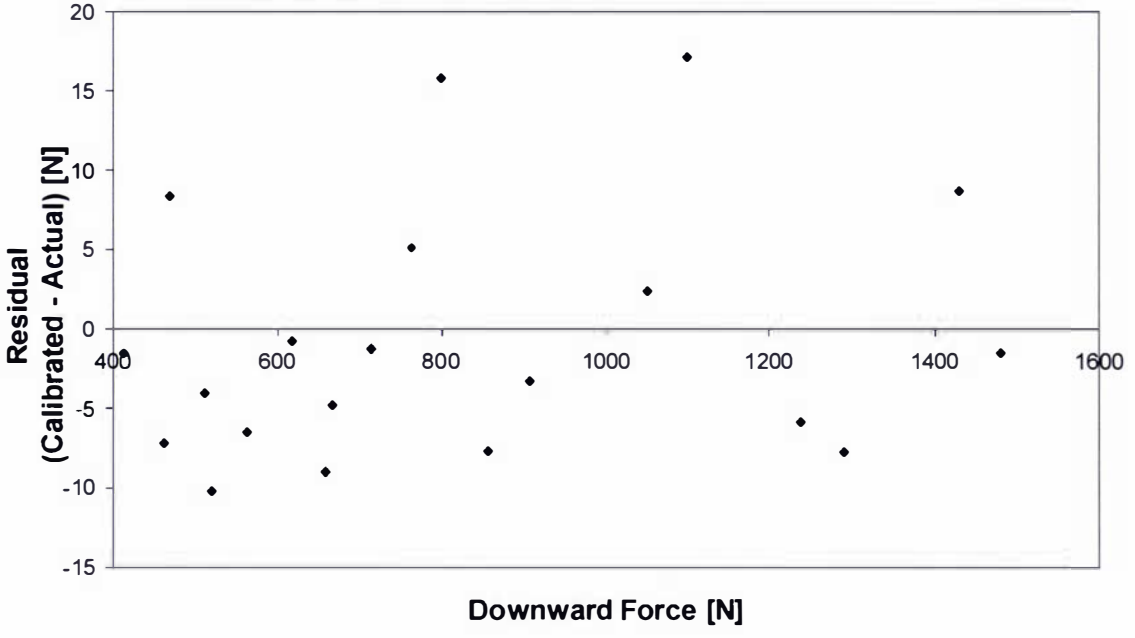

Figure A.6 Downward Force Load Cell Calibration Residuals

9.1.3. Exit Height Meter

The thickness of the sheet, as it left the sheeter, was measured with a wheel attached to a rotary encoder (Figure A.7). When the dough was passed under the wheel the angle angle, α, was measured by the rotary encoder which sent a digital output (proportional to the exit height of the dough, h_e) to the data collection computer. The wheel was mounted 810 mm from the nip gap.

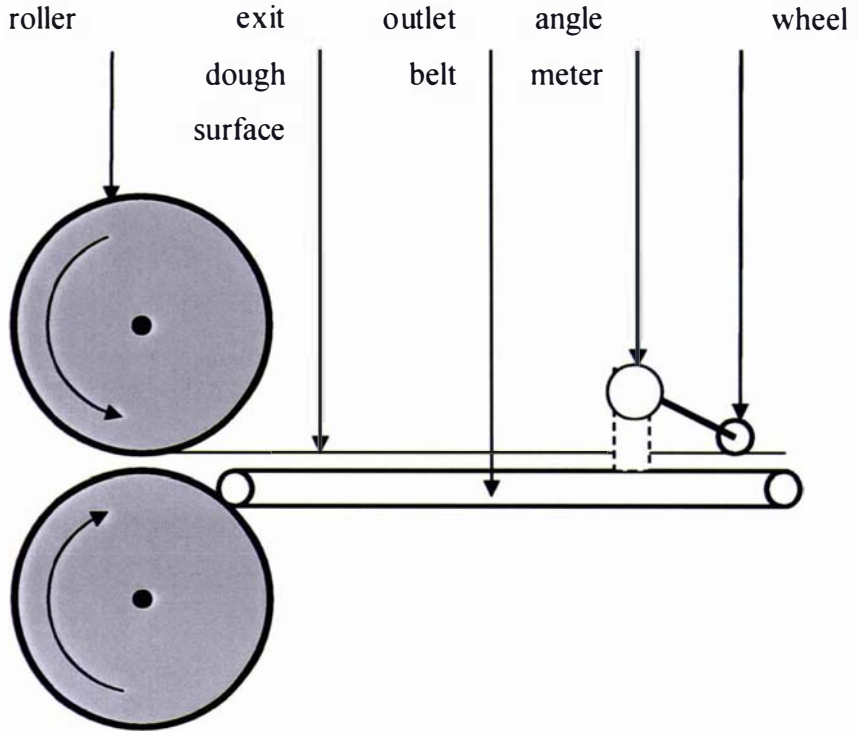

Figure A.7 Exit Height Meter

The curve used to calibrate the digital output of the exit height sensor is given in Figure A.8. The equation of the calibration curve was:

$$h_e = 0.0976(DS) - 185.7 \qquad \text{(A.3)}$$

where, DS = the digital signal. The R^2 value of the curve is 0.999.

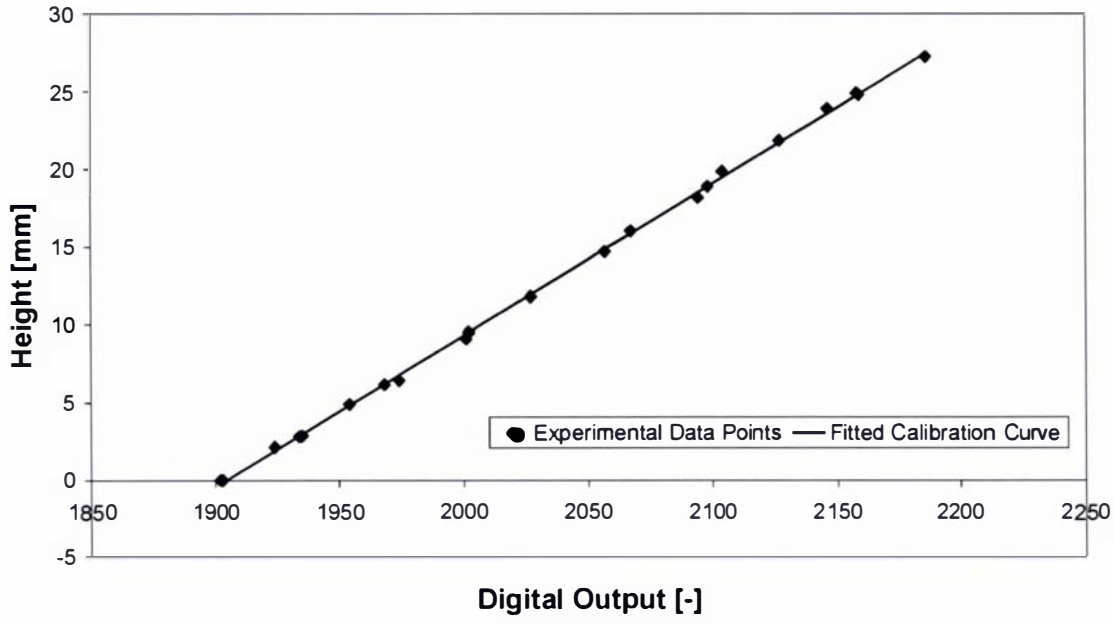

Figure A.8 Exit Height Meter Calibration Curve

The residuals of the calibrated data are shown in Figure A.9. The residuals are distributed about zero, confirming the linear relationship. The accuracy of the height sensor is ± 0.4 mm.

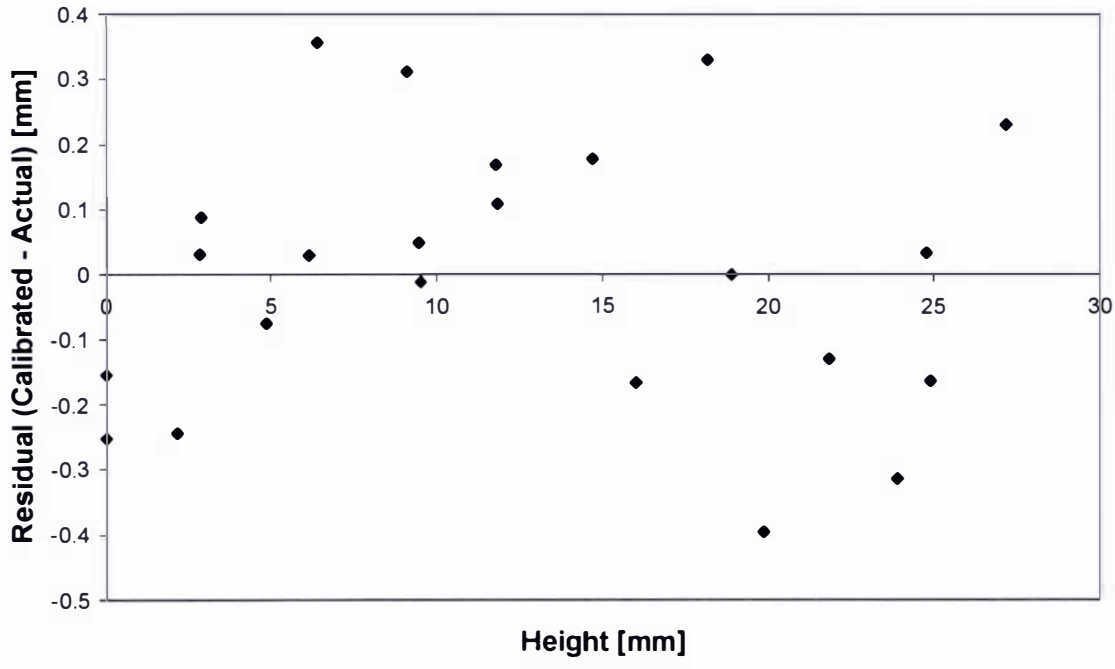

Figure A.9 Exit Height Calibration Residuals

10. Appendix B: Mathematical Details.

10.1. Derivation of Normal Stress, Force and Torque Equations

A simplified diagram of the sheeting system is given in Figure B.1

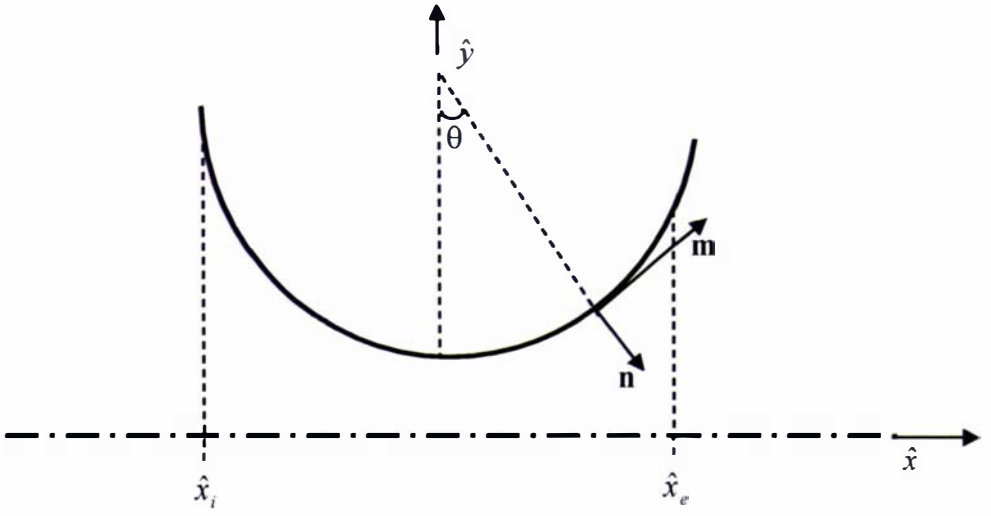

Figure B.1 Simplified sheeting system. n and m are the unit vectors normal and tangential to the roller surface, respectively.

The following procedure was used to determine the normal stress, total upward force and total torque equations for the system.

First, the unit normal and tangential vectors (relative to the roller surface) were resolved into $(\hat{x}, \hat{y}, \hat{z})$ components, demonstrated in Figure B.2.

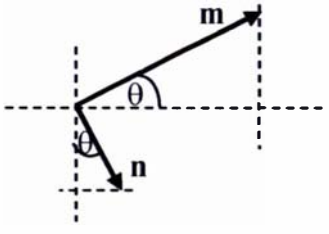

Figure B.2 Resolving vectors into $(\hat{x}, \hat{y}, \hat{z})$ components.

$$\mathbf{n} = (\sin(\theta), -\cos(\theta), 0) \tag{B.1}$$

$$\mathbf{m} = (\cos(\theta), \sin(\theta), 0) \tag{B.2}$$

Then, the traction vector, **T**, on roller surface (facing in direction **n**) was defined as:

$$\mathbf{T}^{(n)} = \left(T_x^{(n)}, T_y^{(n)}, T_z^{(n)}\right) \tag{B.3}$$

From Cauchy's Law:

$$T_i^{(n)} = \sum_j \sigma_{ij} n_j \tag{B.4}$$

Therefore:

$$T_x^{(n)} = \sigma_{xx} \sin(\theta) - \sigma_{xy} \cos(\theta) \tag{B.5}$$

$$T_y^{(n)} = \sigma_{yx} \sin(\theta) - \sigma_{yy} \cos(\theta) \tag{B.6}$$

$$T_z^{(n)} = 0 \tag{B.7}$$

In order to conform to boundary conditions (Section 1.6.6) it was necessary to determine the normal stress acting on the roller. This was calculated by taking the dot product of the traction tensor and the vector, **n**, normal to the roller surface:

$$\hat{\mathrm{T}}_n^{(n)} = \mathbf{T}^{(n)} \cdot \mathbf{n} \tag{B.8}$$

$$\hat{\mathrm{T}}_n^{(n)} = \left(T_x^{(n)}, T_y^{(n)}, T_z^{(n)}\right) \cdot (\sin(\theta), -\cos(\theta), 0) \tag{B.9}$$

$$\hat{\mathrm{T}}_n^{(n)} = \left(\sigma_{xx} \sin(\theta) - \sigma_{xy} \cos(\theta), \sigma_{xy} \sin(\theta) - \sigma_{yy} \cos(\theta), 0\right) \cdot (\sin(\theta), -\cos(\theta), 0) \tag{B.10}$$

$$\hat{\mathrm{T}}_n^{(n)} = \sigma_{xx} \sin^2(\theta) - 2\sigma_{xy} \sin(\theta)\cos(\theta) + \sigma_{yy} \cos^2(\theta) \tag{B.11}$$

By definition (Bird et al., 1986), (note that some authors use a different sign convention),

$$\boldsymbol{\sigma} = \delta\hat{\mathbf{p}} + \hat{\boldsymbol{\tau}} = \begin{pmatrix} \hat{p} + \hat{\tau}_{xx} & \hat{\tau}_{xy} & 0 \\ \hat{\tau}_{xy} & \hat{p} + \hat{\tau}_{yy} & 0 \\ 0 & 0 & 0 \end{pmatrix} \tag{B.12}$$

Therefore:

$$\hat{\mathrm{T}}_n^{(n)} = \hat{p} + \hat{\tau}_{xx} \sin^2(\theta) + \hat{\tau}_{yy} \cos^2(\theta) - 2\hat{\tau}_{xy} \sin(\theta)\cos(\theta) \tag{B.13}$$

Next the force in the upward, *y*, direction at a point was determined from the dot product of the traction vector and a unit vector facing in the *y* direction, that is:

$$\hat{F}_y = \mathbf{T}^{(n)} \cdot \delta_y \tag{B.14}$$

$$\hat{F}_y = \left(T_x^{(n)}, T_y^{(n)}, T_z^{(n)}\right) \cdot (0,1,0) \tag{B.15}$$

$$\hat{F}_y = T_y^{(n)} \tag{B.16}$$

$$\hat{F}_y = \sigma_{xy} \sin(\theta) - \sigma_{yy} \cos(\theta) \tag{B.17}$$

$$\hat{F}_y = \hat{\tau}_{xy} \sin(\theta) - \left(\hat{p} + \hat{\tau}_{yy}\right)\cos(\theta) \tag{B.18}$$

Then to establish the total upward force (per width) on the roller, it was necessary to integrate over the region of contact between the roller and the process material. (*ds* = surface element, on the roller)

$$\frac{\sum \hat{F}_y}{W} = \int_{s_i}^{s_g} \hat{F}_y ds = \int_{s_i}^{s_g} \hat{\tau}_{xy} \sin(\theta) - (\hat{p} + \hat{\tau}_{yy}) \cos(\theta) ds \tag{B.19}$$

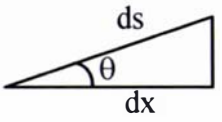

Figure B.3 Geometric relationship between surface and co-ordinate derivative.

From Figure B.3,

$$\frac{dx}{ds} = \cos(\theta) \tag{B.20}$$

Therefore:

$$\frac{\sum \hat{F}_y}{W} = \int_{\hat{x}_i}^{\hat{x}_g} \hat{\tau}_{xy} \sin(\theta) - (\hat{p} + \hat{\tau}_{yy}) \cos(\theta) \frac{d\hat{x}}{\cos(\theta)} \tag{B.21}$$

$$\frac{\sum \hat{F}_y}{W} = \int_{\hat{x}_i}^{\hat{x}_g} [\hat{\tau}_{xy} \tan(\theta) - (\hat{p} + \hat{\tau}_{yy})] d\hat{x} \tag{B.22}$$

which is evaluated at the roller surface.

Then the torque, $\hat{M}$, per unit area, acting on the roller of radius, $\hat{R}$, was determined from the dot product of the traction vector and the unit vector, **m**, tangential to the roller surface:

$$\frac{\hat{M}}{Area} = \hat{R}\mathbf{T} \cdot \mathbf{m} = R(T_x^{(n)}, T_y^{(n)}, T_z^{(n)}) \cdot (\cos(\theta), \sin(\theta), 0) \tag{B.23}$$

$$\frac{\hat{M}}{Area} = \hat{R}(\sigma_{xx} \sin(\theta) - \sigma_{xy} \cos(\theta), \sigma_{yx} \sin(\theta) - \sigma_{yy} \cos(\theta), 0) \cdot (\cos(\theta), \sin(\theta), 0) \tag{B.24}$$

$$\frac{\hat{M}}{Area} = \hat{R}(\sigma_{xx} \sin(\theta)\cos(\theta) - \sigma_{xy} \cos^2(\theta) + \sigma_{yx} \sin^2(\theta) - \sigma_{yy} \sin(\theta)\cos(\theta)) \tag{B.25}$$

$$\frac{\hat{M}}{Area} = \hat{R}((\sigma_{xx} - \sigma_{yy}) \sin(\theta)\cos(\theta) + \sigma_{xy} (\sin^2(\theta) - \cos^2(\theta))) \tag{B.26}$$

$$\frac{\hat{M}}{Area} = \hat{R}((\hat{\tau}_{xx} - \hat{\tau}_{yy}) \sin(\theta)\cos(\theta) + \hat{\tau}_{xy} (\sin^2(\theta) - \cos^2(\theta))) \tag{B.27}$$

Then the total torque (per width) on the roller was calculated by integrating over the roller surface:

$$\frac{\sum \hat{M}}{W} = \int_{s_i}^{s_e} \left[\hat{R}\left(\left(\hat{\tau}_{xx} - \hat{\tau}_{yy}\right)\sin(\theta)\cos(\theta) + \hat{\tau}_{xy}\left(\sin^2(\theta) - \cos^2(\theta)\right)\right)\right] ds \tag{B.28}$$

$$\frac{\sum \hat{M}}{W} = \int_{\hat{x}_i}^{\hat{x}_e} \left[\hat{R}\left(\left(\hat{\tau}_{xx} - \hat{\tau}_{yy}\right)\sin(\theta)\cos(\theta) + \hat{\tau}_{xy}\left(\sin^2(\theta) - \cos^2(\theta)\right)\right)\right] \frac{d\hat{x}}{\cos(\theta)} \tag{B.29}$$

$$\frac{\sum \hat{M}}{W} = \hat{R}\int_{\hat{x}_i}^{\hat{x}_e} \left[\left(\left(\hat{\tau}_{xx} - \hat{\tau}_{yy}\right)\sin(\theta) + \hat{\tau}_{xy}\left(\tan(\theta)\sin(\theta) - \cos(\theta)\right)\right)\right] d\hat{x} \tag{B.30}$$

which is evaluated at the roller surface.

10.2. Choosing Dimensionless Forms

It was required to find dimensionless forms of equations, (5.10) to (5.15). The aim was to rewrite the equations as a dimensionless, power series of a perturbation variable, ε.

10.2.1. Co-ordinate Variables

From geometry considerations the order of the coordinate variables were estimated:

$$\hat{x} \approx O\left(\hat{R}\right) \tag{B.31}$$

$$\hat{y} \approx O\left(\hat{\delta}\right) \tag{B.32}$$

That is:

$$\hat{x} = x\hat{R} \tag{B.33}$$

$$\hat{y} = y\hat{\delta} \tag{B.34}$$

These appeared to be the most natural selection for the dimensionless forms of the coordinate variables. However, using these forms resulted in a difficulty with the equation of the height of the roller surface (see Figure B.4). Under this scheme the height was:

$$h = 1 + \frac{1}{\varepsilon} - \frac{\sqrt{1 - x^2}}{\varepsilon} \tag{B.35}$$

where:

$$\varepsilon = \frac{\delta}{R} \tag{B.36}$$

The Taylor series expansion of (B.35), in terms of ε, was:

$$h = \frac{1}{\varepsilon}\left(1 - \sqrt{1 - x^2}\right) + 1 \tag{B.37}$$

The presence of a negative order term made this expansion difficult to work with. Therefore a new scheme to make the co-ordinate variables dimensionless was devised.

$$\hat{x} = x\sqrt{\hat{\delta}\hat{R}} \tag{B.38}$$

$$\hat{y} = y\hat{\delta} \tag{B.39}$$

This led to the following form for the height boundary condition:

$$h = 1 + \frac{x^2}{2} + \varepsilon^2 \frac{x^4}{8} + \varepsilon^4 \frac{x^6}{16} + \ldots \tag{B.40}$$

where:

$$\varepsilon = \sqrt{\frac{\hat{\delta}}{\hat{R}}} \tag{B.41}$$

This form of h was more suitable to work with.

10.2.2. Velocity Variables

Again from geometry considerations, it was noted that:

$$\hat{u} = \hat{u}_r u \tag{B.42}$$

Substituting the dimensionless forms into (5.10) gave:

$$\hat{v} = \hat{u}_r \sqrt{\frac{\hat{\delta}}{\hat{R}}} v = \hat{u}_r \varepsilon v \tag{B.43}$$

where:

$$u = u_0 + \varepsilon u_1 + \varepsilon^2 u_2 + \ldots \tag{B.44}$$

$$v = v_0 + \varepsilon v_1 + \varepsilon^2 v_2 + \ldots \tag{B.45}$$

10.2.3. The Viscometric Functions

It is desirable to have the dimensionless forms of the three viscometric functions approximately equal to each other. It was noted that:

$$O\left(\hat{\Psi}_1, \hat{\Psi}_2\right) \approx \hat{\eta}\dot{\gamma} \approx \frac{\hat{\eta}\hat{\delta}}{\hat{u}_r} \tag{B.46}$$

Therefore the following dimensionless forms of the viscometric functions were proposed:

$$\hat{\eta} = \hat{\eta}\eta, \text{ i.e. } \eta = 1 \tag{B.47}$$

$$\hat{\Psi}_1 = \Psi_1 \frac{\hat{\eta}\hat{\delta}}{\hat{u}_r} \tag{B.48}$$

$$\hat{\Psi}_2 = \Psi_2 \frac{\hat{\eta}\hat{\delta}}{\hat{u}_r} \tag{B.49}$$

10.2.4. Stress Term

Substituting the dimensionless forms into (5.13), taking into account that $\hat{\delta} < \hat{R}$, gave:

$$\hat{\tau}_{nn} = \frac{\hat{\eta}\hat{u}_r}{\hat{\delta}} T_{nn} \tag{B.50}$$

where:

$$T_{nn} = T_{nn,0} + \varepsilon T_{nn,1} + \varepsilon^2 T_{nn,2} + \ldots \tag{B.51}$$

10.2.5. Pressure

Substituting the dimensionless forms into (5.11), taking into account that $\hat{\delta} < \hat{R}$, gave

$$\hat{p} - \hat{p}_a = P\frac{\hat{u}_r \eta}{\hat{\delta}} \tag{B.52}$$

Or substituting the dimensionless forms into (5.12) gave:

$$\hat{p} - \hat{p}_a = P\frac{\hat{u}_r \hat{\eta}}{\hat{\delta}} \tag{B.53}$$

But, when this dimensionless form was used for the pressure, then the zeroth order term of (5.11) was found to be:

$$\frac{\partial P_0}{\partial x} = \frac{1}{\varepsilon}\frac{\partial^2 u_0}{\partial y^2} \tag{B.54}$$

This was unacceptable, as the perturbation variable, ε, remained in the equation. Therefore a new dimensionless form for the pressure was used, to eliminate this problem:

$$\hat{p} - \hat{p}_a = P\frac{\hat{u}_r \hat{\eta}}{\hat{\delta}}\sqrt{\frac{\hat{R}}{\hat{\delta}}} \tag{B.55}$$

where:

$$P = P_0 + \varepsilon P_1 + \varepsilon^2 P_2 + \ldots \tag{B.56}$$

10.2.6. Force and Torque Equations

Figure B.4 shows the sheeter geometry, with dimensions.

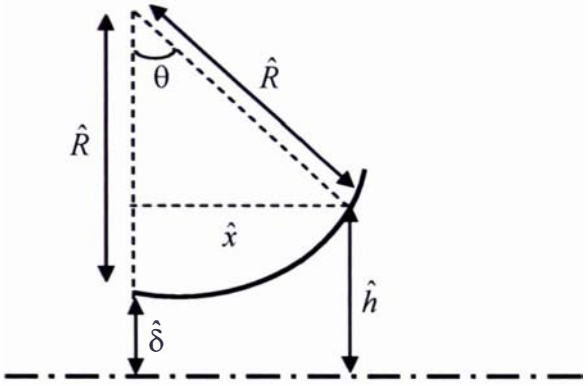

Figure B.4 Sheeter geometry with dimensions.

Therefore, from the geometry:

$$\tan(\theta) = \frac{\hat{x}}{\hat{R} + \hat{\delta} - \hat{h}} \tag{B.57}$$

$$\cos(\theta) = \frac{\hat{R} + \hat{\delta} - \hat{h}}{\hat{R}} \tag{B.58}$$

$$\sin(\theta) = \frac{\hat{x}}{\hat{R}} \tag{B.59}$$

$\hat{h}$ was also determined from the geometry:

$$\hat{h} = \hat{R} + \hat{\delta} - \sqrt{\hat{R}^2 - \hat{x}^2} \tag{B.60}$$

Therefore:

$$\tan(\theta) = \frac{\hat{x}}{\sqrt{\hat{R}^2 - \hat{x}^2}} \tag{B.61}$$

$$\cos(\theta) = \frac{\sqrt{\hat{R}^2 - \hat{x}^2}}{\hat{R}} \tag{B.62}$$

$$\sin(\theta) = \frac{\hat{x}}{\hat{R}} \tag{B.63}$$

The dimensionless forms given above were then substituted in:

$$\tan(\theta) = \frac{\varepsilon x}{\sqrt{1 - \varepsilon^2 x^2}} \tag{B.64}$$

$$\cos(\theta) = \sqrt{1 - \varepsilon^2 x^2} \tag{B.65}$$

$$\sin(\theta) = \varepsilon x \tag{B.66}$$

Or taking Taylor approximations:

$$\tan(\theta) = \varepsilon x + \varepsilon^3 \frac{x^3}{2} + \ldots \tag{B.67}$$

$$\cos(\theta) = 1 - \varepsilon^2 \frac{x^2}{2} + \ldots \tag{B.68}$$

$$\sin(\theta) = \varepsilon x \tag{B.69}$$

Then these were substituted into the total upward force equation:

$$\frac{\sum \hat{F}_y}{W} = \frac{\sum F_y}{W}\left(\dim_{\sum F_y}\right) = \int_{\hat{x}_i}^{\hat{x}_e} \left[\hat{\tau}_{xy} \tan(\theta) - \left(\hat{p} + \hat{\tau}_{yy}\right)\right] d\hat{x} \tag{B.70}$$

$$\frac{\sum F_y}{W}\left(\dim_{\sum F_y}\right) = \sqrt{\delta R} \int_{x_i}^{x_e} \left[\frac{\eta u_r}{\delta} \mathrm{T}_{xy} \tan(\theta) - \left(\frac{\eta u_r}{\delta \varepsilon} P + \frac{\eta u_r}{\delta} \mathrm{T}_{yy}\right)\right] dx \tag{B.71}$$

$$\frac{\sum F_y}{W}\left(\dim_{\sum F_y}\right) = \frac{\sqrt{\delta R}\eta u_r}{\delta \varepsilon} \int_{x_i}^{x_e} \left[\varepsilon \mathrm{T}_{xy}\left(\varepsilon x + \varepsilon^3 \frac{x^3}{2} + \ldots\right) - \left(P + \varepsilon \mathrm{T}_{yy}\right)\right] dx \tag{B.72}$$

$$\frac{\sum \hat{F}_y}{W} = \frac{\sum F_y}{W} \frac{\eta u_r}{\varepsilon^2}\left(= \left[Pa.s. \frac{m}{s}.\right] = \left[\frac{N}{m}\right]\right) \tag{B.73}$$

$$\frac{\sum F_y}{W} = -\int_{x_i}^{x_e} \left[P_0\right] dx - \varepsilon \int_{x_i}^{x_e} \left[P_1 + \mathrm{T}_{yy,0}\right] dx + \varepsilon^2 \int_{x_i}^{x_e} \left[x \mathrm{T}_{xy,0} - \left(P_2 + \mathrm{T}_{yy,1}\right)\right] dx + \ldots \tag{B.74}$$

An equivalent substitution was also made into the total torque equation:

$$\frac{\sum \hat{M}}{W} = \frac{\sum M}{W}(\dim_M)$$
$$= R\int_{\hat{x}_i}^{\hat{x}_g}\left[\left(\left(\hat{\tau}_{xx} - \hat{\tau}_{yy}\right)\sin(\theta) + \hat{\tau}_{xy}\left(\tan(\theta)\sin(\theta) - \cos(\theta)\right)\right)\right]d\hat{x} \tag{B.75}$$

$$\frac{\sum M}{W}\left(\dim_{\sum M}\right) = \sqrt{\delta R}\frac{R}{\delta}\eta u_r\int_{x_i}^{x_g}\left[\begin{array}{l}\left(T_{xx} - T_{yy}\right)(\varepsilon x) \\ + T_{xy}\left(\begin{array}{l}(\varepsilon x)\left(\varepsilon x + \varepsilon^3\frac{x^3}{2} + \ldots\right) \\ -\left(1 - \varepsilon^2\frac{x^2}{2}\right)\end{array}\right)\end{array}\right]dx \tag{B.76}$$

$$\frac{\sum \hat{M}}{W} = \frac{\sum M}{W}\frac{\eta R u_r}{\varepsilon}\left(=\left[Pa.s.\frac{m}{s}.m\right] = \left[\frac{N}{m^2}.s.\frac{m}{s}.m\right] = [N]\right) \tag{B.77}$$

$$\frac{\sum M}{W} = \int_{x_i}^{x_g}\left[-T_{xy,0}\right]dx + \varepsilon\int_{x_i}^{x_g}\left[\left(T_{xx,0} - T_{yy,0}\right)x - T_{xy,1}\right]dx$$
$$+ \varepsilon^2\int_{x_i}^{x_g}\left[\left(T_{xx,1} - T_{yy,1}\right)x + T_{xy,0} - T_{xy,2} + \frac{x^2}{2}T_{xy,0}\right]dx + \ldots \tag{B.78}$$

10.3. Boundary Conditions (Dimensionless, Perturbation Forms)

The boundary conditions were also needed in a dimensionless form.

10.3.1. No Slip at the Roller Surface

At the roller surface, $\hat{h}$, the dough velocity is equal to the roller velocity, $\hat{u}_r$. The dimensionless perturbation form of the condition was easily derived from the dimensionless forms of *h*, u and *v*:

$$\text{at } y = h = 1 + \frac{x^2}{2} + \varepsilon^2\frac{x^4}{8} + \ldots, \tag{B.79}$$

$$u = u_0 + \varepsilon u_1 + \varepsilon^2 u_2 + \ldots = 1 - \varepsilon^2\frac{x^2}{2} - \varepsilon^4\frac{x^4}{8} + \ldots \tag{B.80}$$

$$v = v_0 + \varepsilon v_1 + \varepsilon^2 v_2 + \ldots = x \tag{B.81}$$

10.3.2. Line of Symmetry

At $\hat{y}=0$, there is a line of symmetry, which means: $\hat{v}=0$ and $\frac{\partial \hat{u}}{\partial \hat{y}}=0$. Again this is simply rewritten with the dimensionless forms of u and *v*::

at $y=0$, (B.82)

$$\frac{\partial u}{\partial y}=\frac{\partial u_0}{\partial y}+\varepsilon\frac{\partial u_1}{\partial y}+\varepsilon^2\frac{\partial u_2}{\partial y}+\ldots=0 \quad \text{(B.83)}$$

$$v=v_0+\varepsilon v_1+\varepsilon^2 v_2+\ldots=0 \quad \text{(B.84)}$$

10.3.3. Inlet Condition

At the point of inlet $(\hat{x}_i,\hat{h}_i)$, there is a free surface, at which the total stress on the roller surface is equal to zero.

The point of inlet was easily rewritten, with the dimensionless forms of *h*:

$$\text{at } y=h_i=1+\frac{x_i^{\,2}}{2}+\varepsilon^2\frac{x_i^{\,4}}{8}+\ldots \text{and } x=x_i, \quad \text{(B.85)}$$

The total normal stress is given in a dimensioned form above, into which the dimensionless forms of pressure and stress were substituted:

$$\hat{\mathrm{T}}_n^{(n)}=\mathrm{T}_n^{(n)}\left(\dim_{\hat{T}}\right)=\hat{p}+\hat{\tau}_{xx}\sin^2(\theta)+\hat{\tau}_{yy}\cos^2(\theta)-2\hat{\tau}_{xy}\sin(\theta)\cos(\theta) \quad \text{(B.86)}$$

$$\mathrm{T}_n^{(n)}\left(\dim_{\hat{T}}\right)=\frac{\eta u_r}{\delta}\sqrt{\frac{R}{\delta}}\begin{bmatrix}P+\varepsilon^3x^2\mathrm{T}_{xx}+\varepsilon\left(1-\varepsilon^2x^2+\ldots\right)\mathrm{T}_{yy}\\-2\varepsilon^2x\left(1-\varepsilon^2\frac{x^2}{2}\right)\mathrm{T}_{xy}\end{bmatrix} \quad \text{(B.87)}$$

$$\hat{\mathrm{T}}_n^{(n)}=\mathrm{T}_n^{(n)}\frac{\eta u_r}{\delta\varepsilon}\left(=\left[Pa.s.\frac{m}{s}.\frac{1}{m}\right]=[Pa]\right) \quad \text{(B.88)}$$

$$\mathrm{T}_n^{(n)}=P_0+\varepsilon\left(P_1+\mathrm{T}_{yy,0}\right)+\varepsilon^2\left(P_0+\mathrm{T}_{yy,1}-2x\mathrm{T}_{xy,0}\right)+\ldots=0 \quad \text{(B.89)}$$

10.3.4. Outlet Condition

At the point of outlet $(\hat{x}_e,\hat{h}_e)$, there is a free surface, at which the total stress on the roller surface is equal to zero. In dimensionless form this is:

$$\text{at } y=x_e=1+\frac{x_e^{\,2}}{2}+\varepsilon^2\frac{x_e^{\,4}}{8}+\ldots \text{and } x=x_e, \quad \text{(B.90)}$$

$$\mathrm{T}_n^{(n)}=P_0+\varepsilon\left(P_1+\mathrm{T}_{yy,0}\right)+\varepsilon^2\left(P_2+\mathrm{T}_{yy,1}-2x\mathrm{T}_{xy,0}\right)+\ldots=0 \quad \text{(B.91)}$$

10.3.5. Conservation of Mass

At any value of $\hat{x}$ the integral of the horizontal velocity component by $\hat{y}$, from $\hat{y} = 0$ to $\hat{y} = \hat{h}$, is equal to a constant. Assuming that the exit velocity profile is flat, and obeying the outlet boundary condition, then the constant is equal to $\hat{u}_e \hat{h}_e$. From the dimensionless forms of *h* and *u* this was written as:

$$\forall x \tag{B.92}$$

$$u_e h_e = 1 + \frac{x_e^{\,2}}{2} - \varepsilon^2 \frac{x_e^{\,2}}{8}\left(x_e^{\,2} + 4\right) - \ldots \tag{B.93}$$

$$u_e h_e = \int_0^h u dy. \tag{B.94}$$

$$u_e h_e = \int_0^{1+\frac{x^2}{2}} u_0 dy + \varepsilon \int_0^{1+\frac{x^2}{2}} u_1 dy + \varepsilon^2 \left(\int_0^{\frac{x^4}{8}} u_0 dy + \int_0^{1+\frac{x_e^{\,2}}{2}} u_2 dy \right) + \ldots \tag{B.95}$$

10.4. Solution Details

10.4.1. Zero Order Solution

Below are the details of the zeroth order solution. A similar method was used for the higher orders. The symbolic processing package, MACSYMA, was used to perform the mathematical operations.

First (5.39) was integrating by *y*:

$$P_0 = B_0 + C_0(x) \tag{B.96}$$

Where C_0 is an unknown function of *x*, and B_0 is an unknown constant. (B.96) was then differentiated by *x*:

$$\frac{\partial P_0}{\partial x} = \frac{dC_0}{dx} \tag{B.97}$$

(B.97) was then substituted into (5.38).

$$\frac{\partial^2 u_0}{\partial^2 y} = \frac{1}{\eta}\frac{dC_0}{dx} \tag{B.98}$$

(B.98) was then integrated by y.

$$\frac{\partial u_0}{\partial y} = \frac{y}{\eta}\frac{dC_0}{dx} + D_0 \tag{B.99}$$

Where D_0 is an unknown constant. The Line of Symmetry boundary condition was then used to determine the value of D_0.

$$D_0 = 0 \tag{B.100}$$

$$\frac{\partial u_0}{\partial y} = \frac{y}{\eta}\frac{dC_0}{dx} \tag{B.101}$$

(B.101) was then integrated by y:

$$u_0 = \frac{y^2}{2\eta}\frac{dC_0}{dx} + E_0 \tag{B.102}$$

Where E_0 is another unknown constant. The No Slip at the Roller Surface boundary condition was used to determine the value of E_0.

$$E_0 = 1 - \frac{1}{2\eta}\frac{dC_0}{dx}\left(1 + x^2 + \frac{x^4}{8}\right) \tag{B.103}$$

$$u_o = 1 + \frac{y^2 - \left(1 + x^2 + \frac{x^4}{8}\right)}{2\eta}\frac{dC_0}{dx} \tag{B.104}$$

Then the Mass Conservation boundary condition was used, to determine the derivative of C_0, with regard to x.

$$\int_0^h u_0 dy = \left(1 + \frac{x_e^{\,2}}{2}\right) \therefore \frac{dC_0}{dx} = 12\eta\frac{(x - x_e)(x + x_e)}{(x^2 + 2)^3} \tag{B.105}$$

Then substituting (B.102) gave:

$$u_0 = \frac{3x_e^{\,2} - x^2 + 4}{2(x^2 + 2)} - \frac{6y^2(x_e - x)(x_e + x)}{(x^2 + 2)^3} \tag{B.106}$$

Substituting this into (5.37) and applying the Line of Symmetry boundary condition allowed v_0 to be solved for:

$$v_0 = \frac{3xy(x_e^{\,2} + 2)}{(x^2 + 2)^2} - \frac{4xy^3(3x_e^{\,2} - 2x^2 + 2)}{(x^2 + 2)^4} \tag{B.107}$$

Equation (B.105) was then integrated by x. The constant of integration (an arbitrary function of neither x nor y) can be discarded, as it is already included as B_0.

$$C_0 = -\eta\frac{3}{8}\left(\frac{x(10x_e^{\,2} + 4) + x^3(3x_e^{\,2} - 2)}{(x^2 + 2)^2} + \frac{3x_e^{\,2} - 2}{\sqrt{2}}\tan^{-1}\left(\frac{x}{\sqrt{2}}\right)\right) \tag{B.108}$$

This expression was then substituted into (B.96), to give an expression for P_0.

$$P_0 = -\eta\frac{3}{8}\left(\frac{x(10x_e^{\,2} + 4) + x^3(3x_e^{\,2} - 2)}{(x^2 + 2)^2} + \frac{3x_e^{\,2} - 2}{\sqrt{2}}\tan^{-1}\left(\frac{x}{\sqrt{2}}\right)\right) + B_0 \tag{B.109}$$

The inlet boundary condition was then used to solve for B_0.

$$B_0 = \eta\frac{3}{8}\left(\frac{x_i\left(10x_e^{\,2}+4\right)+x_i^{\,3}\left(3x_e^{\,2}-2\right)}{\left(x_i^{\,2}+2\right)^2}+\frac{3x_e^{\,2}-2}{\sqrt{2}}\tan^{-1}\left(\frac{x_i}{\sqrt{2}}\right)\right) \tag{B.110}$$

Therefore:

$$P_0 = -\eta\frac{3}{8}\left(\begin{array}{l}\dfrac{x\left(10x_e^{\,2}+4\right)+x^3\left(3x_e^{\,2}-2\right)}{\left(x^2+2\right)^2}-\dfrac{x_i\left(10x_e^{\,2}+4\right)+x_i^{\,3}\left(3x_e^{\,2}-2\right)}{\left(x_i^{\,2}+2\right)^2}\\ +\dfrac{3x_e^{\,2}-2}{\sqrt{2}}\left(\tan^{-1}\left(\dfrac{x}{\sqrt{2}}\right)-\tan^{-1}\left(\dfrac{x_i}{\sqrt{2}}\right)\right)\end{array}\right) \tag{B.111}$$

Finally the earlier solutions were substituted into (5.40), (5.41) and (5.42) to give:

$$T_{yy,0} = -144\Psi_2 y^2\frac{(x_e-x)^2(x_e+x)^2}{\left(x^2+2\right)^6} \tag{B.112}$$

$$T_{xy,0} = 12\eta y\frac{(x_e-x)(x_e+x)}{\left(x^2+2\right)^3} \tag{B.113}$$

$$T_{xx,0} = -144(\Psi_1+\Psi_2)y^2\frac{(x_e-x)^2(x_e+x)^2}{\left(x^2+2\right)^6} \tag{B.114}$$

This completes the zero order solution. The first and second order solutions proceeded similarly, using the appropriately perturbated boundary conditions.

10.4.2. Confirming Boundary Conditions

After the zero, first and second order solutions were completed (5.37) to (5.54) it was confirmed that the boundary conditions were met. This means that the solution may have proceeded without error.